1. Report No. FHWA/TX-12/0-6992-2	2. Government Accession No.	3. Recipient's Catalog No.
4. Title and Subtitle COMPREHENSIVE EVALUATION OF COMPACTION OF ASPHALT PAVEMENTS AND DEVELOPMENT OF COMPACTION MONITORING SYSTEM		5. Report Date Submitted: January 2012 Published: April 2012
		6. Performing Organization Code
7. Author(s) Emad Kassem, Tom Scullion, Eyad Masad, Arif Chowdhury, Wenting Liu, Cindy Estakhri, and Samer Dessouky		8. Performing Organization Report No. Report 0-6992-2
9. Performing Organization Name and Address Texas Transportation Institute The Texas A&M University System College Station, Texas 77843-3135		10. Work Unit No. (TRAIS)
		11. Contract or Grant No. Project 0-6992
12. Sponsoring Agency Name and Address Texas Department of Transportation Research and Technology Implementation Office P. O. Box 5080 Austin, Texas 78763-5080		13. Type of Report and Period Covered Technical Report: September 2009–August 2011
		14. Sponsoring Agency Code
15. Supplementary Notes Project performed in cooperation with the Texas Department of Transportation and the Federal Highway Administration. Project Title: Develop Practical Field Guidelines for the Compaction of HMA or WMA URL: http://tti.tamu.edu/documents/0-6992-2.pdf		

16. Abstract

This study aimed to conduct a comprehensive evaluation of compaction of asphalt pavements and develop software for monitoring field compaction in real time. In the first phase of this study, the researchers built several test sections that were constructed using different asphalt mixtures and various compaction methods. The results of these experiments were used to determine the effects of compaction temperature, compaction method, mixture design, and base type on the compactability of asphalt mixtures. The researchers found that the efficiency of the compactive effort across the steel rollers was non-uniform. A point on the mat closer to the center of the roller was subjected to more compaction than a point closer to the edge of the roller. The compaction temperature was found to have a great effect on compaction irrespective of mixture type. The researchers presented a method for predicting the density of asphalt pavements in real time. This method utilizes the location of the roller on the mat and the compaction curves for each roller to predict the density. The predicted density was close to the measured one.

In the second phase of this study, the researchers developed a system for monitoring and documenting the compaction process of asphalt mixtures. This system is called the compaction monitoring system (CMS). The CMS uses the latest global positioning system technologies and various sensors to provide full coverage of the newly constructed mat. The CMS shows maps of coverage, compaction index, and temperature of the first roller pass in real time. The CMS was found to be simple and easy to install and use. The CMS was able to show some inconsistencies in the compaction process, for example, unequal converge across the mat, non-uniform temperature, and significant delay in compaction after placement of the mixtures. The CMS documents the compaction process for the whole project, and the data are saved on the computer. The data can be opened using the same software for reviewing the whole compaction process.

17. Key Words Asphalt Mixtures, HMA, WMA, Compaction, Temperature, Effectiveness Factor, Uniformity, CMS	18. Distribution Statement No restrictions. This document is available to the public through NTIS: National Technical Information Service Alexandria, Virginia 22312 http://www.ntis.gov		
19. Security Classif. (of this report) Unclassified	20. Security Classif. (of this page) Unclassified	21. No. of Pages 162	22. Price

COMPREHENSIVE EVALUATION OF COMPACTION OF ASPHALT PAVEMENTS AND DEVELOPMENT OF COMPACTION MONITORING SYSTEM

by

Emad Kassem
Associate Research Scientist

Tom Scullion
Senior Research Engineer

Eyad Masad
Research Engineer

Arif Chowdhury
Assistant Research Engineer

Wenting Liu
Assistant Research Engineer

Cindy Estakhri
Research Engineer,
Texas Transportation Institute

and

Samer Dessouky
Assistant Professor
University of Texas at San Antonio

DISCLAIMER

The contents of this report reflect the views of the authors, who are responsible for the facts and the accuracy of the data presented herein. The contents do not necessarily reflect the official view or policies of the Federal Highway Administration (FHWA) or the Texas Department of Transportation (TxDOT). This report does not constitute a standard, specification, or regulation, nor is it intended for construction, bidding, or permit purposes. The United States Government and the State of Texas do not endorse products or manufacturers. Trade or manufacturers' names appear herein solely because they are considered essential to the object of this report. The researcher in charge was Tom Scullion, P.E. (Texas, #62683).

ACKNOWLEDGMENTS

TABLE OF CONTENTS

LIST OF FIGURES

x

LIST OF TABLES

CHAPTER 1
INTRODUCTION AND BACKGROUND

OVERVIEW

TxDOT 0-5261 conducted a comprehensive literature search on compaction of hot asphalt mixtures (Masad et al. 2009a). This chapter presents a summary of previous studies and recent technologies in field compaction of asphalt mixtures.

Compaction is the process by which the volume of an asphalt mixture is reduced, leading to an increase in unit weight of the mixture and interlock among aggregate particles (Corps of Engineers 2000; Roberts et al. 1996). The level of compaction of asphalt mixtures influences the performance. Insufficient compaction leads to several distresses in asphalt mixtures such as premature permanent deformation or rutting, excessive aging, and moisture damage even if all desirable mixture design characteristics are met.

The compaction process is influenced by many factors including the properties of the materials in the mixture, environmental variables, conditions at the lay down site, and method of compaction (Corps of Engineers 2000). The required compaction effort increases with an increase in aggregate angularity, nominal maximum aggregate size, and aggregate hardness. The grade and amount of asphalt binder also influence the compaction process. A mixture produced with too little asphalt is stiff and usually requires more compactive effort than a mixture with high asphalt binder content. Temperatures of the air, mixture, and base are important factors that influence compaction (Corps of Engineers 2000). The compaction effort increases with an increase in layer thickness.

Although compaction is an important process in determining the overall performance of flexible pavements, researchers devoted little effort in the past to this topic. Some studies have attempted to examine the relationship between field compaction methods, laboratory compaction methods, and mechanical properties. Consuegra et al. (1989) assessed the applicability of producing laboratory specimens similar to the ones from the field. They found that the Texas gyratory compactor produces specimens with mechanical properties closer to field cores than other laboratory compaction devices. However, Harvey and Monismith (1993) carried out a similar study and found that the laboratory roller compactor produced specimens with mechanical properties similar to the ones from the field. Peterson et al. (2004) conducted a study to examine the influence of changing the compaction parameters in the Superpave gyratory compactor (SGC) on hot mix asphalt (HMA) mechanical properties. The evaluated parameters included angle of gyration,

specimen height, gyratory compaction pressure, and temperature of the compaction mold. The angle of gyration was found to be the most important parameter that influenced the mechanical properties. They found that using a compaction angle of 1.5° with a specimen height of 50 to 75 mm would produce SGC specimens similar to field cores in terms of the mechanical properties.

Masad et al. (1999) evaluated the air void distribution in SGC specimens using image analysis techniques. They found that air void distribution is not uniform, and there is a higher air void content at the top and the bottom than in the middle. Tashman et al. (2001) evaluated the effect of the compaction pattern in the field on the mechanical properties and air void distribution, and compared the results to SGC laboratory specimens. The results revealed that the compaction pattern was not significant in changing the distribution of the air voids. They found that SGC parameters can be modified to produce SGC specimens that better simulate field cores in terms of air void distribution and mechanical properties.

Sebaaly et al. (2008) evaluated the effectiveness of various joint geometries and compaction techniques in order to increase longitudinal joint density and improve the overall performance of asphalt pavements. The results of this study did not propose a specific joint geometry or a compaction technique that would ensure achieving proper joint compaction.

RESEARCH PROJECT 0-5261

The following sections provide a summary of the main findings of TxDOT Research Project 0-5261.

Field Study

The study aimed to provide a better understanding of the compaction factors that influence uniformity and degree of compaction and the resulting mechanical properties of asphalt mixtures. Such understanding is necessary in order to compact more uniform asphalt pavements with improved performance. In this study, researchers identified roadway projects with different types of mixtures, compaction patterns, and compaction equipment, and followed different compaction patterns in the field. Field cores were obtained from the test sections. Number of passes and the position of each compactor's pass were recorded across the mat, and their influence on measured percent air voids in the recovered field cores were studied. Figure 1-1 shows the number of passes and percent air voids across the mat for a field project.
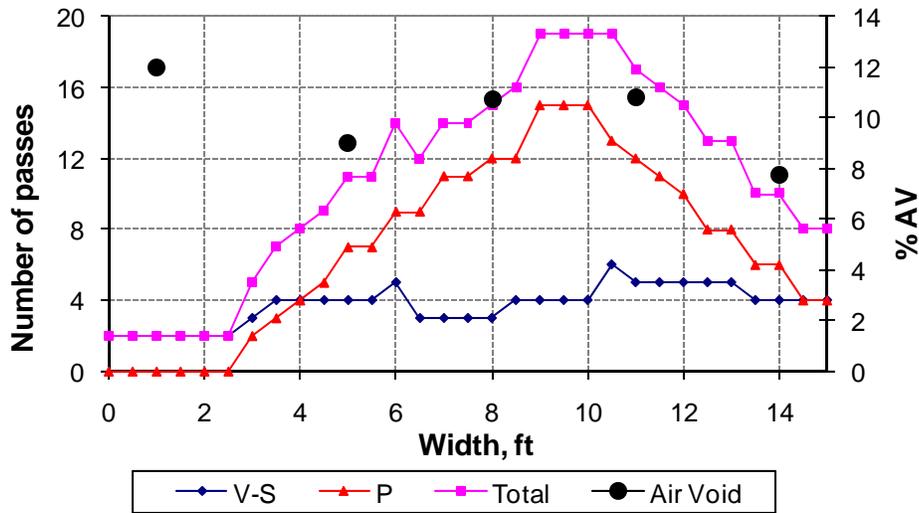
Figure 1-1. Number of Passes and Percent Air Voids (%AV) across the Mat in the US 259 Test Section (Masad et al. 2009a).

The research team observed that cores compacted close to the center of the roller width (static or vibratory) tended to have a higher density than cores compacted at the edge of the compactor even if cores were taken from the middle of the mat and away from the joint. Therefore, researchers conducted an analysis to determine the relationship of percent air voids as a function of number of passes of static and vibratory rollers and the location of the core with respect to the compactor width. Each pass was multiplied by an effectiveness factor, which is a function of the location of the core with respect to roller width.

The efficiency of compaction at a given point is a function of the location of this point with respect to the roller width. Therefore, a new index referred to as the compaction index (CI) was proposed to quantify the compaction effort at any point in the pavement. The CI is a function of number of passes at a point and the position of the point with respect to the compaction roller width. The efficiency of compaction across the roller width was found to be non-uniform. Figure 1-2 shows the effectiveness of one pass across the roller width. A point on the mat closer to the center of the roller is subjected to more effective compaction than a point closer to the edge of the roller. The percent air voids was plotted against the summation of number of passes multiplied by the effectiveness factor corresponding to each pass. This summation is termed CI. The CI correlated very well with the percent air voids for the test sections evaluated in research study 0-5261. Figure 1-3 shows an example of the relationship between CI and percent air voids.
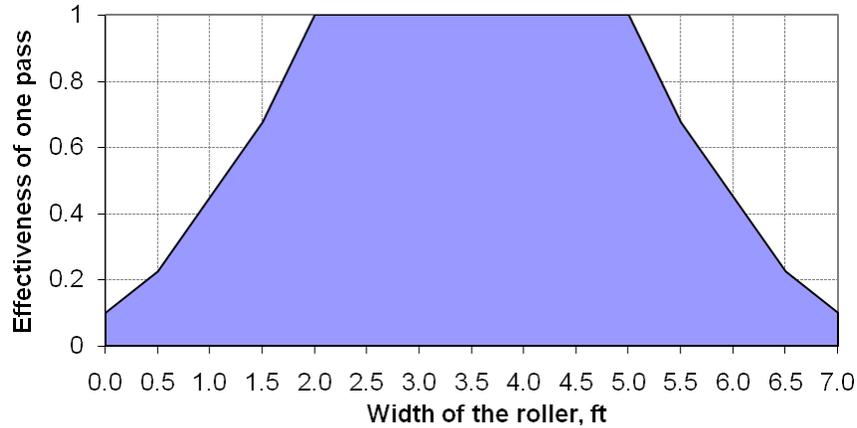
Figure 1-2. Effectiveness Distribution across Roller Width (Masad et al. 2009b).
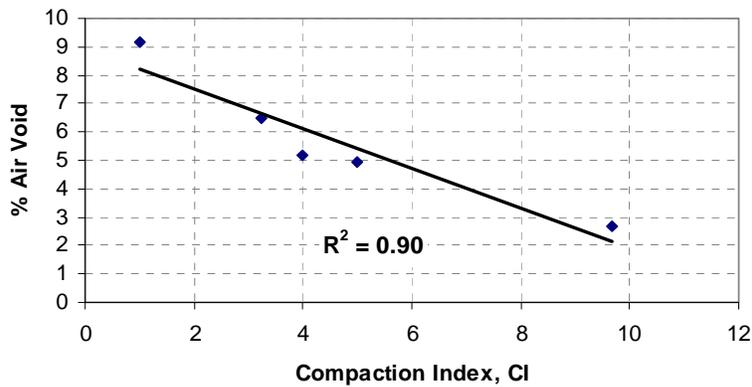
Figure 1-3. CI versus the Percent of Air Voids in the IH 35 Test Section (Masad et al. 2009a).

The relationship between percent air voids and CI can be very useful to set up the compaction pattern (number of passes and location of these passes). The compaction pattern can be set up in order to achieve uniform CI distribution across the pavement section, which corresponds to uniform air void distribution. This point is illustrated in Figure 1-4, which shows a map of percent air voids (Figure 1-4[a]) and relationship between CI and percent air voids (Figure 1-4[b]). As the figure shows, higher CI corresponded to lower air voids and vice versa. The map of percent air void (Figure 1-4[a]) was generated by inputting the location of each core and its percent air voids to the Matlab 7.1[®] software. Then an interpolation algorithm in Matlab was used to predict percent air voids in the whole pavement section.

4

Lab vs. Field

      The compactability of given asphalt mixtures in the field can be predicted based on laboratory measurements. The CI, calculated based on field compaction data, was plotted against corresponding percent air voids for different asphalt mixtures. Figure 1-5 shows such a relationship for some roadway projects (Masad et al. 2009b). In the laboratory, four SGC specimens (6-inch diameter and approximately 2.5 inches in height) were fabricated at a 1.25° gyration angle, and two specimens were compacted at a 2.0° gyration angle from different asphalt mixtures. The slope of percent air voids to number of gyrations in logarithmic scale was calculated. Figure 1-6 shows the relationship between the average slopes calculated from the initial compaction point to the point of 8 percent air voids in the laboratory versus the CI at this percent air voids for all asphalt mixtures included in this project. Mixtures with higher slope in the laboratory needed less CI in the field (less compaction effort). This relationship offers the potential to estimate the required compaction effort in the field (i.e., CI) based on the slope of number of gyrations and percent air voids in the laboratory.
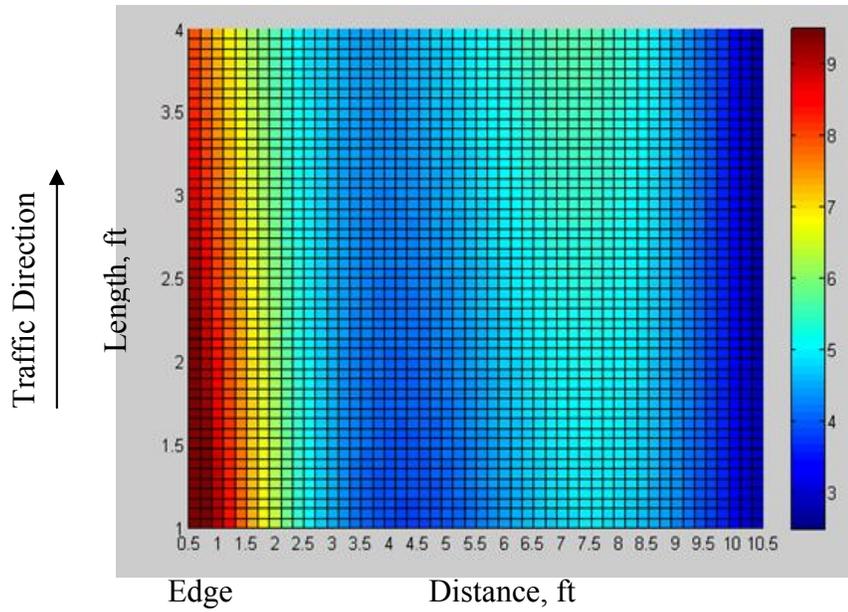
(a)
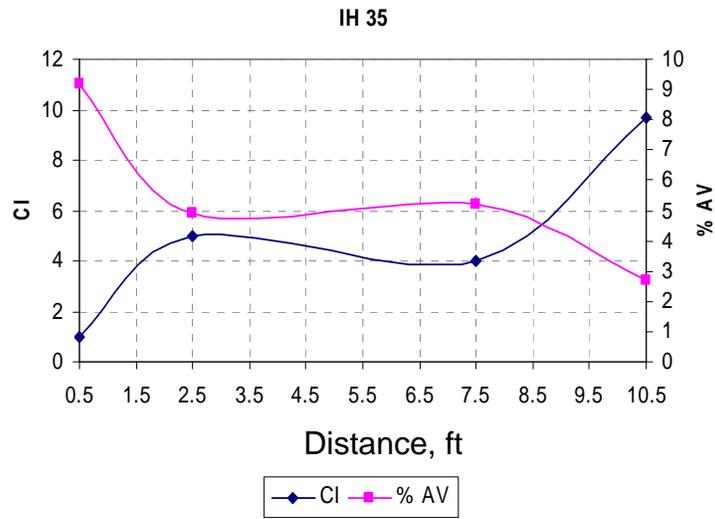
(b)

Note: The total width of the mat is 15 ft (Masad et al. 2009a).

Figure 1-4. (a) Air Void Distribution (%) across the Mat for the IH 35 Job;
(b) the CI and Average Percent of Air Voids across the Mat for the IH 35 Test Section.
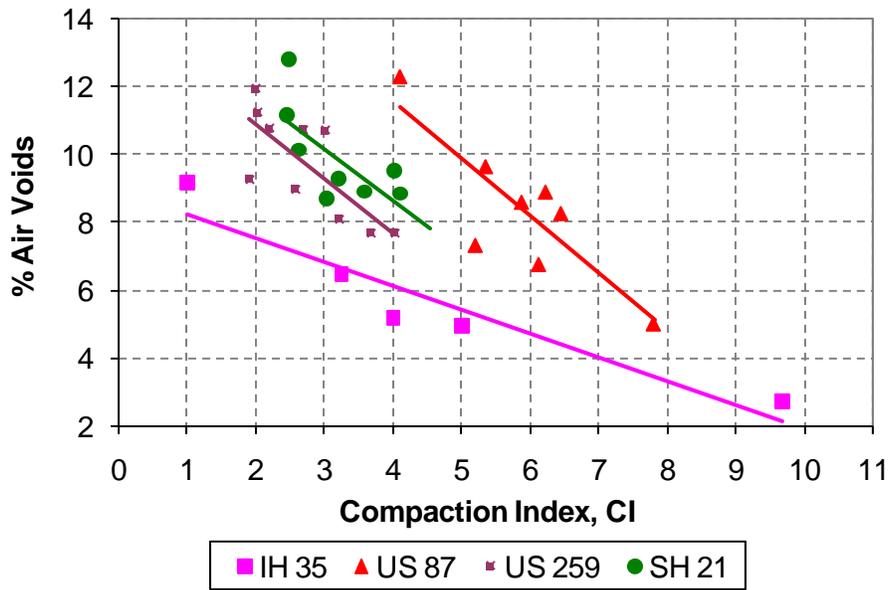
Figure 1-5. CI versus the Percent of Air Voids (Masad et al. 2009b).
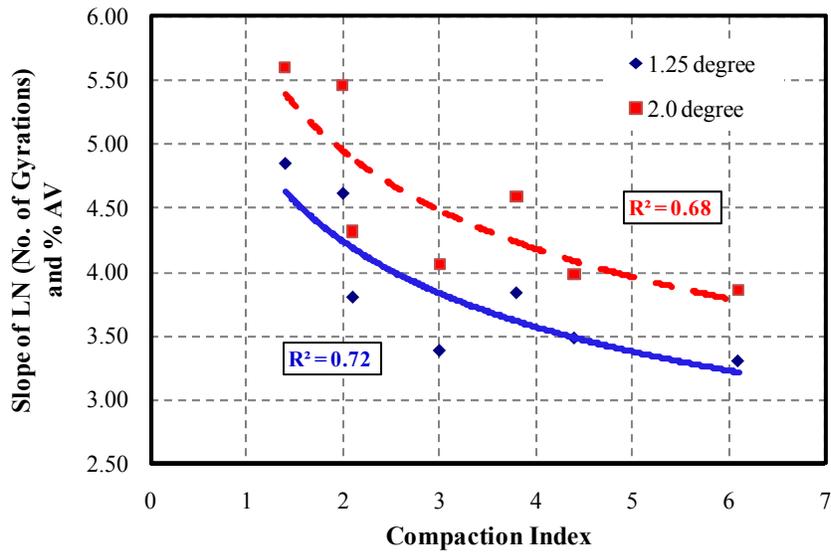
Figure 1-6. Compaction Index versus Slope of Compaction Curve from SGC for Different Mixes (Masad et al. 2009b).

INFLUENCE OF MIXTURE DESIGN ON COMPACTABILITY

The asphalt mixture properties affect the compactability in both the laboratory and field. It is very useful to determine the ability to compact a given asphalt mixture prior to pavement construction. Leiva and West (2008) evaluated the compactability of asphalt mixtures in the field and in the laboratory by measuring mixture characteristics. They examined the following laboratory characteristics and parameters: compaction energy index, number of gyrations, compaction slope, locking point, and Bailey method ratios. The accumulated compaction pressure was also evaluated in the field. That study did not find a simple relationship between field and laboratory compaction for different asphalt mixtures. However, the researchers used a multiple regression analysis to relate field compaction and mixture characteristics.

Muras (2010) conducted a comprehensive study to develop a correlation between asphalt mixture properties and laboratory compaction parameters. In this study, he evaluated 22 different asphalt mixtures. These mixtures included TxDOT's dense-graded mixtures (B, C, and D), stone matrix asphalt (SMA), porous friction course (PFC), and crack attenuating mixtures (CAM). These mixtures had a wide range of gradations, maximum aggregate size, and binder content. For each mixture, a number of parameters or characteristics were measured, which included binder content, binder viscosity, aggregate angularity, aggregate sphericity, aggregate texture, and gradation. He compacted four SGC specimens (6-inch diameter and 2.5 inches in height) from each mixture in the laboratory. He recorded the compaction curves that show the change in the percent air voids with the number of gyrations. The results of this study showed that gradation parameters, binder content, and aggregate angularity significantly influenced the slope of the compaction curves, while gradation parameters, binder content, and aggregate sphericity affected the percent of air voids in the compacted samples after the first gyration. A dense and coarser aggregate gradation, high binder content, and high angularity were found to aid the compaction of the evaluated mixtures in this study. In addition, a dense aggregate gradation, high binder content, high sphericity, and high texture contributed to low percent air voids in the samples after the first gyration.

Stakston et al. (2002) evaluated the effect of the fine aggregate angularity (FAA) on the compaction characteristics of asphalt mixtures in the laboratory. Different asphalt mixture designs—a fine gradation and a coarse-shaped gradation—were evaluated. In addition, the researchers varied the proportions of the manufactured sand to the natural sand from each aggregate source while maintaining the overall gradation in order to vary the FAA values of the fine

aggregates. The laboratory compaction data for SGC specimens were analyzed to estimate the effect of the FAA on compaction of asphalt mixtures to 92 percent of theoretical maximum density (Gmm) and above 92 percent Gmm. The results of this study showed that the effect of the FAA on the densification of the asphalt mixtures is highly dependent on aggregate source. Authors suggested that the mixture design be based on the limits of densification characteristics rather than a target value for the FAA for different mixture types.

TEMPERATURE SEGREGATION DETECTION

Researchers at the Texas Transportation Institute (TTI) developed an infrared temperature monitoring system to detect the temperature segregation in hot mix asphalt and evaluate the uniformity and the overall quality of paving construction (Sebesta et al. 2006; Scullion et al. 2006). This system employs a bar with an array of infrared sensors bar that are mounted onto the rear end of a paver, as Figure 1-7 shows. As the paver moves forward, the sensors measure the surface temperature of uncompacted mixture. Figure 1-8 displays an example of thermal infrared data collected in real time. Based on the collected thermal imaging data in these studies, different thermal distribution categories were observed. These categories included the following:

- Uniform, with little thermal variation (less than 25°F) observed in 95 percent of the measured temperatures.
- Uniform within the truckload, but with a variation in the mean placement temperature between the truckloads.
- Truck-end cold spot, with significant cold spots between the truckloads observed.
- Seemingly random temperature variation, requiring the most corrective action. This type of temperature variation could be due to many factors, which include poor control of the temperature at the plant, truck-end segregation, poor mixing in the material transfer vehicle, and poor temperature control in the heater of the paver.

Sebesta et al. (2006) recommended including this system as a tool to certify the uniformity of paving construction. The contractor should be able to provide the TxDOT engineer with thermal plots to ensure that the mix is placed at uniform temperature. TxDOT then can certify the operation. Also, Sebesta et al. (2006) recommended using the ground-penetrating radar (GPR) as a quality assurance in order to determine if the problem areas in the thermal data became low density spots after rolling.

Figure 1-7. The Infrared System Installed on a Paver (Scullion et al. 2006).
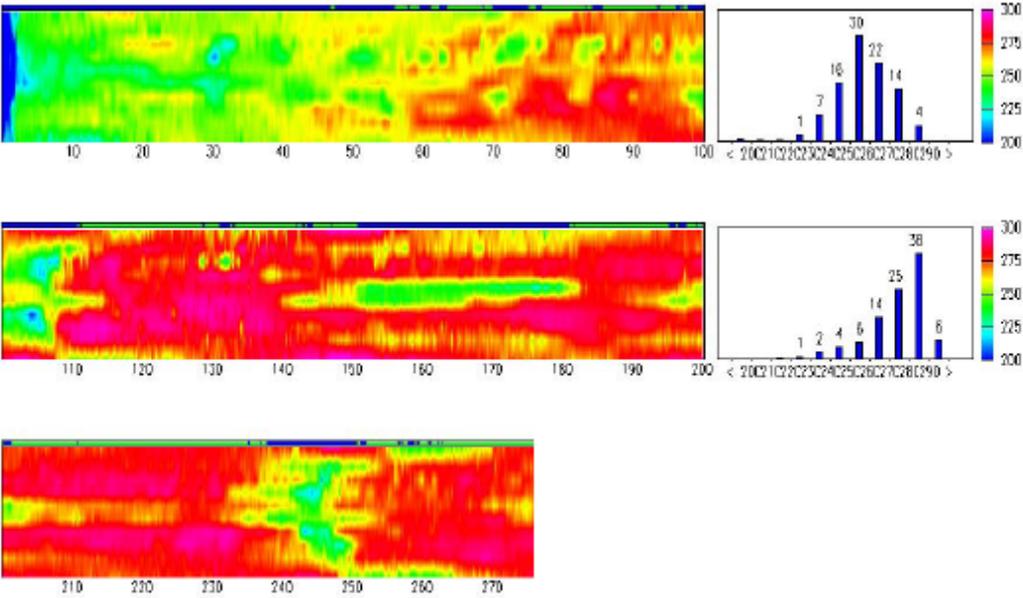
Figure 1-8. Infrared Data Displayed in Real Time (Sebesta et al. 2006).

WARM MIX ASPHALT TECHNOLOGY

Warm mix asphalt (WMA) technology, recently developed in Europe, is gaining strong interest in the United States. By lowering the viscosity of asphalt binder and/or increasing the workability of mixture using minimal heat, WMA technology allows the mixing, transporting, and paving process at a significantly lower temperature. Using this new technology, asphalt mix can be produced as much as 100°F lower than traditional hot mix asphalt. Several benefits of lower mixing and compaction temperature include less emissions, savings in energy cost, longer construction season, less odor, and construction during non-peak periods. In the last few years, dozens of field test sections have been constructed throughout the United States using different WMA technologies. It is too early to report the performance, but so far, no negative performance has been reported in the literature. In the last few years, several large national- and state-level research projects have been initiated to evaluate, validate, and implement this new technology (Chowdhury and Button 2009).

Researchers identified as many as 15 different types of WMA technologies available worldwide. Among them, eight types are commercially available in the United States. Some state departments of transportation are beginning to accept WMA technologies. TxDOT currently includes five different WMA technologies in its list of pre-approved materials. Table 1-1 presents the WMA technologies pre-approved for use on department projects. In the past year, TxDOT has placed more than 600,000 tons of warm mix around the state, which has included all of the processes listed in Table 1-1.

Table 1-1. TxDOT's Pre-Approved List of WMA Technologies.

WMA Technology	Process Type	WMA Supplier
Advera	Foaming Process	PQ Corporation
Double Barrel Green	Foaming Process	Astec Industries Inc.
Evotherm	Chemical Additive	MeadWestvaco Asphalt Innovations
Redi-Set WMX	Chemical Additive	Akzo Nobel Surfactants
Sasobit	Organic Additive	Sasol Wax Americas Inc.

The FHWA conducted a recent study (D'Angelo et al. 2008) to evaluate the various WMA technologies in Europe. The FHWA scan team visited four European countries: Belgium, France, Germany, and Norway. The team reported the benefits of using the WMA technology, which

11

included reduced fuel and emissions, improved field compaction, better working conditions, and ability to haul mixtures for long distances and pave in cooler temperatures. Below are the main findings of this research.

In Norway, the team visited six WMA pavement sections. Two sections were constructed using stone matrix asphalt (SMA), and four sections were dense-graded mixtures. The team observed rutting in the pavements, but it was not related to the WMA technology, as Norway allows the use of studded tires, which cause significant wear to the pavements.

In Germany, the team constructed trial WMA field pavement sections and collected field data during the construction that included mixing temperature, emission data, mix samples, and initial profile. The team constructed these test sections side by side with HMA pavement sections. A total number of seven WMA test sections were constructed between 1998 and 2001. One test section was a dense-graded mixture, and the rest were SMA mixtures. The WMA test sections had the same performance as the control HMA sections and in some cases were even better (Table 1-2). In addition, some suppliers presented to the search team the results of some WMA commercial projects that they carried out. The results showed that the performance of the WMA sections was the same or even better than the performance of the HMA sections. Some of the WMA additives used in Germany have the ability to increase the stiffness of the binder at high temperatures; also, they may affect the properties of the binder at low temperatures.

In France, the researchers conducted laboratory studies and field trials on various WMA projects. The laboratory test results showed that rutting resistance and fatigue testing of the WMA was the same as that of the HMA. The moisture resistance results were slightly lower for the WMA. The workability of the WMA tended to improve in the laboratory. In 2004, the city of Paris constructed six WMA projects in conjunction with HMA. When the team conducted its search on WMA in Europe, these WMA projects were still under evaluation. In the meantime, a private toll road operator evaluated the trial WMA section compared to the performance of the HMA section. The in-place voids for the WMA (7.3 percent) were higher than for the HMA (6.5 percent); however, the modulus of the HMA (10,414 MPa) was slightly lower than the modulus of the WMA (11,376 MPa).

Table 1-2. Evaluation of WMA Sections Compared to Control Sections (D'Angelo et al. 2008).

		SmB 35 B 209 (preblended Sasobit)	50/70 Pen + 4% Sasobit (added at plant) Hamburg	50/70 Pen + Asphaltan B B 193	50/70 Pen + Asphaltan B L 303	50/70 Pen + Aspha-min B3	Sübit VR 45 B283	Sübit VR 35 B 51
	Section Number	**1**	**2**	**3**	**4**	**5**	**6**	**7[3]**
Field Measurements	Rutting[1]	Equal	Equal	Equal	Equal	Equal	Equal	Low
	Post-compaction densification in the wheelpaths	Equal	Better	Equal	Better	Better	Equal	None
	Cracking	Equal[2]	Equal[2]	Equal[2]	Equal[2]	Equal[2]	Equal[2]	
Laboratory Investigations	Thermal stability	Better	Better	Equal	Better	Equal	Better	Very Good
	Low-temperature performance	Equal	Equal or Better	Equal	Equal	Equal or Better	Equal or Better	Good
	Aging of the binder	Equal or Better	Equal or Better	Equal or Better	Equal or Better	Equal	Equal	Low
	Adhesion	Equal or Better	Equal or Better	Better	Equal	Equal or Better	Equal or Better	Good

[1]Low level = <10 mm (0.4 in)
[2]Equal = none
[3]No control section available

Newcomb (2010) pointed out that since certain WMA technologies require a mixing process that is different from conventional HMA, new guidelines need to be developed for proper quality control/quality assurance (QC/QA) of the mix. He further stated that the suitability of WMA for the high production rates of asphalt plants in the United States needs to be examined. Some engineers are concerned that those WMA products that utilize moisture may induce some clogging in bag houses; however, the literature has reported no such problems.

Chowdhury and Button (2009) noted that except for the temperature of the mat, there are generally no differences in construction activities, whether using HMA or WMA, after the product leaves the plant. The experience of the authors has shown that Evotherm can be stored in a silo in a manner similar to HMA. Romier et al. (2004) indicated this is also true for low-energy asphalt (LEA).

When studying WAM-Foam, Koenders et al. (2002) recommended keeping the breakdown roller directly behind the paver; otherwise, the compaction effort required seemed to be considerably increased. This recommendation is likely to maximize the advantages of the lubricating effects of the moisture in the mat before it dissipates. Chowdhury and Button (2009) also mentioned that compaction temperature of a WMA mat is apparently less critical than that of HMA,

but it is still important to complete compaction quickly and efficiently while the mat temperature is within the appropriate window for the specific WMA product.

ON-SITE POSITIONING AND TRACKING TECHNOLOGIES

On-site positioning and tracking technologies can facilitate tracking of construction rollers and provide an automated data collection means for sophisticated, data-driven analytical techniques. In the past, there were some efforts for developing automated methods for monitoring the compaction during the paving construction. These automated methods include the compaction documentation system (CDS), laser, and global positioning system (GPS). The CDS system is an old system that was developed in the mid-1980s in Sweden. This system was utilized to provide a conceptual system for monitoring compaction during construction (Li et al. 1996). In this system, the data include lane change, direction change, number of passes, layer numbers, and start and stop of the compactor. Initially, the operator of the compactor had to follow a fixed route that was decided beforehand due to the unavailability of the automatic sensors that detected the location of the roller in real time. Later, studies began to use new technologies to track the position of the compactors in real time. These technologies include the laser and GPS. The laser positioning system is very accurate but requires many laser targets, which act as receivers (Li et al. 1996). The GPS is relatively less expensive, and its measurements should be accurate enough to be applicable in the pavement project application. Li et al. (1996) reported the accuracy of using GPS on real-time quality control of compaction operations in highway construction by applying differential GPS. Roberts et al. (1999) applied the GPS positioning to aid autonomous control and guidance of construction plants. Their system provided coordinate precision of a few millimeters when a reference receiver was located at a nearby point with well-defined coordinates. The application setting was limited to an open-air road construction site and real-time communication between the reference receiver and the GPS unit on board that the construction plant required for line of sight. Peyret et al. (2000) also evaluated the precision of using the real-time kinematic (RTK) GPS for the elevation control of the screed of an asphalt paver. The researchers found that the drift error due to the multipath effects of GPS signals rendered the raw positioning measurements not accurate enough for supporting the control systems. Oloufa (2002) showed the applicability of using a GPS-based positioning system for monitoring multiple compactors in real time during paving construction.

Lu et al. (2007) demonstrated the drawback of using GPS in highly dense urban areas due to the blockage of satellite signals and the multipath effect, which is due mainly to deflection and distortion of satellite signals by neighboring buildings and temporary structures/facilities on the site. In contrast with the open, outdoor settings of earth-moving and mining operations, the use of GPS for tracking the movement of construction equipment and vehicles on and off building sites situated in a highly dense urban area presents distinctive challenges to the technology itself (Mattos 2003).

NEW TECHNOLOGIES IN FIELD COMPACTION

Recently, intelligent compaction (IC) has drawn attention as a tool to determine the degree of compaction of asphalt mixtures in the field. The concept of IC is to use rollers that can adapt the compactive effort to produce asphalt pavements with the desired stiffness. Maupin (2007) conducted a study to evaluate the correlation between the stiffness measured by a particular IC roller and the density of a thin surface layer of asphalt being compacted. In this study, two types of rollers were used in the field. The first roller was an IC breakdown tandem vibratory roller, BOMAG BW190-4 AM, while the second was a conventional Sakai 800 series tandem vibratory roller. These rollers were used in the pavement construction of two adjacent test sections in Smoketown Road near Dale City, Virginia, as Figure 1-9 shows. The nuclear density gauge was used to record the density in the field after the construction; in addition, field cores were extracted for density and permeability tests. The nuclear density measurements were more than the recovered cores. The author believed that the density measurements for the extracted cores give more consistent results than nuclear density measurements. The researcher applied correction factors to the density measurements recorded by the nuclear gauge based on the density of the recovered cores. The density values were plotted against the roller stiffness measurements for each site, as Figure 1-10 illustrates. Results showed that the correlation between IC stiffness measurements and density of the pavements was very poor. The results also showed that the IC roller was not more efficient than the conventional vibratory roller. The IC roller could not provide more compactive effort when needed. The researcher believed that relatively small thickness of the asphalt layer hindered the IC roller from using its intelligent features of applying more compactive effort when it was needed. This study concluded that the IC was not ready to be used in asphalt construction at the time.

In a recent study, Commuri et al. (2011) developed a neural network-based intelligent asphalt compaction analyzer (IACA) to estimate the level of compaction in the field using a steel vibratory compactor. The researchers reported that density measured using the IACA correlated well with the field cores densities. However, there is still a need for further developments of new methods to better predict density of asphalt pavements in real time during construction.
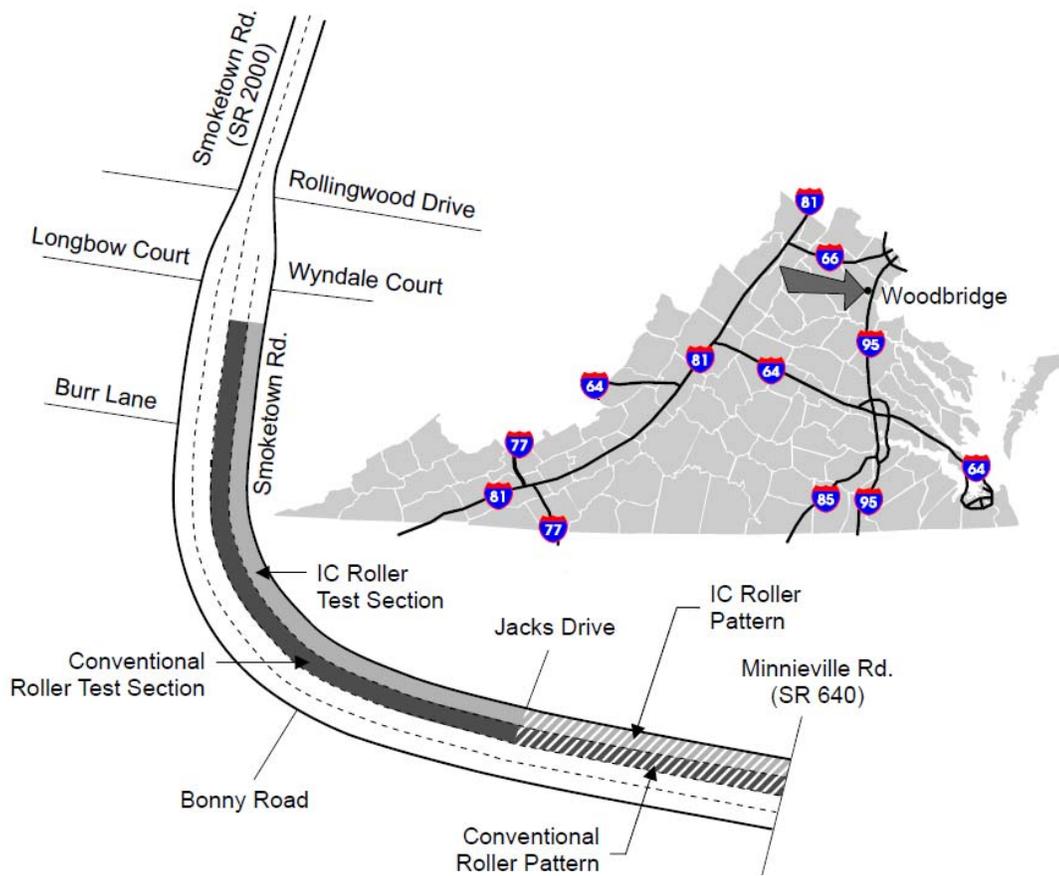
Figure 1-9. Locations of the Test Sections (Maupin 2007).
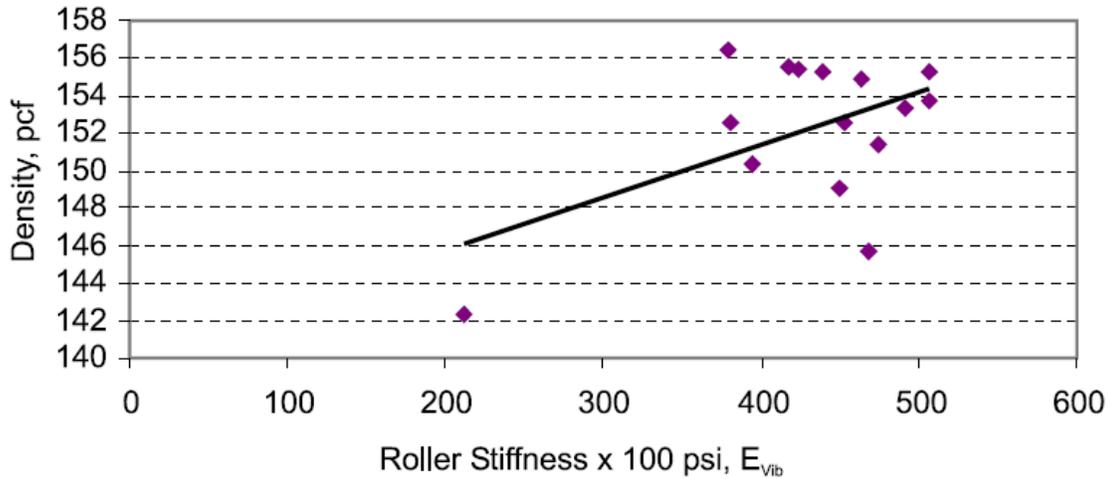
Figure 1-10. Roller Stiffness Measurements vs. Field Density (Maupin 2007).

One of the members of the current research team in TxDOT Project 0-6992 attended a webinar organized by the Asphalt Institute (AI) in March 2010 to collect relevant information on using IC in pavement construction. This webinar provided an overview of the IC and its implementation in pavement construction in the United States. Figure 1-11 shows a couple of instrumented rollers for the intelligent compaction process. The requirements of an IC roller include a roller measurements value (RMV), GPS-based documentation system, on-board color-coded display, surface temperature measurements system, and optional automatic feedback system. The IC rollers are designed to help in achieving the in-place density, which is very important for good performance. The conventional compaction rollers and procedures have many limitations that yield poor results in the field (AI 2010). These limitations include on-the-fly feedback during construction and over- and under-compaction (non-uniform density) paving. Also, the density measurements on extracted cores are conducted after the compaction is completed, which makes it impossible to apply more compactive effort if needed. There is a need for real-time feedback to guide the roller operator during pavement construction. Such a system is very fruitful, as it makes the compaction more effective and efficient. In this webinar, the presenter showed many IC rollers manufactured by different suppliers, including Ammann/Case, Volvo, Dynapac, Bomag-America, Caterpillar®, and Sakai America. The presenter presented some of the findings of applying the IC in pavement construction. The first outcome was improving the rolling pattern by mapping the number of passes during the construction in real time, as Figures 1-12 through 1-14 illustrate. The second finding was mapping the underplaying layer prior to placing the surface asphalt mixture layer. The results of this

17

finding are quite important, as they show that the roller measurement values taken after placing the asphalt mixture layer were influenced by the soft or hard spots within the underplaying layers, as Figure 1-15(a) demonstrates. Also, the good correlation (R-squared = 0.69) between the roller measurement values for the sub-base and the HMA explained clearly that roller measurement values of the HMA were highly influenced by the stiffness of the sub-base (Figure 1-15[b]). This could be due to the thin HMA layer. Figure 1-16 illustrates the correlation between the roller measurement values and the density of extracted cores in one of the projects where the IC roller was utilized. This poor correlation (R-squared = 0.20) questions the applicability of using the IC in HMA pavement construction in terms of measuring stiffness rather than mapping the rolling patterns.

Figure 1-11. Intelligent Compaction Rollers (Asphalt Institute 2010).
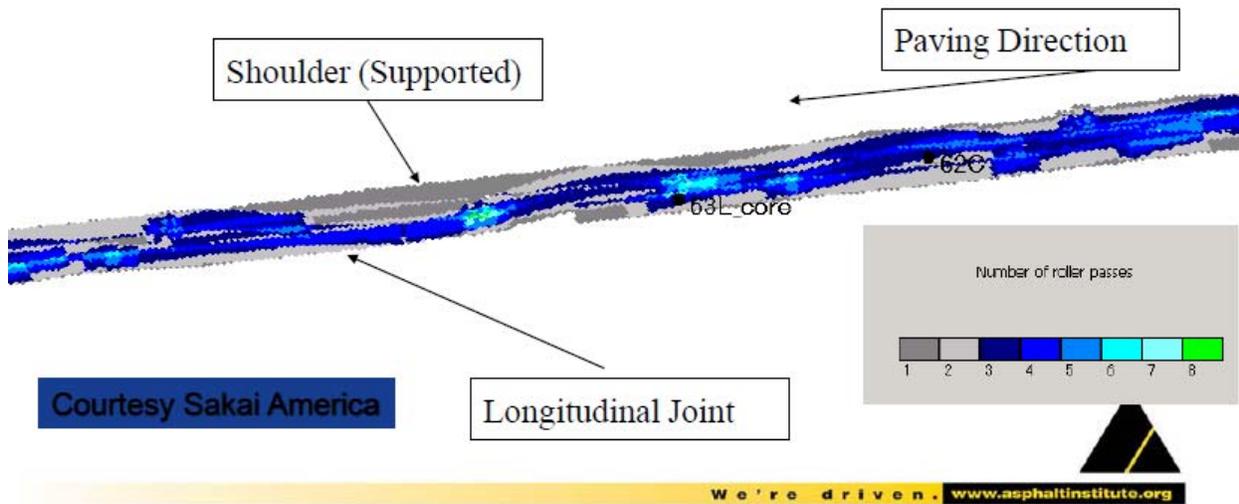
Figure 1-12. Mapping the Compaction Patterns (Asphalt Institute 2010).
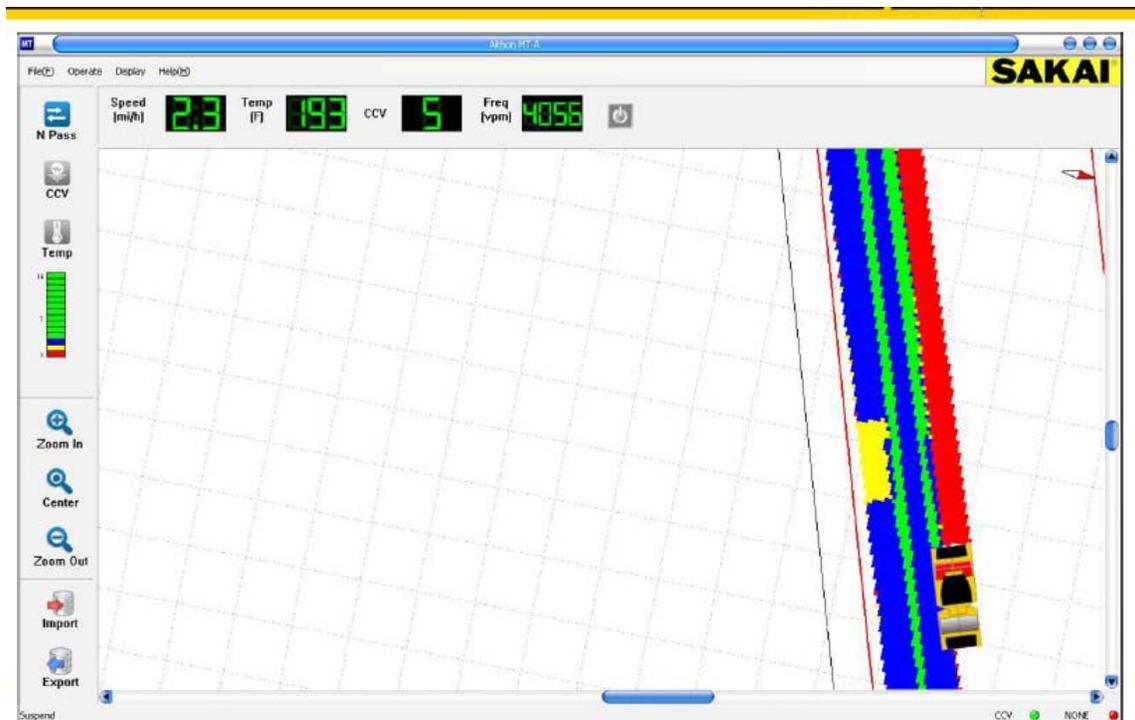
Figure 1-13. Color-Coded On-Board Display (Asphalt Institute 2010).
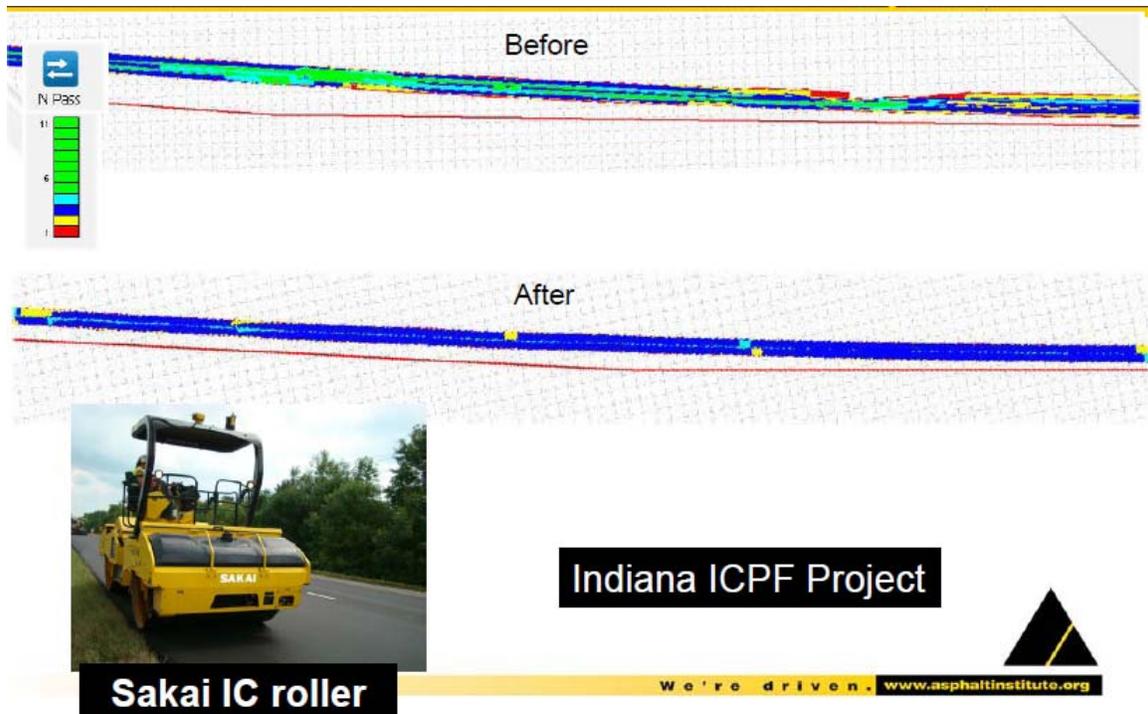
Figure 1-14. Improving Rolling Pattern (Asphalt Institute 2010).
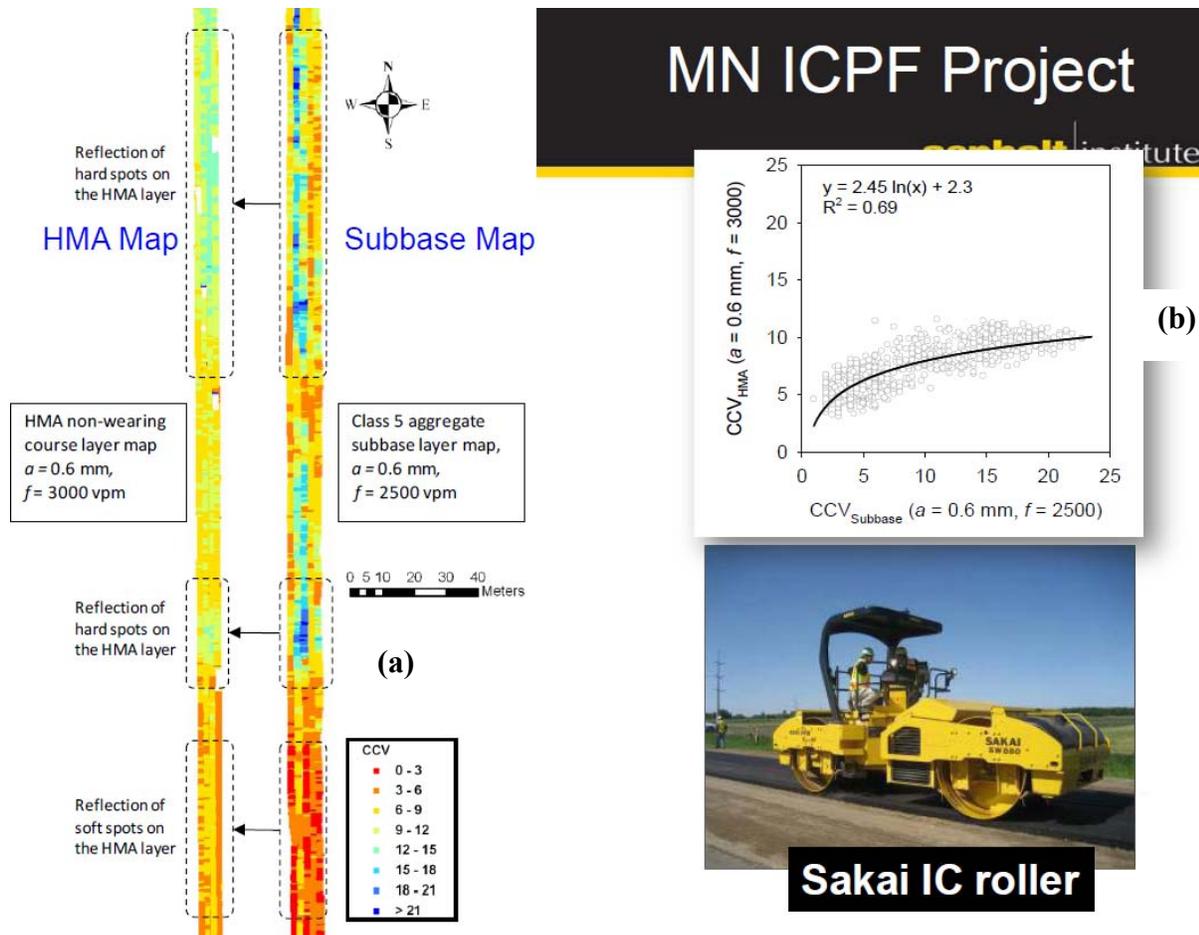
Figure 1-15. (a) Maps of the Roller Measurements before and after Placing the HMA; (b) the Correlation between the Roller Measurement Values before and after Placing the HMA (Asphalt Institute 2010).

21
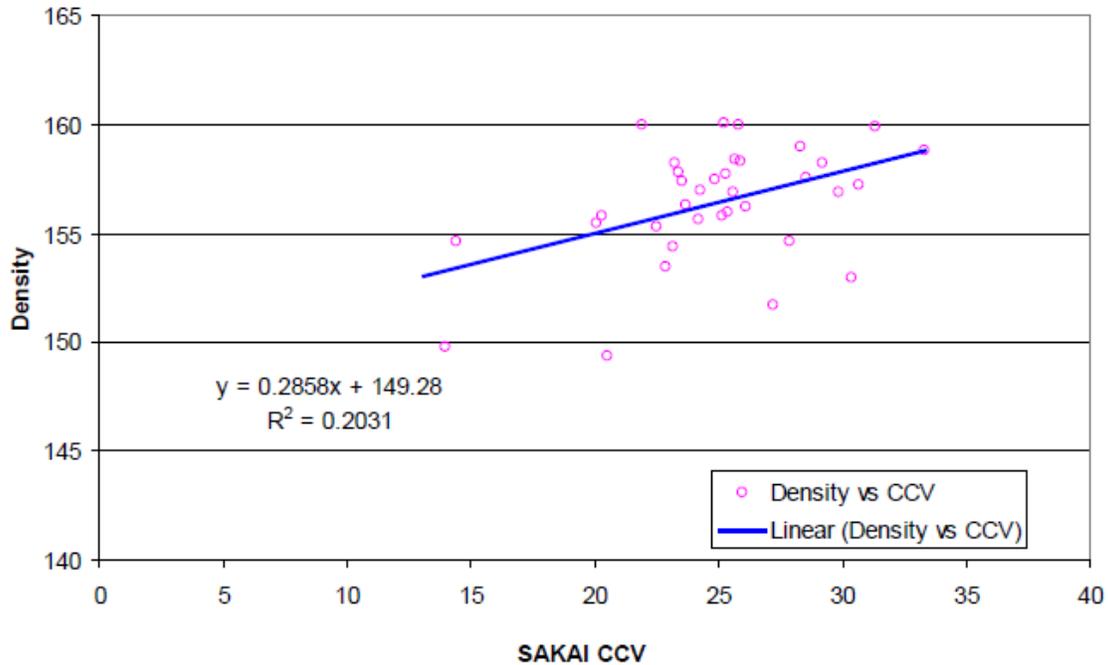
Figure 1-16. Roller Measurement Values vs. Field Density (Asphalt Institute 2010).

MONITORING DENSITY IN THE FIELD

Harris and McNaught (1978) developed a system that gives a direct reading of the maximum resultant peak particle velocity of a vibration. These readings are measured using a velocity-type, triaxial geophone, apparently mounted on the ground.

In 1978, Dynapac introduced the compactometer system to monitor and analyze the signals of the first harmonics of the vibrations. The system continuously reads relative values of the bearing capacity or modulus of elasticity of the materials and reports instantly to the roller operator (Forssblad 1992).

The density on the run (DOR) is the first attempt at continuous density reading measurements. This device can be removed from the roller in minutes and mounted on a two-wheeled cart to measure and optimize density performance of the asphalt paver. Seamon (1988) reported that DOR can be used to take stationary readings and provide moisture data for base course construction. Density on the run can be used to:

- Deal with shortcomings of nuclear and conventional coring specifications in which one test in 1200 lane-ft is often considered adequate agency acceptance.
- Reduce rolling hours and optimize asphaltic concrete paver performance to avoid penalties and solve problem variables of compaction.

22

- Measure density of large areas, furnishing the added data to statistically analyze uniformity of density and its relationship to quality in flexible pavements.

- Offset the shortcomings of stationary nuclear density meters.

- Implement high-speed nuclear testing and pneumatic roller compaction testing and measure the density of thin-lift overlays as small as 0.75 inch in 1-inch increments.

In 1987, Troxler introduced Model 4545, a roller-mounted continuous density gauge similar to DOR. The gauge is mounted on the compactor near the pavement surface with capability to store and download compaction data. Gamma photons emitted by the source radiate into the pavement and are scattered back to detectors located in the gauge. Density is continually measured in sections with the average being automatically updated (James Informational Media 1987).

Investigators from Japan developed a method that uses the behavior of an exciter that vibrates on the ground and relates it to the ground stiffness (Tateyama et al. 1995). They reported satisfactory results with the method except for when measuring the base layer under the ground.

Saarenketo (1997) presented a study on using ground-penetrating radar and capacitance-based dielectric surface probe measurements to measure the fluctuations in voids, bitumen content, or both in newly compacted asphalt pavement. Both methods rely on the compaction of asphalt to reduce the proportion of air, low dielectric, in the material, which increases the volumetric proportions of higher dielectric bitumen and rock and thus results in an increase in the measured mat dielectric value. GPR has the additional advantage that readings can be taken at short intervals: for example, 1 foot intervals.

Geodynamik developed a system based on the continuous measurement of the most important compaction parameter in hot-mix construction process, i.e., the mat temperature. Geodynamik has long had a compactor-mounted compaction meter that is designed for embankments and other soil layers (Thurner 1998).

Jaselskis et al. (2001) presented another approach to monitor asphalt density. The study described the use of two antennas to measure differential microwave signals to indicate when optimal compaction is achieved. A roller-mountable real-time asphalt pavement density sensor was used.

At the University of Wisconsin-Madison, a path planning system for asphalt compaction operations, called AUTOPAVE, was developed to estimate the number of passes to be made by the roller and generate a motion path that ensures coverage of the entire pavement area and controls the

overlap regions between subsequent passes. Instrumented with an on-board guidance system using GPS and compass orientation, the path planning system provides a semi-automated hybrid to track the paver and roller path and perform real-time processing of the motion information (Veeramani et al. 1998; Krishnamurthy et al. 1998). This system operates together with another system called the instantaneous motion planning and controlling tool (IMPACT). IMPACT uses RTK-GPS for multiple construction equipment. The system measures the location of equipment, as well as static obstacles, to plan the shortest collision-free paths for equipment to increase productivity and safety (Tserng and Russell 1997). Figure 1-17 provides a description of the system.
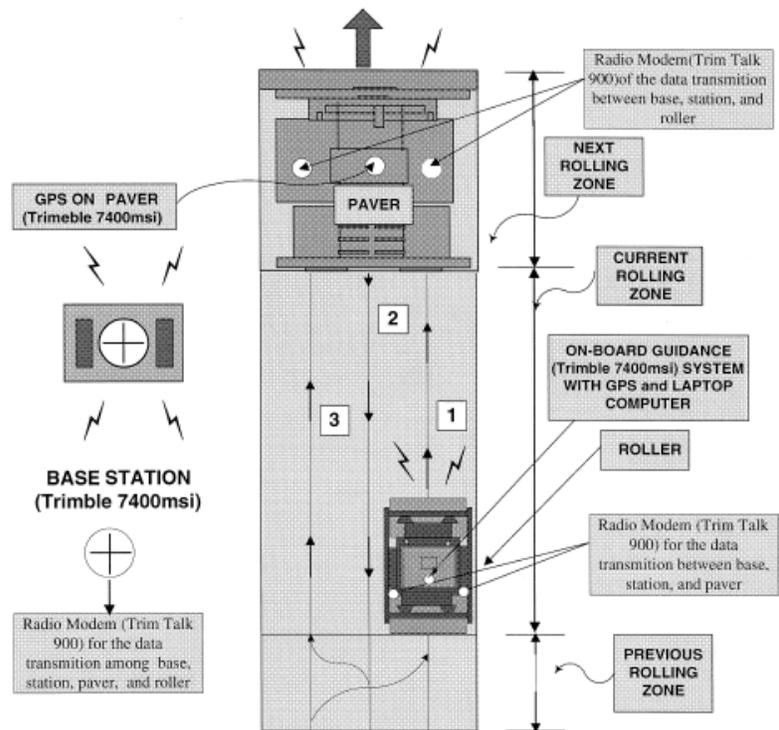
Figure 1-17. Top View of Semi-Automated System (Krishnamurthy et al. 1998).

Rinehart and Mooney (2008) described the development of a comprehensive instrumentation system to monitor the vibration of a roller compactor. Their paper discussed the selection and placement of accelerometers to capture the three-dimensional response of critical roller components and the measurement of the rotating eccentric mass position within the drum to reproduce the input force time history. Instrumentation was placed at the drum, and frame vibration was monitored in three dimensions using accelerometers. Figure 1-18 shows the position of the rotating eccentric mass, which monitors using sensors connected through a data acquisition system.

The location of the rotating eccentric mass inside the drum enables the determination of the forcing function that the roller compactor inputs to the soil and pavement layers, as well as the phase lag of drum displacement with respect to eccentric force, both of which are important to determine compactor-soil system parameters. The installed sensors also enable the position of the eccentric mass to be monitored. The measurement of eccentric position and the determination of phase lag were found to be very important in properly characterizing the contact force between the drum and the soil and in understanding fundamental roller and soil responses.

Figure 1-18. Schematic of the Front Drum and Frame Showing Axis Orientation, Six Degree-of-Freedom Motion, and Sensor Locations (Rinehart and Mooney 2008).

Recently, commercial IC systems have been developed to facilitate and track highway construction and compaction processes. For instance, Amman-America Inc. and Bomag-America Inc. have taken the lead in the development of a commercially feasible intelligent compaction system. Amman has developed rollers that continuously and automatically change roller parameters based on measured materials' stiffness and inputted stiffness criteria. This system, called the Amman Compaction Expert (ACE), stores data in the continuous compaction control (CCC) computerized system and offers GPS technology as an option. Following are descriptions of the five most widely used commercially available IC systems.

Caterpillar® Compaction System

Caterpillar has developed three measuring systems to monitor compaction of soil and pavements, machine drive power (MDP) measurements, compaction meter value (CMV), and Caterpillar compaction value (CCV), which is the commercial version of CMV.

The CMV technology uses accelerometers installed on the vibratory drum to measure accelerations during compaction operations. It is defined as:

$$CMV = C * \frac{A_1}{A_0}$$ (1)

where C is a constant equal to 300 to give a full-scale reading of about 100, and A_1 and A_0 are the amplitudes of the first harmonic and the fundamental frequency. White et al. (2005) correlated the ratio of the amplitudes to conventional in-situ field compaction measurements for several soils.

The use of MDP determines the stresses acting on the drum and the energy necessary to overcome the resistance to motion to relate the soil properties controlling drum sinkage (Komandi 1999; Muro and O'Brien 2004). White et al. (2005) documented using MDP for describing soil compaction, where higher power indicates soft or weak material and lower power indicates compact or stiff material.

CCV follows the same theoretical background of CMV with the integration of a GPS system and an on-board compaction monitor that displays the real-time roller location, vibration amplitude and frequency, and roller speed. The technology enables a roller operator to make judgments regarding the condition of the compacted material.

In field evaluation testing, soil properties (e.g., dry unit weight, moisture content, strength, and modulus) of the clean sand material were determined using in-situ testing devices and compared to the above system outputs. White et al. (2007) documented that intelligent compaction technology may not accurately indicate compaction for unbound granular materials that do not compact at the surface. Clean sands often lack sufficient confining pressure and base friction to achieve high density immediately under the roller. Also, they found no correlation between CMV measurements and MDP for loose layers.

The White et al. (2005) study also implied that based on CCV data, little compaction occurred after the initial roller pass. The CCV was an effective tool in indicating uniformity of compacted materials. However, poor correlation with in-situ test results was noticed because insufficient variation was observed in the smaller compacted areas.

Ammann Compaction System

The Ammann system calculates kB—soil stiffness—as a measure of stability and the level of compaction achieved with the roller. The roller-measured stiffness is reportedly independent of machine-related parameters such as the frequency and rotating eccentric shaft mass (Anderegg 2000). The Ammann system combines soil stiffness measurement with automatic feedback control of both amplitude and frequency parameters based on existing materials characteristics.

Using six test strips compacted with the Ammann vibratory smooth-drum roller and tested using a lightweight deflectometer, dynamic cone penetrometer, Clegg impact hammer, and static plate load tests, the researchers found strong relationships between kB and in-situ test results for strips with a relatively wide range of stiffness. However, comparatively weak relationships for strips with more uniform conditions were found. The roller-measured stiffness measurements were also useful to identify sections with weak compaction that showed rutting by test roller (White et al. 2007).

Sakai Compaction System

The basis of the Sakai IC system is the IC roller (equipped with CCV measurement system, temperature sensors, and GPS radio/receiver) and a GPS with radio base station. All measurements are consolidated to the CIS display. IC data can then be transferred to personal computers (PCs) via universal serial bus (USB) ports for further reporting/documenting and integrating with computer-aided design (CAD) systems (FHWA 2009).

The Sakai CCV is a unit-less, vibratory-based technology that makes use of an accelerometer mounted to the roller drum to create a record of machine-ground interaction. Its value represents the stiffness of the compacted pavement layers underneath. The concept behind the CCV is that as the ground stiffness increases, the roller drum starts to enter into a "jumping" motion, which results in vibration accelerations at various frequency components. The current Sakai IC system does not yet consist of auto-feedback.

Dynapac Compaction System

The Dynapac compaction system DCA system measures CMV as an indicator of compaction quality. The CMV technology uses accelerometers to measure drum accelerations in response to soil behavior during compaction operations. The ratio between the amplitude of the first

harmonic and the amplitude of the fundamental frequency provides an indication of the soil compaction level. An increase in CMV value indicates increasing compaction.

CMV is a dimensionless parameter that depends on roller dimensions (i.e., drum diameter, weight) and roller operation parameters (i.e., frequency, amplitude, and speed). The machine used on this project reported a measurement value approximately every 0.5 m at the drum center along the direction of travel. The machine also reported a bouncing value (BV), which provides an indication of the drum behavior (e.g., continuous contact, partial uplift, double jump, rocking motion, and chaotic motion).

Roller Integrated Measuring and Documentation Systems (Bomag)

Bomag developed a wide range of smooth-drum vibratory intelligent rollers for granular base and asphalt pavement compaction. Similar to the Amman system, the Bomag system, called the VARIOMATIC, is capable of reading the stiffness of the lift being compacted and also can change the roller parameters based on measured material stiffness and inputted stiffness criteria (Minchin et al. 2003).

The Bomag E_{VIB} meter BEM provides the first step to reducing the cost of soil compaction. The E_{VIB} meter enables the determination of a measuring magnitude directly related with the deformation modulus E_V of the soil and the interrelationship between force and immersion of the roller into the ground. The measuring value is called vibration modulus E_{VIB}.

Bomag has developed a system called the Terrameter BTM, which consists of a recorder unit with two acceleration sensors, an electronic unit, a travel sensor, an operating and display unit, and a printer. The Terrameter display continuously shows the E_{VIB} value, working speed, frequency, and amplitude. The paper strip documents the recorded E_{VIB} value as a continuous line record and documents the operating parameters of the compaction equipment. Weak points and areas with a low bearing capacity can be precisely localized along the measuring route.

The BCM 05 software creates detailed data summaries with calculations of areas and static examination of the E_{VIB} values for assessing compaction quality both on the BCM display for the roller driver and in the site office for the data evaluator (Figure 1-19). During the compaction process, any measured data are displayed graphically and numerically to the roller driver on a color display and are analyzed, managed, and documented on a PC. The M3 method works as a spot-check test of the working procedure. The compaction status is displayed to the roller driver during the

compaction process using the documentation system. Altogether, this leads to uniform, quality-assured, and cost-optimized compaction. In addition, the quality control tests demanded by the contractor can be carried out in a targeted way using the documentation functions of the BCM 05 system.

Figure 1-19. Components of the Bomag IC Software (Kloubert et al. 2007).

CHAPTER 2
COMPREHENSIVE EVALUATION OF COMPACTION OF ASPHALT PAVEMENTS AND A PRACTICAL APPROACH FOR DENSITY PREDICTIONS*

The degree of compaction has a significant influence on the performance of asphalt pavements. Providing all desirable mixture design characteristics without adequate compaction could lead to premature permanent deformation, excessive aging, and moisture damage. These distresses reduce the useful life of asphalt pavements. In practice, the compaction pattern to achieve the desired density in a certain project is established based on experience and trial and error. This is a time-consuming and expensive process. Consequently, there is a need for developing a systematic method to quantify the compactive effort and predict the density of the mat in real time during asphalt pavement compaction. Such a method should be developed based on a clear understanding of the factors that affect the compactability of asphalt mixtures.

OBJECTIVES

The objectives of this part of the study were as follows:
- Study the effect of the following factors on mixture compactability:
  - Compaction methods (vibratory steel roller, static steel roller, pneumatic tire roller).
  - Mixture type (coarse versus fine, or HMA versus WMA).
  - Support condition (flexible base versus rigid concrete base).
  - Asphalt pavement temperature.
- Verify the concept of the compaction index developed by Kassem et al. (2008) as a tool to control uniformity of asphalt pavement compaction.
- Study the effect of joint conditions (restricted versus unrestricted) on the density of the longitudinal joints.
- Propose a method for predicting the density of asphalt pavements in the field.

_____

RESEARCH TASKS

Researchers carried out the following tasks in order to achieve the objectives:

1. Construct a number of field test sections using different asphalt mixtures and compaction methods.
2. Monitor and record different construction parameters, including the roller movement.
3. Extract field cores from different locations across the mat.
4. Measure percent air voids in the recovered cores and develop maps of air void distribution in the test sections.
5. Analyze the relationship between compaction method, mixture type, mixture design, compaction temperature, base support, and joint condition on the compactability of asphalt mixtures.
6. Use the data to develop a method for predicting density of asphalt pavements.

DESCRIPTION OF THE TEST SECTIONS

The research team constructed five test sections at the Riverside Campus of Texas A&M University using different asphalt mixtures. Test Sections No. 1 and 4 were HMA constructed using Type C mix with PG 76-22 binder, Test Sections No. 2 and 5 were HMA constructed using Type D mix with PG 64-22 binder, and Test Section No. 3 was WMA Type D mix with PG 64-22 binder. Table 2-1 describes the properties of different mixtures used in these test sections. Both Type C and Type D are dense-graded mixtures commonly used by the Texas Department of Transportation. Type C has coarser gradation than Type D (TxDOT 2004). They are comparable to 0.5 inch (12.5 mm) and 0.375 inch (9.5 mm) Superpave mixture, respectively. The appendix provides the mixture designs of these mixtures.

Table 2-1. Properties of Mixtures Used in the Test Sections.

Section No.	Mix Type	NMAS[1], inch	Binder Type	Aggregate Type	Binder Content	Comment
1	Type C	0.5	PG 76-22	Limestone	4.8	1% lime
2	Type D	0.375	PG 64-22	Limestone	5.2	1% lime & 20% RAP[2]
3	Type D with WMA	0.375	PG 64-22	Limestone	5.2	1% lime & 20% RAP
4	Type C	0.5	PG 76-22	Limestone	4.8	1% lime
5	Type D	0.375	PG 64-22	Limestone	5.2	1% lime & 20% RAP

[1]Nominal Maximum Aggregate Size
[2]Recycled Asphalt Pavement

Test sections 1, 2, and 3 were constructed on a rigid base site (Location 1) located on Runway 35C, as shown in Figure 2-1(a) and (b) (Location 1). Test sections 4 and 5 were constructed on a flexible base site (Location 2) located on the southern taxiway, as shown in Figure 2-1(a) and (c).

Figure 2-1. (a) The Location of the Test Sections at the Riverside Campus; (b) Rigid Pavement Site; (c) Flexible Pavement Site.

The research team conducted GPR and falling weight deflectometer (FWD) testing at both the rigid and flexible sites before the construction and GPR testing after the construction. Figure 2-2 and Figure 2-3 show the GPR data before the construction for the rigid pavement and the flexible pavement sites, respectively. The dimensions of the concrete slabs in the rigid base side were 12-ft wide and 20-ft long. The GPR results showed that a uniform support condition was provided, and the FWD data showed the load transfer efficiency (LTE) was around 95 percent, as Figure 2-4

34

illustrates. The flexible site had uniform layer thickness, 3 inches of HMA above 14 inches of flexible base on a sandy subgrade. Figure 2-5 presents the FWD deflections for the flexible site.
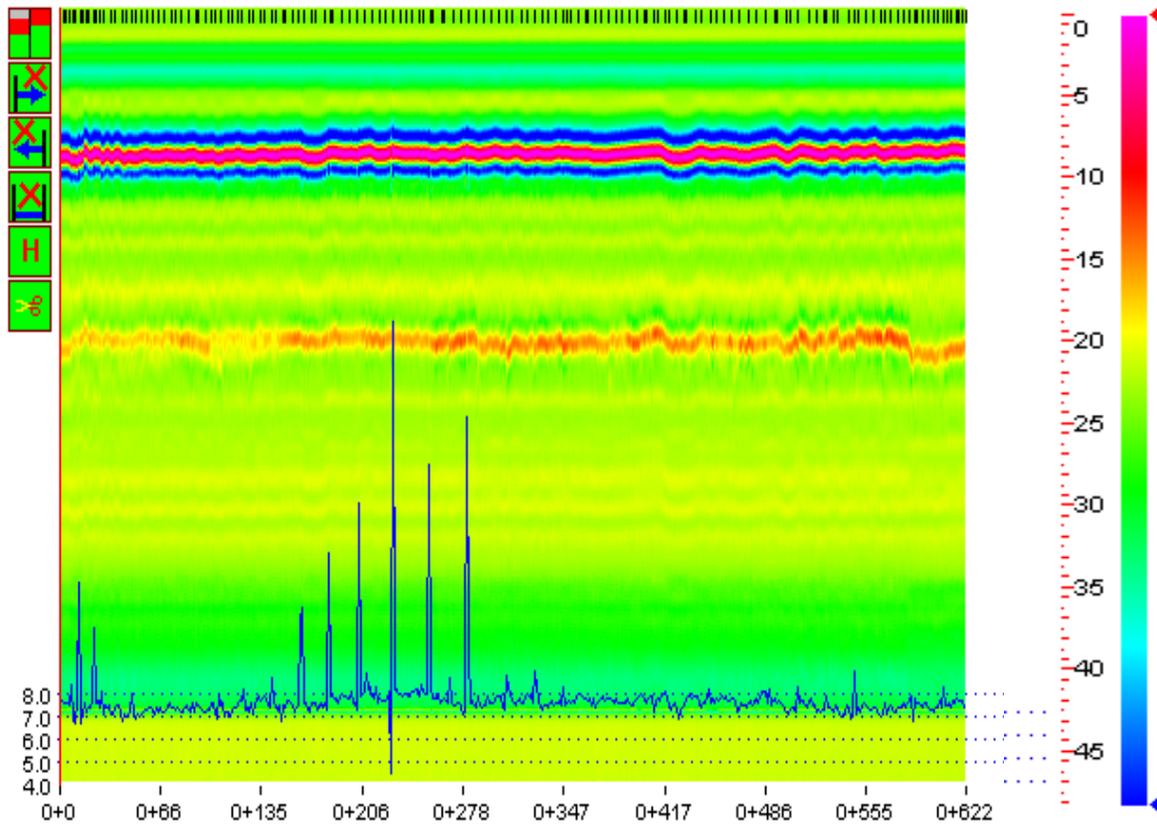
Figure 2-2. GPR Results for the Rigid Base Site.
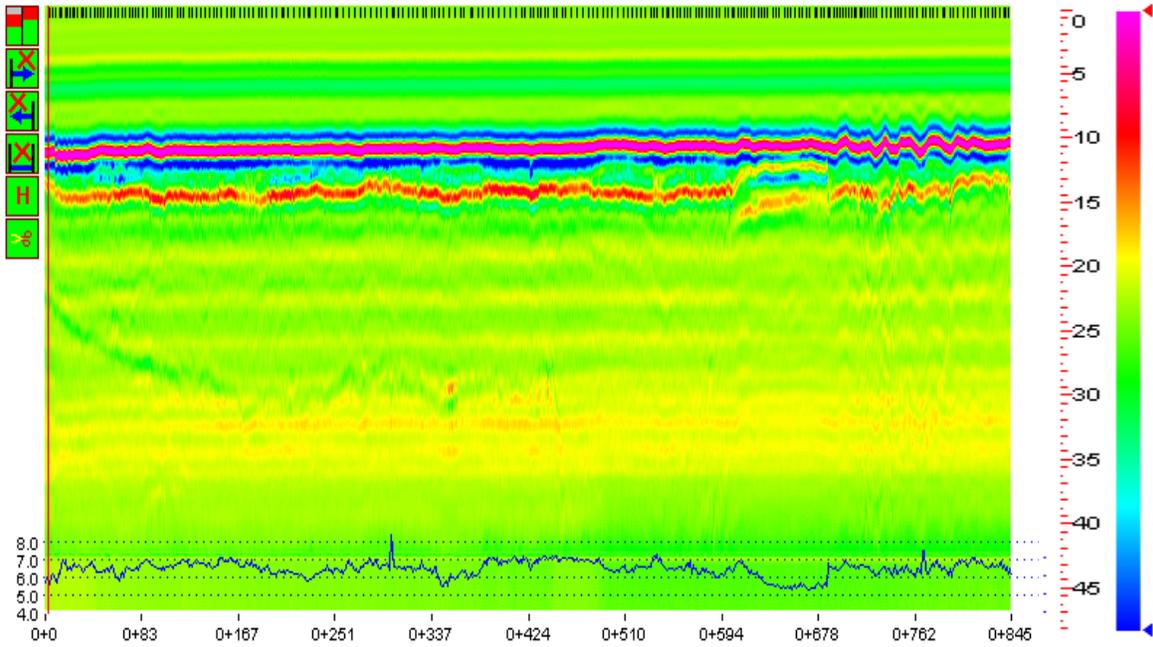
Figure 2-3. GPR Results for the Flexible Base Site.
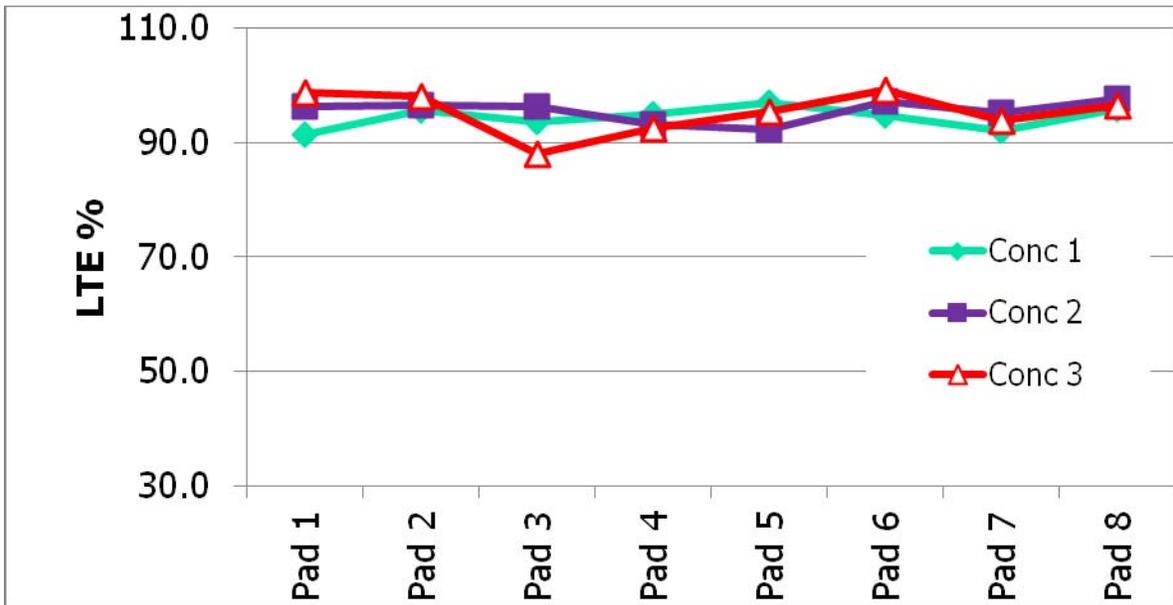
Figure 2-4. Load Transfer Efficiency for the Rigid Base Site.
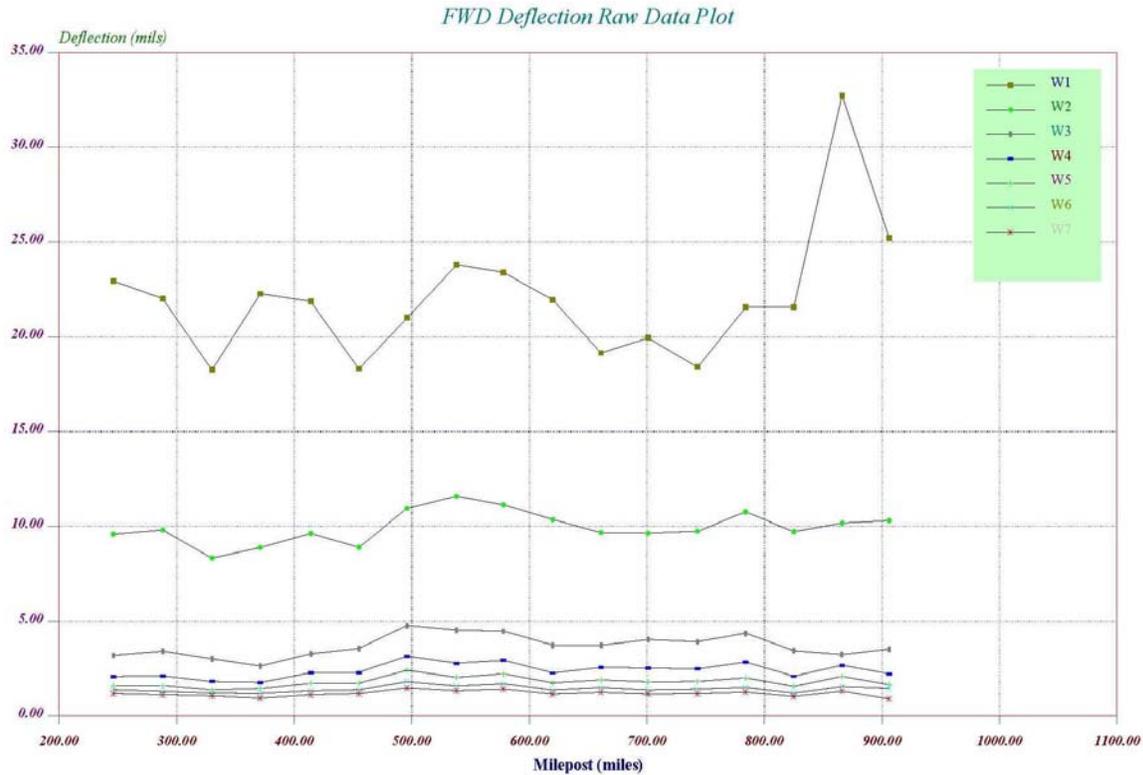
Figure 2-5. FWD Deflections for the Flexible Base Site.

Each test section was 9-ft wide and 700-ft long, and lift thickness was about 2 inches. Figures 2-6 through 2-10 present the schematic layouts and the rolling patterns for each test section. Each test section was divided into sub-test sections that were compacted using different compaction methods. Each sub-test section was then divided into several smaller strips (approximately 30-ft long) that were compacted using a varying number of roller passes. Researchers used different compaction rollers—static steel roller, vibratory steel roller, and pneumatic tire roller— to construct these test sections. Three of these test sections (sections 1, 2, and 3) were constructed over a jointed rigid (concrete) base, and sections 4 and 5 were constructed over a flexible base. Different joint conditions—free edge, restricted, and semi-restricted—were considered in the test sections to evaluate the effect of the joint conditions on the density of the longitudinal joints. A free longitudinal joint refers to one that is not confined by any material to the side during compaction. A restricted joint refers to one that is compacted against an existing asphalt layer, which provides confinement to the compacted mix. The semi-restricted joint is one that is compacted against a newly placed loose asphalt mixture.

37

As Figures 2-6 through 2-10 illustrate, each of these five test sections was divided into a number of sub-test sections as follows:

- Sub-test section 1 was compacted at a temperature of 180°F, which is lower than the designed one for each mix. This sub-test section was compacted using a vibratory steel roller.

- Sub-test section 2 was compacted using a static steel roller.

- Sub-test section 3 was compacted using a vibratory steel roller.

- Sub-test section 4 was compacted using both vibratory and static steel rollers.

- Sub-test section 5 was compacted using a vibratory steel roller for breakdown, and then a pneumatic tire roller was used to conduct the compaction. Earlier attempts to compact this test sub-section with only a pneumatic tire roller did not work, as the rubber tire was picking loose the mix.

FIELD CORE EXTRACTION

Researchers extracted field cores from different locations across the mat from each strip. As Figure 2-11 displays, two rows of cores (seven cores in each row) were taken from each strip that was subjected to a different number of passes. The field cores were exacted for saturated surface dry (SSD) density, vacuum sealed density, and performance testing. Figure 2-11 shows a typical coring layout. About 1200 field cores were extracted from the constructed test sections—240 cores from each test section. In addition to the laboratory density measurements, field density was measured using nuclear and non-nuclear density gauges on the same locations where the cores were extracted.

AIR VOID DISTRIBUTION IN ASPHALT PAVEMENT SECTIONS

Researchers developed maps for the air void distribution across the width of the mat for all the test sections, as Figures 2-6 through 2-10 demonstrate. These maps of air void distribution were generated by inputting the location of each core and its percent air voids into the Matlab 7.1® software (Matlab 2004). Then, an interpolation algorithm in Matlab was used to predict and plot a color map of percent air voids in a whole strip.
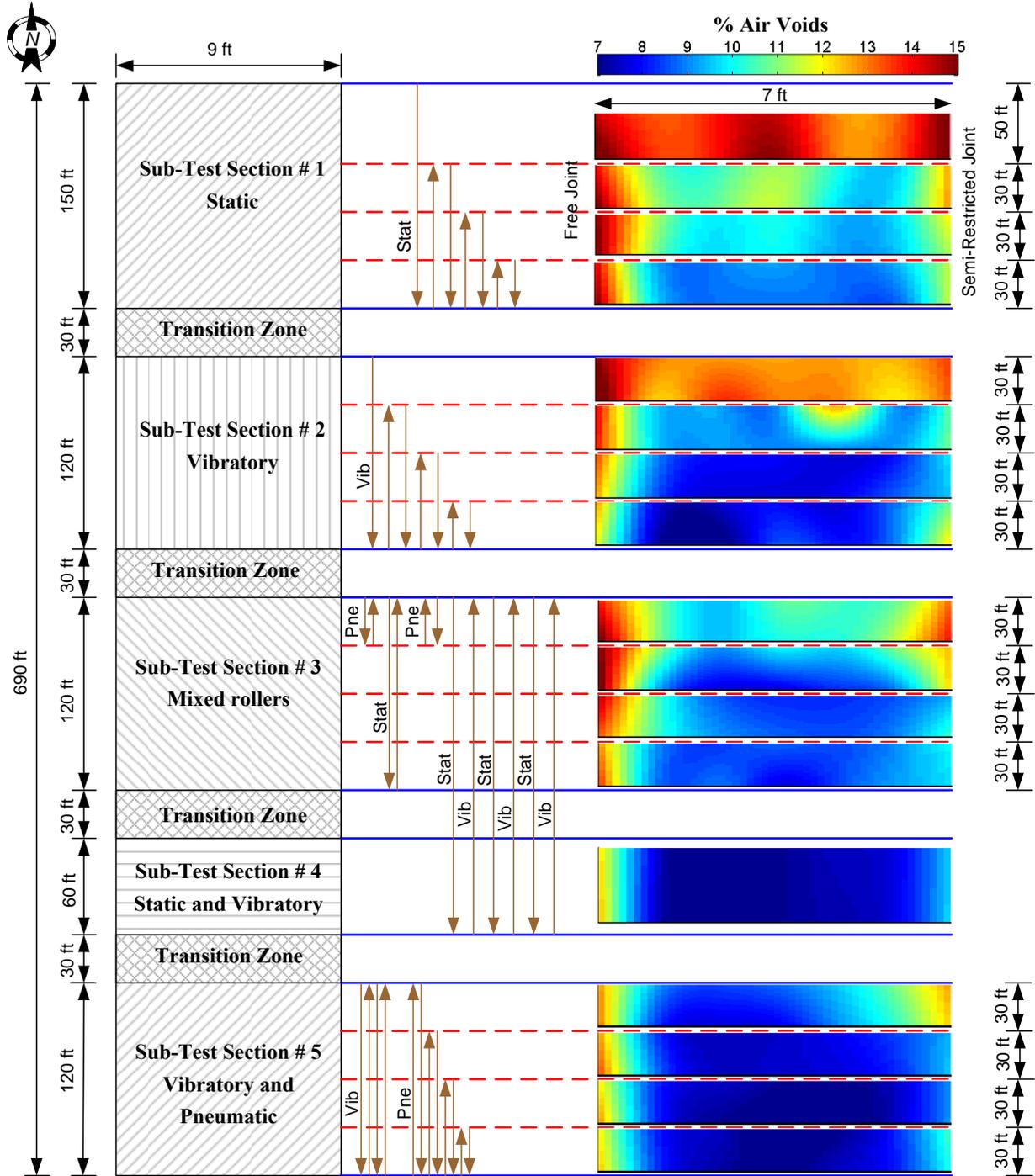
Figure 2-6. Test Section # 1, Schematic of Sub-Test Sections and Rolling Patterns, and Maps of Air Void Distribution.
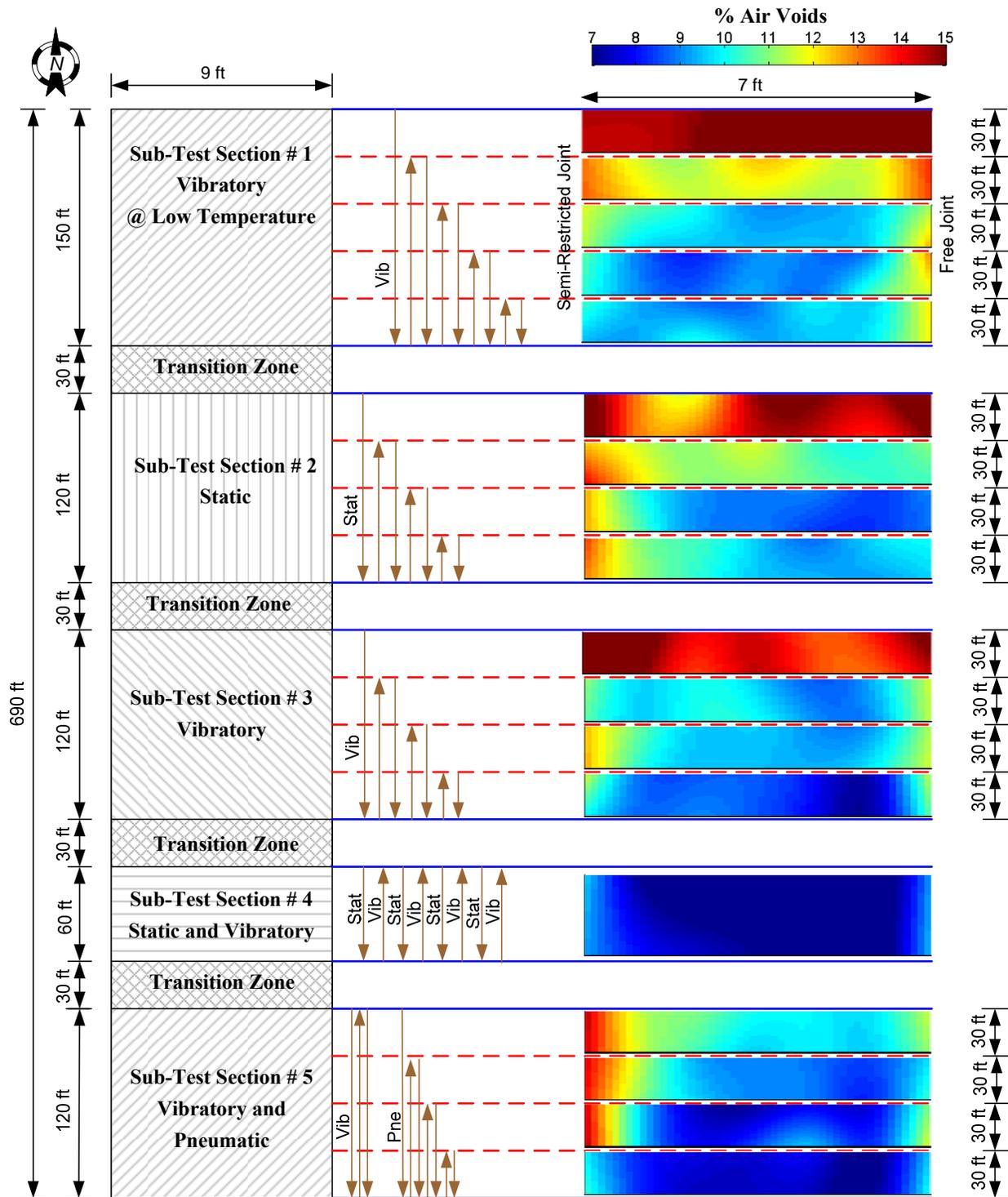
Figure 2-7. Test Section # 2, Schematic of Sub-Test Sections and Rolling Patterns, and Maps of Air Void Distribution.
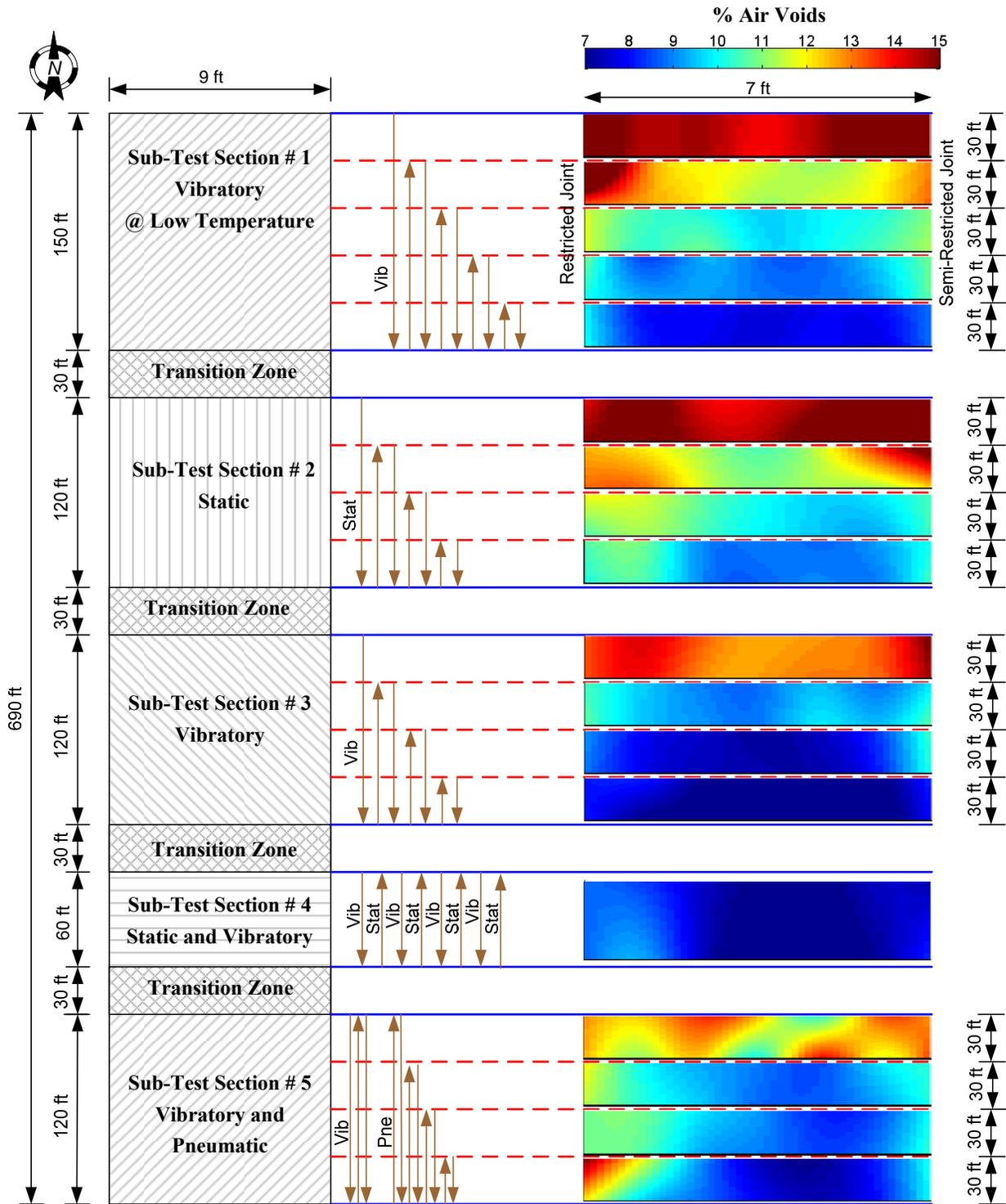
Figure 2-8. Test Section # 3, Schematic of Sub-Test Sections and Rolling Patterns, and Maps of Air Void Distribution.

41
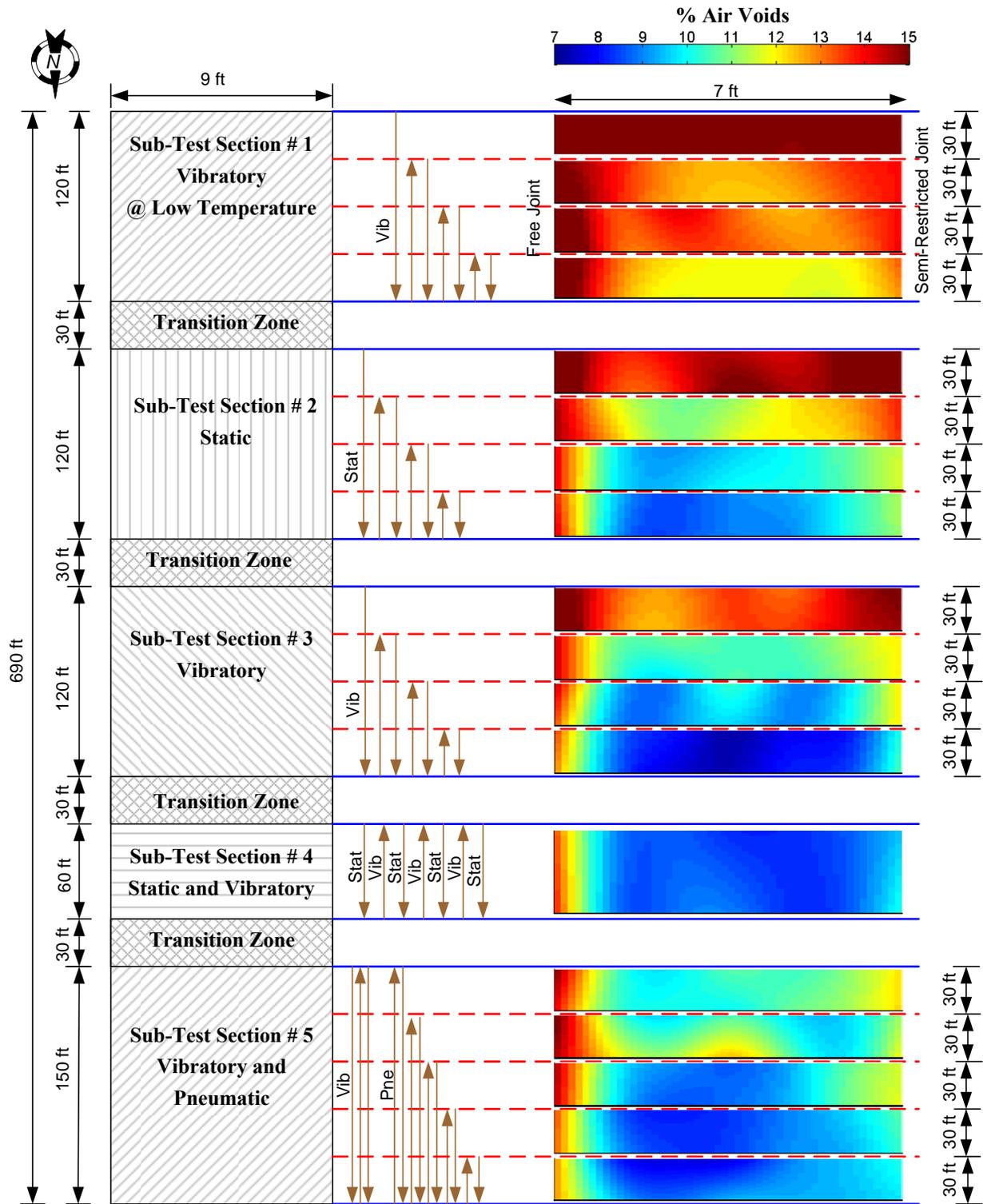
Figure 2-9. Test Section # 4, Schematic of Sub-Test Sections and Rolling Patterns, and Maps of Air Void Distribution.
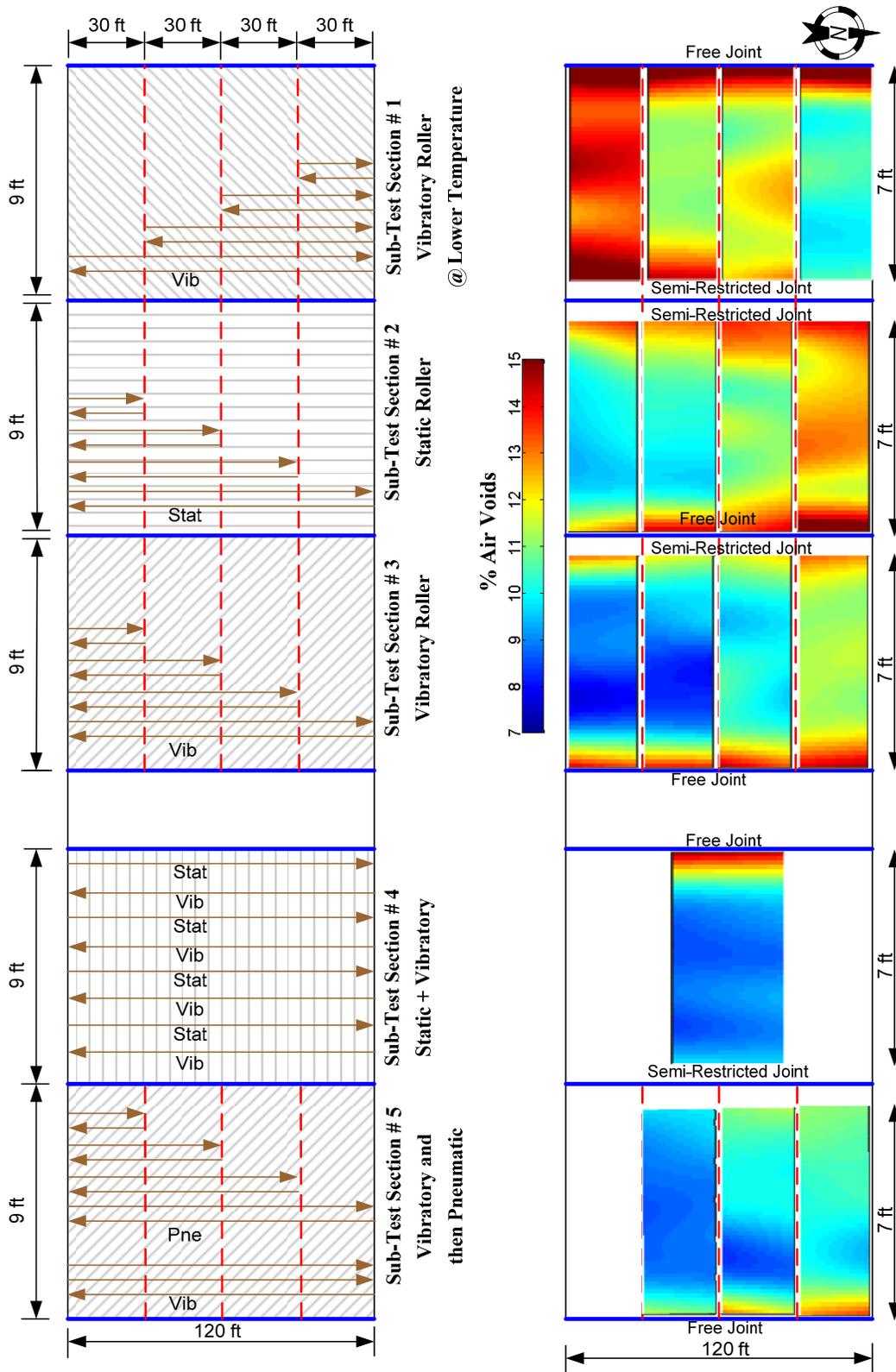
Figure 2-10. Test Section # 5, Schematic of Sub-Test Sections and Rolling Patterns, and Maps of Air Void Distribution.

43
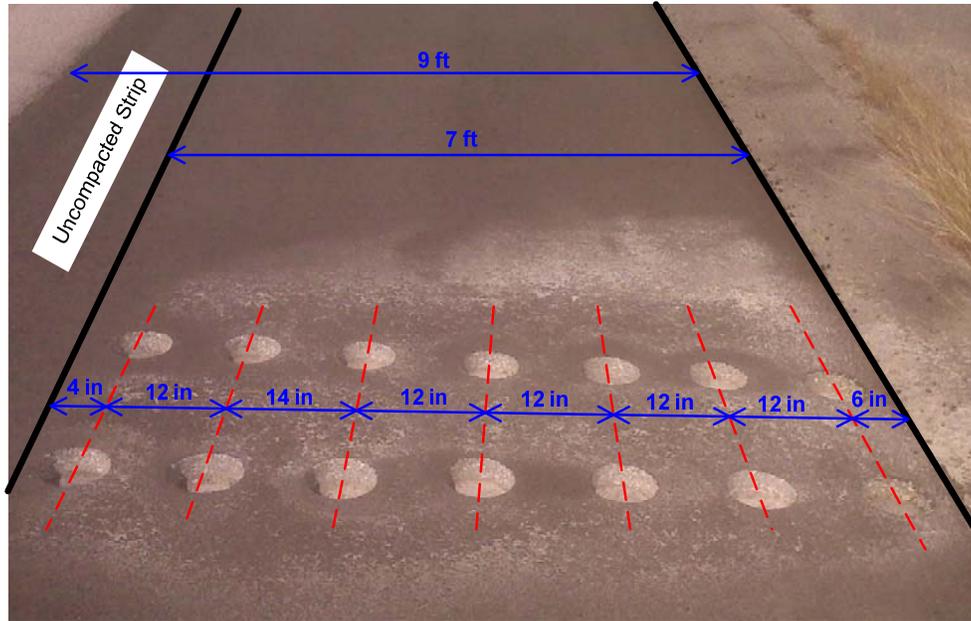
Figure 2-11. Layout of Coring in Test Sections.

COMPACTION EFFORT UNDER THE ROLLER AND ITS RELATIONSHIP TO DENSITY UNIFORMITY

The paving width was 9 ft, but only 7 ft from one edge was compacted by driving a roller with a width of 7 ft straight back and forth to evaluate uniformity of the density across the roller width. Field cores were extracted from seven locations across the mat width with two replicates at each location, as shown in Figure 2-11. The density of these cores was measured in the laboratory. The percent air voids for all the extracted cores were plotted against the number of passes for each sub-test section. Examples of such correlation are given in Figures 2-12 and 2-13 for test sections 1 and 5, respectively. Figures A-4 through A-13 in the appendix show the results for the remaining test sections. These results clearly indicate that uniform density cannot be achieved simply by applying a uniform number of passes; this finding is consistent with the previous work of Kassem et al. (2008).

Kassem et al. (2008) showed that cores compacted close to the center of the steel roller (static or vibratory) tend to have a higher density (less air voids) than cores compacted at the edge of the compactor. They also showed that the compaction efficiency can be described well by the CI, which is defined as the summation of the number of passes multiplied by an effectiveness factor corresponding to each pass. The effectiveness factor describes the efficiency of compaction across the roller width. Kassem et al. (2008) described the statistical and analytical methods used to

44

determine the effectiveness factor in detail. Figure 2-14 shows the effectiveness factor that was found for the test sections constructed in this study.
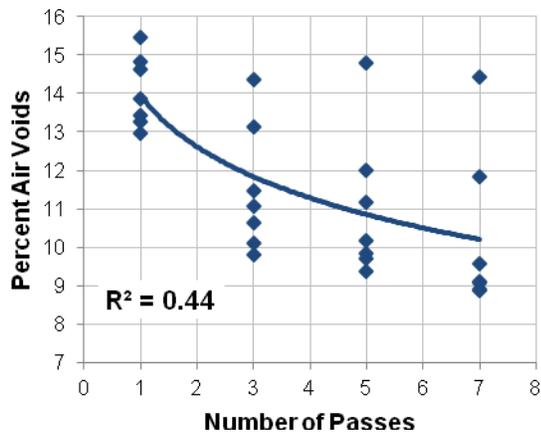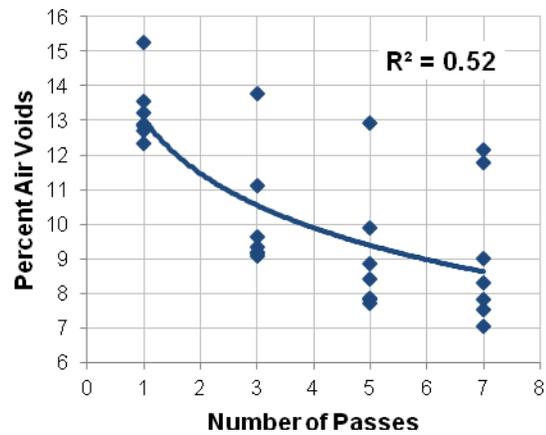
(a) Test Section 1 (Static Roller) (b) Test Section 1 (Vibratory Roller)

Figure 2-12. Percent Air Voids versus Number of Passes for Test Section 1.
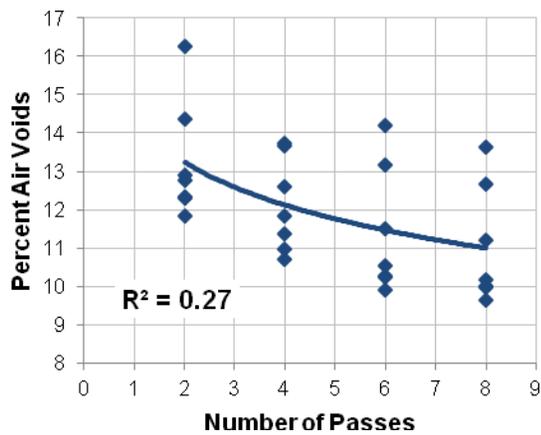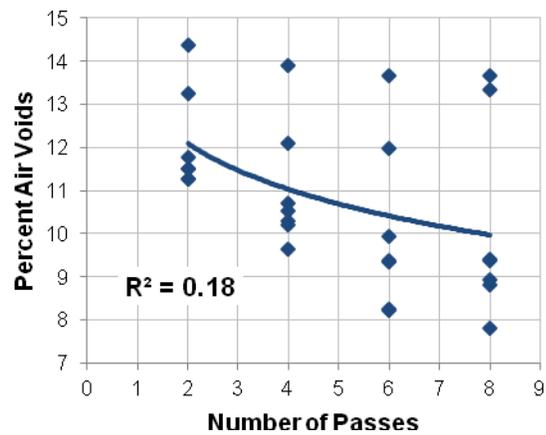
(a) Test Section 5 (Static Roller) (b) Test Section 5 (Vibratory Roller)

Figure 2-13. Percent Air Voids versus Number of Passes for Test Section 5.

45
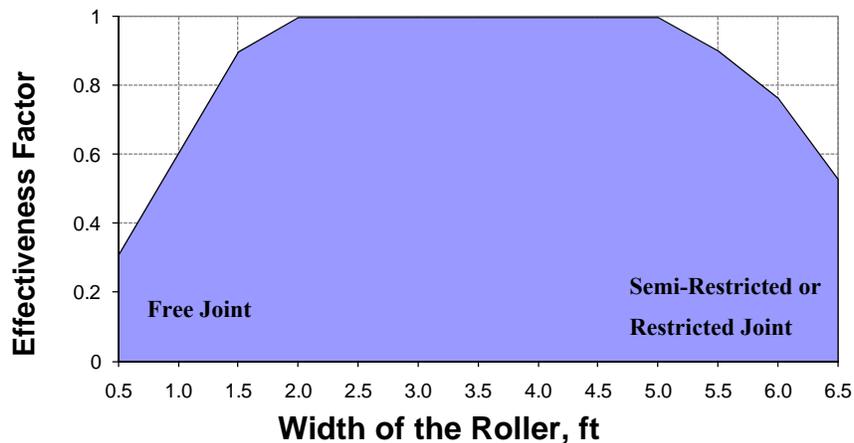
Figure 2-14. Efficiency Distribution of the Compactive Effort across Roller Width.

Figures 2-15 and 2-16 illustrate examples of the relationship between CI and percent air voids, respectively. Figure 2-15(a) and (b) shows this correlation for test section 1 compacted using static and vibratory rollers, respectively. Figure 2-16(a) and (b) shows the correlation for test section 5 compacted using static and vibratory rollers, respectively. Figures A-4 through A-13 in the appendix show the results for the remaining test sections. Table 2-2 summarizes the R-squared values of the correlation between the percent air voids and number of passes (N) and correlation between the percent air voids and CI for the same test sections. The R-squared values show that using the CI improved the correlation for most of the test sections. This finding emphasizes the importance of taking the CI into consideration in order to achieve uniform density distribution across the mat through proper overlapping and overhanging of the roller. Also, it is important to predict the density of the mat across the whole width, as discussed later in this paper.
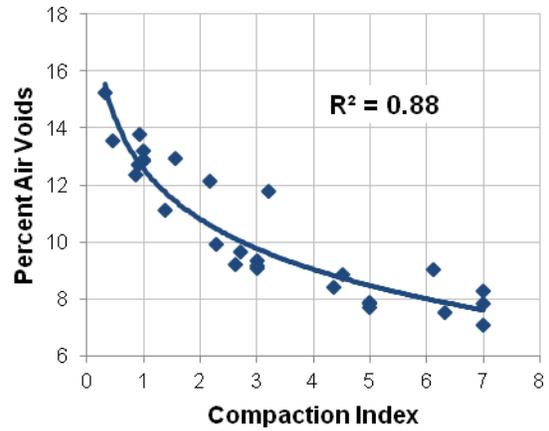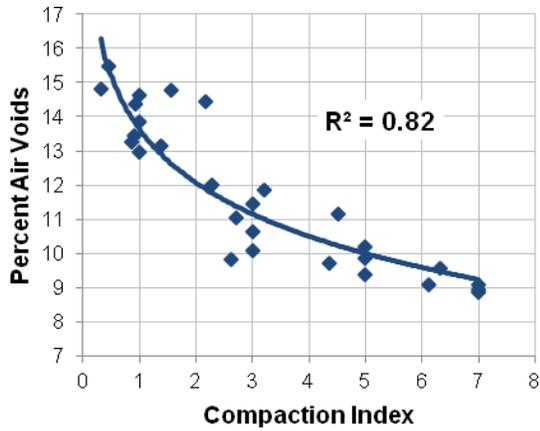
(a) Test Section 1 (Static Roller)   (b) Test Section 1 (Vibratory Roller)

Figure 2-15. Percent Air Voids versus Compaction Index for Test Section 1.
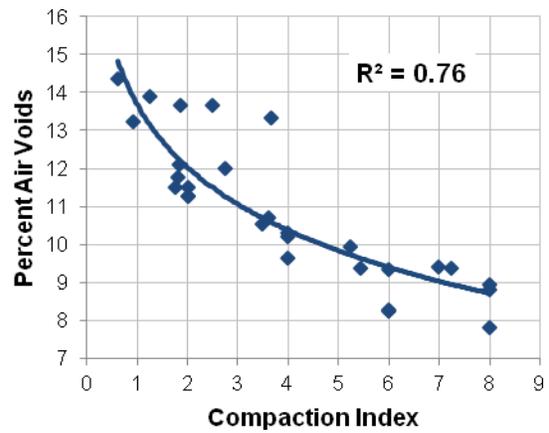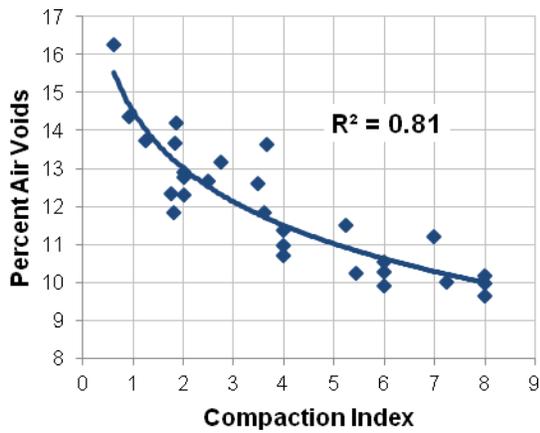
(a) Test Section 5 (Static Roller)   (b) Test Section 5 (Vibratory Roller)

Figure 2-16. Percent Air Voids versus Compaction Index for Test Section 5.

47

Table 2-2. R-Squared Values between Air Voids, Number of Passes, and Compaction Index.

Test Section #	Compaction Method	R^2 Value	
		%AV vs. N	%AV vs. CI
1	Static	0.44	0.83
1	Vibratory	0.52	0.86
2	Static	0.60	0.63
2	Vibratory	0.68	0.81
2*	Vibratory	0.81	0.88
3	Static	0.87	0.79
3	Vibratory	0.89	0.87
3*	Vibratory	0.84	0.91
4	Static	0.64	0.93
4	Vibratory	0.57	0.93
4*	Vibratory	0.47	0.75
5	Static	0.27	0.81
5	Vibratory	0.18	0.76
5*	Vibratory	0.27	0.76

*These test sections were compacted at a lower temperature, below compaction temperatures.

INFLUENCE OF LONGITUDINAL JOINTS ON DENSITY

A major difference between the earlier work of Kassem et al. (2008) and this current study is that the earlier work considered only the influence of the position of the mixture with respect to the roller width on density; however, this study also evaluated the influence of longitudinal joints on density. As discussed earlier, three types of joints were considered: free, semi-restricted, and restricted. Figure 2-6 shows that the free joints to the left of the air void plots had higher air voids than the semi-restricted joints to the right of the plots. The analysis of other sections showed that there was no difference in densities between restricted and semi-restricted joints. Figure 2-14 shows that the effectiveness factor was higher for semi-restricted and restricted joints compared to a free joint. In fact, the effectiveness factor was found to be about 0.55 for the semi-restricted or restricted joint, while it was only 0.32 for the free joint.

INFLUENCE OF COMPACTION METHOD ON DENSITY

Researchers examined the change in density with the CI in each sub-test section to evaluate the influence of the compaction method—vibratory steel roller, static steel roller, and pneumatic roller—on achieving the required compaction level. The densities of the six middle cores from two rows (Figure 2-11) were averaged to represent the average density at a given CI. Figure 2-17(a) and

(b) shows examples of changing the density of the mat with the CI for test sections compacted using vibratory and static steel rollers. Figure A-14 in the appendix shows the results for the remaining test sections. The results were consistent for all test sections and showed, as expected, that the vibratory roller was more effective in increasing the density of HMA and WMA compared to the static steel roller. In order to obtain the compaction curves under the pneumatic roller, the vibratory roller was used for breakdown for only a few passes before applying the pneumatic roller. Researchers attempted to use the pneumatic roller for breakdown, but the pneumatic tires were picking up loose mixtures and compaction could not be accomplished. Therefore, it was decided to use a vibratory roller for breakdown and wait until the temperature dropped before using the pneumatic roller. Figure 2-18(a) and (b) present examples of the compaction curves for sub-test sections compacted using the pneumatic roller. The results showed that the pneumatic roller was still capable of applying compactive effort when it was used as an intermediate compaction roller.

INFLUENCE OF COMPACTION TEMPERATURE ON DENSITY

Sub-test sections in test sections 2, 3, 4, and 5 were compacted using a vibratory roller at a compaction temperature of 180°F, which is lower than the pre-determined compaction temperatures for these mixtures. The field compaction temperatures of Type C PG 76-22, Type D PG 64-22 HMA, and Type D PG 64-22 WMA mixtures were about 270°F, 250°F, and 230°F, respectively. The compaction curves for these sub-test sections were compared to the corresponding sub-test sections that were compacted using a vibratory roller at the designed compaction temperature. Figure 2-19(a) and (b) present examples of the compaction curves for some test sections. Figure A-15 in the appendix shows the results for the remaining test sections. The compaction temperature had a great effect on compaction regardless of mixture type—HMA or WMA. Compaction at a lower temperature shifted up the compaction curves. On average, there was a 10 percent increase in the measured percent air voids per 30°F reduction in the compaction temperature. The sub-test sections compacted at lower compaction temperatures had higher air voids compared to the corresponding ones compacted at the designed compaction temperatures, as Figures 2-7 through 2-10 illustrated. The results of this part demonstrate the importance of real-time recording of mat temperature during the compaction due to its great effect on the compactability of asphalt mixtures.
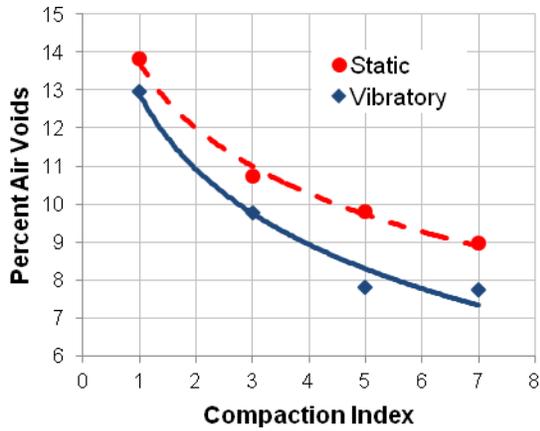
(a) Test Section 1
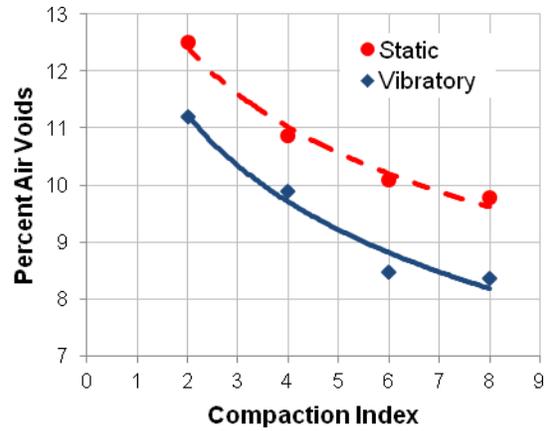
(b) Test Section 5

Figure 2-17. Examples of Percent Air Voids versus Compaction Index for Different Rollers.
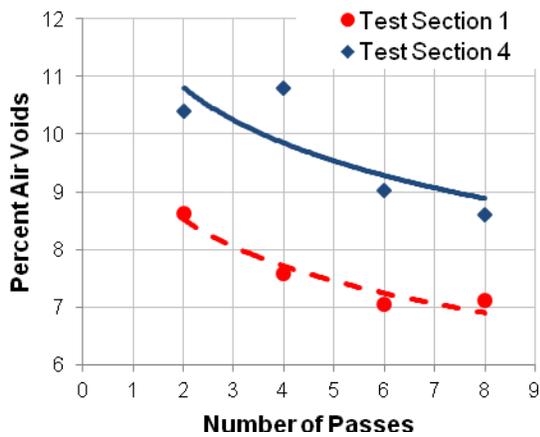
(a) Compaction Curves Using Pneumatic
Roller in Test Sections No. 1 and 4
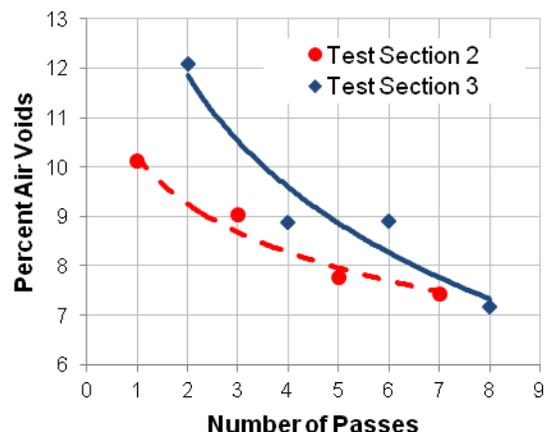
(b) Compaction Curves Using Pneumatic
Roller in Test Sections No. 2 and 3

Figure 2-18. Examples of Percent Air Voids versus Compaction Index Using Different Pneumatic Roller.
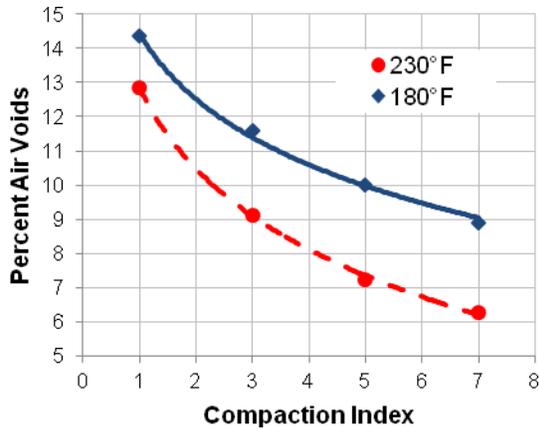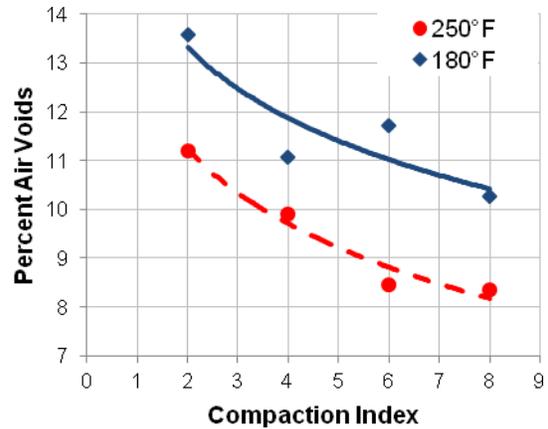
(a) Test Section 3   (b) Test Section 5

Figure 2-19. Examples of Percent Air Voids versus Compaction Index at Different Compaction Temperatures.

INFLUENCE OF MIXTURE DESIGN AND TYPE ON DENSITY

To evaluate the effect of the mixture type (HMA versus WMA) on compaction, researchers compared the compaction curves for test section 2—Type D, HMA—to the corresponding ones for test section 3—Type D, WMA. Figure 2-20(a) and (b) show the change in percent air voids using the vibratory and static rollers, respectively. Figure 2-20(a) demonstrates that the WMA was easier to compact than the HMA. However, the compaction curves for both WMA and HMA using the static roller were comparable and did not show any difference. This could be due to the fact that in general, the static roller applies less compactive effort compared to vibratory rollers, as was discussed earlier.

In order to evaluate the influence of the mixture design on the compactability, the compaction curves for test section 1—Type C, HMA—were compared to the compaction curves for test section 2—Type D, HMA. Both of these test sections were constructed on a rigid (concrete) base. In addition, the compaction curves for test section 4—Type C, HMA—were compared to those for test section 5—Type D, HMA. Both test sections 4 and 5 were constructed on a flexible base. The results showed that HMA Type C was relatively easier to compact than HMA Type D. Type C, a relatively coarse mixture, included PG 76-22 binder, and Type D included PG 64-22 binder, but the Type D mixture had 20 percent RAP. Figure 2-21(a) and (b) show examples of the compaction curves for the Type C mixture and Type D mixture. Figure A-16 in the appendix shows the results for the remaining test sections. The difference between these mixtures was evident when

51

the vibratory roller was used in the compaction. Previous field experience by the research team indicates that typically Type D mixtures with unmodified binder are easier to compact than Type C. However, it seems that incorporating RAP in the Type D mixture made it more difficult to compact.

| (a) Vibratory Roller | (b) Static Roller |
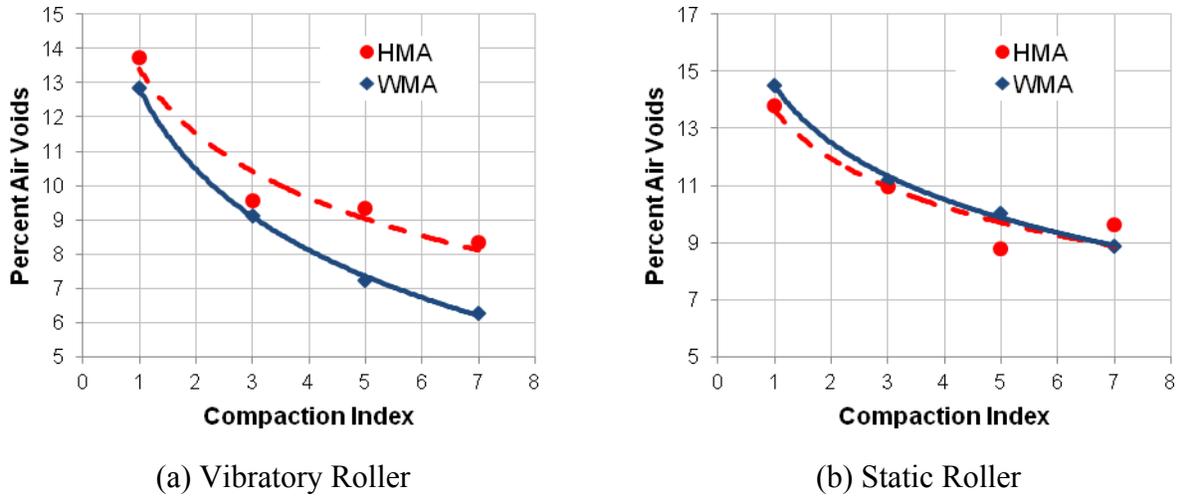
Figure 2-20. Influence of Mixture Type on Density.

| (a) Vibratory Roller | (b) Static Roller |
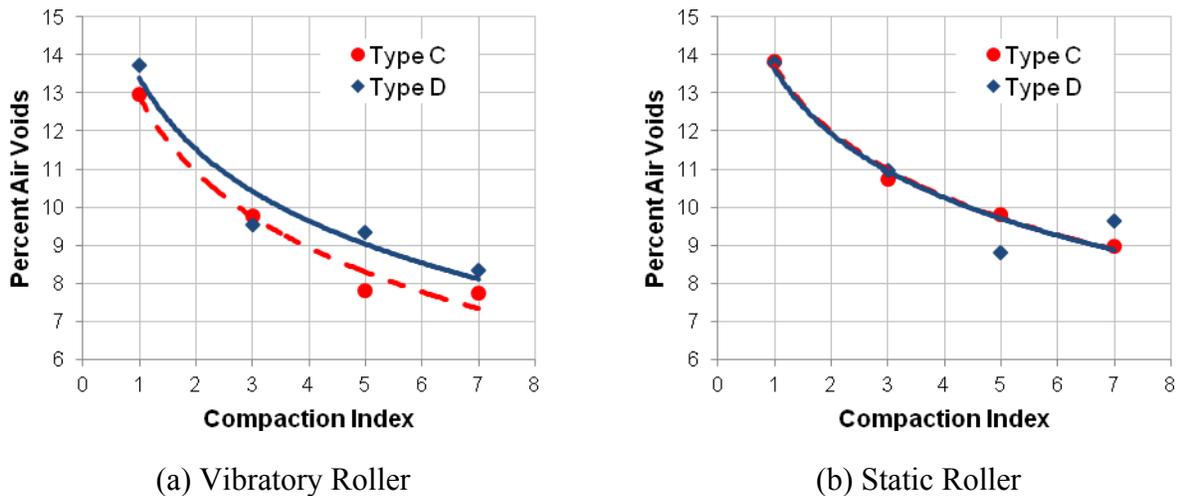
Figure 2-21. Influence of Mixture Design on Density: Test Section 1 vs. Test Section 2.

INFLUENCE OF BASE SUPPORT TYPE ON COMPACTABILITY

To assess the effect of the base conditions (rigid versus flexible) on compactability, the research team compared the compaction curves of mixtures HMA Type C and HMA Type D constructed on a rigid base to the compaction curves of the same mixtures compacted on a flexible base. Figure 2-22(a) and (b) show examples of the compaction curves using vibratory and static rollers. Figure A-17 in the appendix shows the results for the remaining test sections. The results

52

showed that compaction of HMA over a rigid base had slightly higher density than the corresponding mixtures on a flexible base.

(a) Vibratory Roller   (b) Static Roller
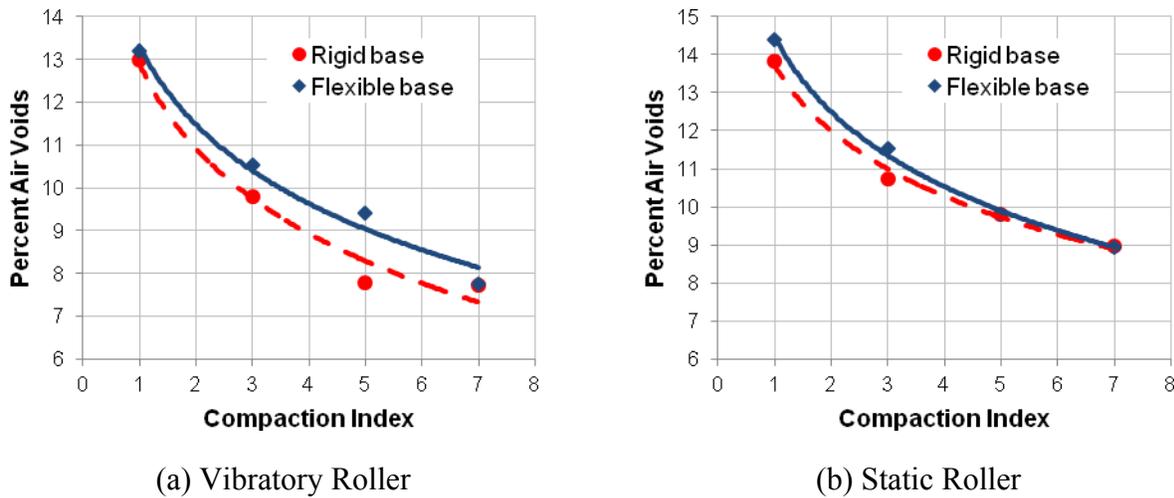
Figure 2-22. Influence of Base Support Type on Compactability: Test Section 1 vs. Test Section 4.

METHOD FOR PREDICTION OF DENSITY IN REAL TIME

Researchers compacted five sub-test sections using different combinations of compaction methods (vibratory and static). Sub-test section 4 in Figures 2-6 through 2-10 shows the rolling patterns. These sub-test sections were constructed to assess the possibility of predicting the density under realistic combinations of compaction methods in real time if the compaction curves for each compaction method are known. For each test section, researchers had the compaction curves for each compaction method (vibratory and static) from the sub-test sections that were compacted using a single compaction method as discussed earlier. Researchers used these curves to predict the density of the sub-test section that was compacted using both vibratory and static methods. Figure 2-23 presents an example of such prediction. The rolling pattern, predicted percent air voids after each pass, and measured final percent air voids of the mat for test section 5 are given in Table 2-3. The procedure can be summarized as follows:

- The percent of air voids after one CI or one pass of vibratory roller, since the density was recorded in the middle of the mat, could be determined from the vibratory roller compaction curve, which was 12.9 percent.

- From this air void level (12.9 percent) on the compaction curve for the static roller, one could determine the percent air void after applying one pass of static roller, by moving

one pass toward the right on the static compaction curve. This would give a percent air void of 12.0 percent.

- From this air void level (12.0 percent) on the vibratory roller compaction curve, one should move one pass toward the right to get the air void after one extra pass of the vibratory roller. This would result in 10.9 percent air void.

The above steps were repeated until the final roller pass, as shown in Figure 2-23 and presented in Table 2-3.
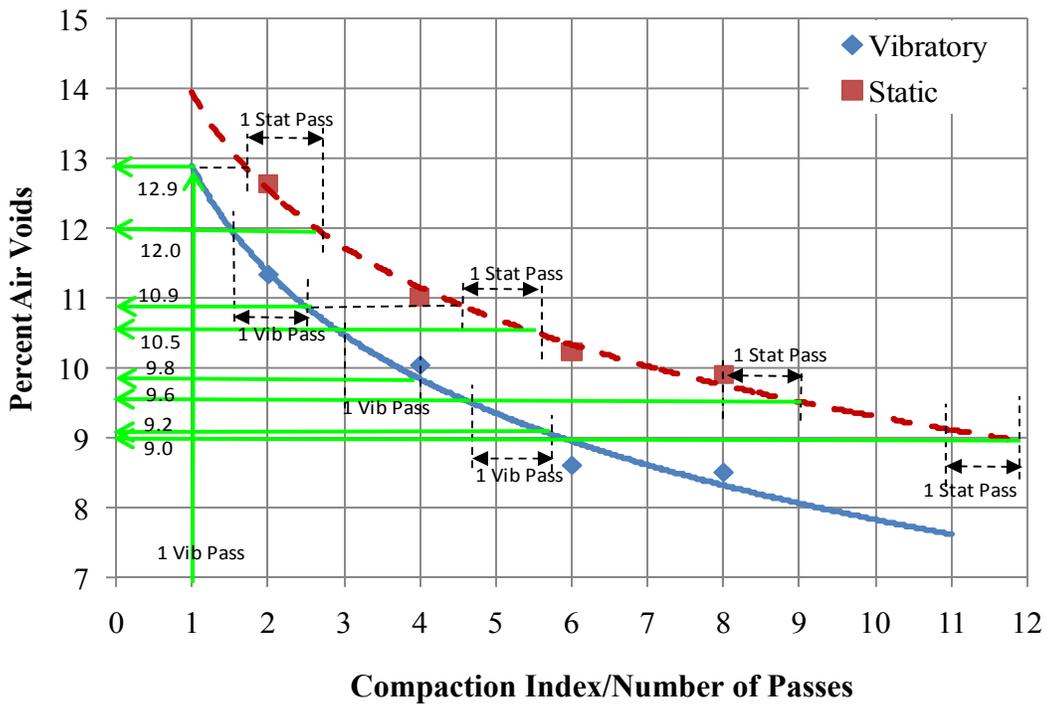
Figure 2-23. Prediction Density Level Using the Compaction Curves: Test Section 5.

Table 2-3. Percent Air Voids for Different Compaction Methods.

No. of Passes	Compaction Method	Predicted %AV	Measured %AV
1	Vibratory	12.9	
2	Static	12.0	
3	Vibratory	10.9	
4	Static	10.5	
5	Vibratory	9.8	
6	Static	9.6	
7	Vibratory	9.2	
8	Static	9.0	8.9

The predicted air void level in all the sub-test sections that were compacted using mixed compaction methods were compared to the measured final density after the compaction was completed, and Figure 2-24 presents the results. The results showed that the predicted densities were very close to the measured values. This means that if the compaction curves for each compaction method can be established at the beginning of a job, the density can be predicted in real time for the remaining part of the job. However, this can only be achieved if the field conditions such as weather, mat thickness, and underlying base remain fairly consistent during construction.

Figure 2-24 shows a comparison between the predicted percent air void and the measured percent air void in the middle of the mat or under the middle of the roller. In order to predict the percent air void across the whole mat, another factor should be introduced, which is the efficiency distribution of the compactive effort (Figure 2-14). After generating the compaction curves for mixed compaction methods as given in Table 2-3, the number of passes should be multiplied by the effectiveness factor across the roller width in order to obtain the density across the mat under the roller. Figure 2-25 and Figure 2-26 show examples of the introduced error (the difference between the measured percent air void and the expected percent air void) for all the cores taken across the mat in two cases. The first case considers only the compaction curves without considering the non-uniform efficiency distribution of the compactive effort, and the second case considers the efficiency distribution. Figures A-18 through A-20 in the appendix show the results for the remaining test sections. For most of the test sections, considering the efficiency distribution reduced the error in predicting the density for the cores taken at the edges of the mat.

These results show that one can develop test sections at the beginning of the work that are compacted by static rollers and vibratory rollers in different modes of operation (vibration amplitude and frequency). Then, one can record the compaction under each roller and combine this information to predict the best combination of compaction pattern to achieve the required density. The number of passes can be combined with the efficiency distribution of the compactive effort in order to produce CI maps in real time. This information can be presented in real time to the roller operator to adjust the compaction patterns (by changing number of passes, overlapping, and overhanging) needed to achieve a uniform CI in order to obtain the required density uniformly across the mat.
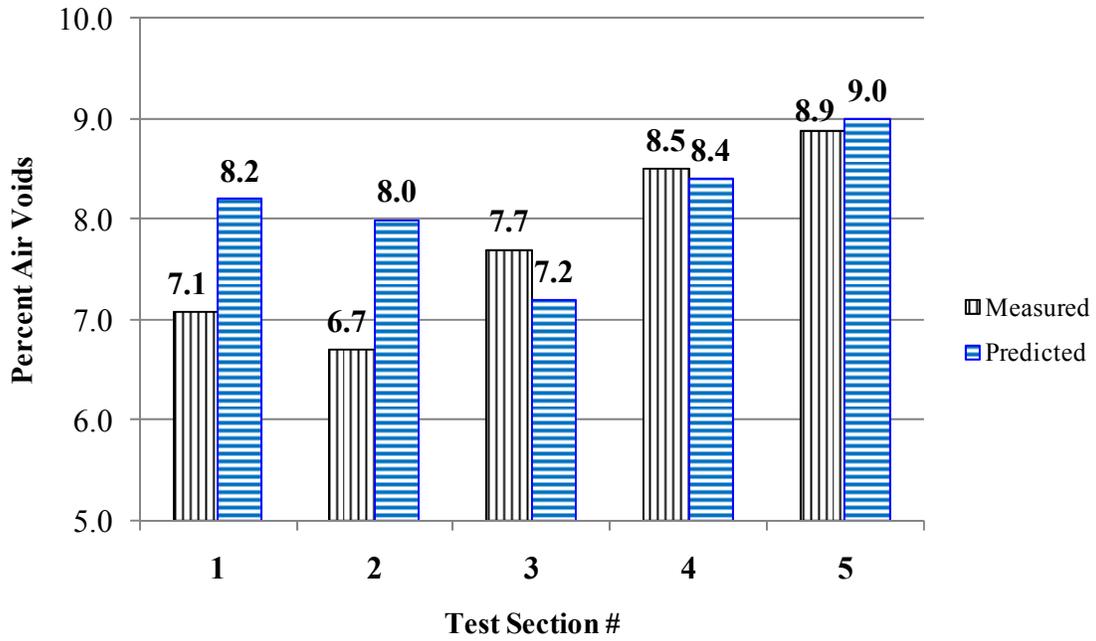
Figure 2-24. Predicted and Measured Percent Air Voids.
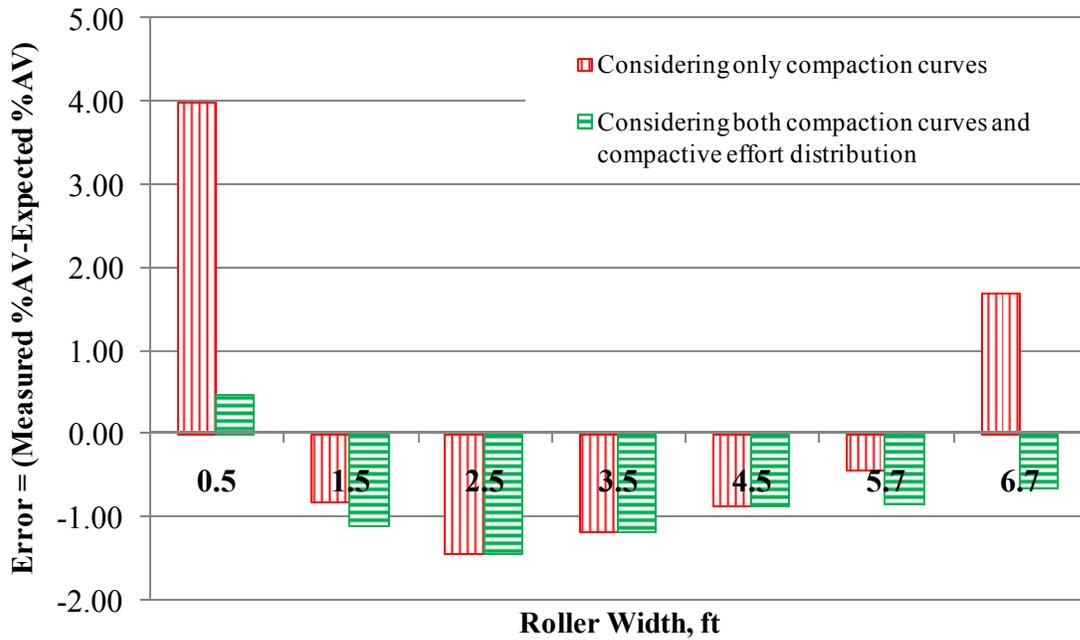
Figure 2-25. Error in Predicting Density Level for Test Section 1.
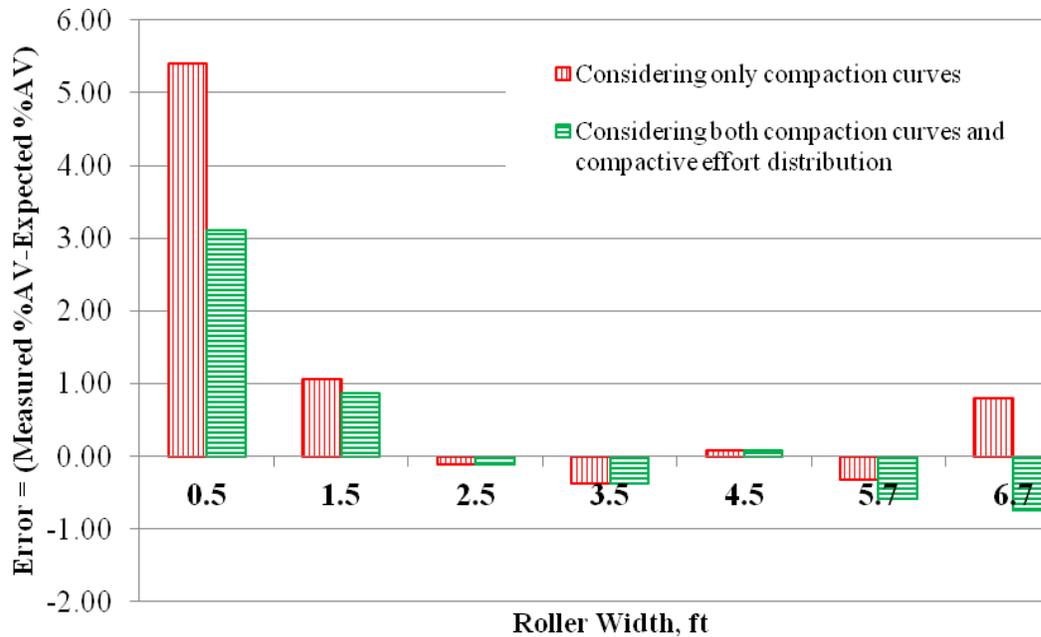
Figure 2-26. Error in Predicting Density Level for Test Section 5.

CONCLUSIONS

This part of the study provided a comprehensive experimental evaluation of important factors that influence the compaction process of asphalt pavements. The main findings of this part are summarized as follows:

- The efficiency of the compactive effort across the steel rollers was found to be non-uniform. A point on the mat closer to the center of the roller was subjected to more compaction than a point closer to the edge of the roller.

- Cores compacted close to restricted or semi-restricted joints had more density than cores near free or unrestricted joints.

- The compaction temperature had a great effect on compaction irrespective of mixture type—HMA or WMA. On average, there was a 10 percent increase in the measured percent air voids per 30°F reduction in the compaction temperature.

- The WMA was relatively easier to compact compared to the HMA, in spite of the fact that WMA was laid and compacted at lower temperatures than HMA.

- Incorporating RAP in asphalt mixtures could require increasing the compaction effort to achieve the desired density compared to mixtures without RAP. However, several other factors besides the use of RAP may affect the compactability of HMA, such as aggregate

57

gradation, voids in the mineral aggregate (VMA), aggregates characteristics, etc.

- HMA compacted on the top of a rigid base had a higher density than the mixture compacted on a flexible base.

- A method was presented for predicting the density of asphalt pavement compacted using static and vibratory rollers. This method utilizes the location of the roller on the mat and the compaction curves for each roller to predict the density. The predicted density was close to the measured one. More work is recommended to validate and further demonstrate this approach. This approach could be used to set up the rolling pattern that is needed to achieve the desired asphalt pavement density.

CHAPTER 3
MEASUREMENTS OF ASPHALT PAVEMENT DENSITY USING GROUND-PENETRATING RADAR AND ITS RELATIONSHIP TO PERFORMANCE

The level of asphalt pavement compaction in the field significantly affects its mechanical properties. The traditional methods of measuring air voids can be destructive, expensive, and time-consuming and can only provide point-specific information. The GPR is a non-destructive tool that has been used to perform structural assessment of asphalt pavements and has been proven to be a successful tool. In this study, the research team utilized GPR as a tool to assess the compaction level in asphalt pavements. Such evaluation was conducted on both HMA and WMA in order to address any compaction concerns of WMA compared to HMA. In addition, the effect of level of compaction on the mechanical properties of asphalt pavements was evaluated through conducting performance tests. The results of these tests shed light on how significant the effect of the percent air voids is on some of the mechanical properties of asphalt mixtures.

OBJECTIVES

The objectives of this part of the study were as follows:
- Examine the feasibility of using GPR as a non-destructive quality control tool to determine density (air void distribution) of asphalt pavements.
- Study the effect of compaction level on the mechanical properties of asphalt mixtures.
- Compare the compactability and mechanical properties of WMA to HMA.

RESEARCH METHODOLOGY

The researchers conducted GPR scanning at different lateral positions for all the test sections described in Chapter 2. They developed maps of percent air void distribution in the test sections using GPR data. The distribution maps developed using GPR were compared to the ones developed using extracted field cores (Figures 2-6 through 2-10). The researchers conducted several performance tests (indirect tensile test, Hamburg, and overlay) on the recovered field cores with different percent air voids.

BACKGROUND ON TEST METHODS

Basics of Ground-Penetrating Radar

The GPR measurements for quality control or forensic study of highway pavements are conducted typically with 1.0 Gigahertz (1-GHz) air-coupled horn antenna. Figure 3-1(a) shows the Texas Transportation Institute's 1-GHz air-launched GPR unit. This system sends discrete pulses of radar energy into the pavement system and captures the reflections from each layer interface within the structure. Radar is an electromagnetic wave and, therefore, obeys the laws governing reflection and transmission of e-m waves in layered media.

Figure 3-1(b) shows the operating principle of GPR. The reflection A_1 is the energy reflected from the surface of the pavement, and A_2 and A_3 are reflections from the top of the base and subgrade, respectively. These are all classified as positive reflections, which indicate an interface with a transition from a lower to a higher dielectric material. These amplitudes of reflection and the time delays between reflections are used to calculate both layer dielectrics and thickness (Scullion and Chen 1999). Figure 3-1(c) shows a typical plot of captured reflected energy versus time for one pulse, as a graph of volts versus arrival time in nanoseconds. The dielectric value of the HMA layer is computed by measuring the amplitude of reflection from the top of the pavement and comparing it with the reflection from a large metal plate which is the 100 percent reflection.

The dielectric constant of a material is an electrical property that is most influenced by moisture content and density. An increase in moisture will cause an increase in layer dielectric; in contrast, an increase in air void content will cause a decrease in layer dielectric. The examples below illustrate how changes in the pavement's engineering properties would influence the typical GPR trace shown in Figure 3-1(b).

- If the thickness of the surface layer increased, then the time interval Δt_1 between A_1 and A_2 would increase.
- If the base layer became wetter, then the amplitude of reflection from the top of the base A_2 would increase.

- For well-compacted hot mix layers, the GPR wave would be reflected at the top of the asphalt layer and the top of the base layer. If the asphalt layer had uniform density with depth, then no intermediate reflections would be observed. If there was a significant defect within the surface layer, then an additional reflection would be observed between A_1 and A_2. This could indicate areas of poor compaction or moisture trapped between pavement layers.

- Large changes in the surface reflection A_1 would indicate changes in either the density or moisture content along the section. The variation in surface reflection is used to check segregation within a new HMA surface layer, and it can also be used to test the quality of longitudinal construction joints.

In most GPR projects, researchers collect several thousand GPR traces. In order to conveniently display this information, color-coding schemes are used to convert the traces into line scans and stack them side by side so that a subsurface image of the pavement structure can be obtained. Figure 3-1(c) illustrates a typical display from a good-quality, thick HMA pavement. This is taken from a section of newly constructed thick asphalt pavement over a thin granular base.

Color coding consists of converting this trace into a single-line scan of different colors where the high positive volt areas are color coded red, the negatives are blue, and the areas around zero volts are green. Using the color-coding and stacking scheme, these data are transformed into Figure 3-1(d), which shows a COLORMAP$^{®}$ subsurface image for a section of highway. The zero on the depth scale is the reflection from the surface of the pavement. The important features of this figure are the lines marked H, I, and J; these are the reflections from the surface, top, and bottom of base, respectively. The pavement is homogeneous, and the layer interfaces are easy to detect. The variation in surface dielectric is shown at the bottom of the figure. For good-quality, uniform-density HMA, this would be almost a horizontal line. Significant areas of high dielectrics would indicate wet areas on the surface. Significant dips in surface dielectric are associated with areas of low density in the mat, typically "truck-end" segregation.

(a) TTI GPR Van Equipped with Air-Launched Antenna
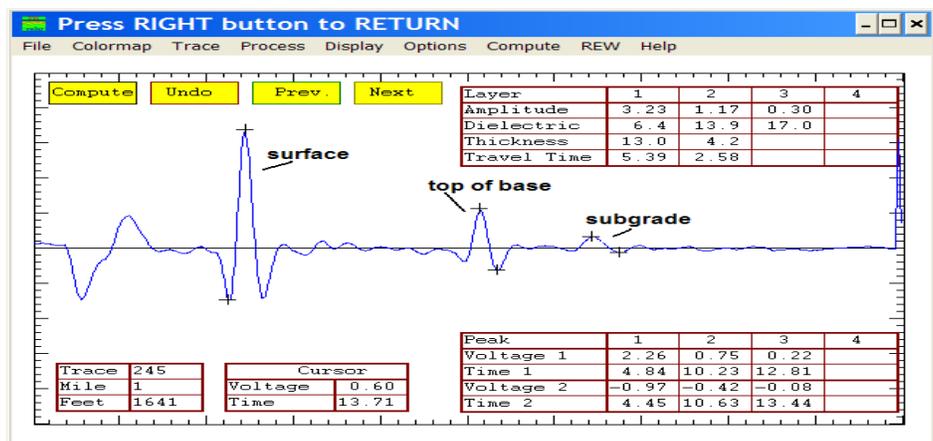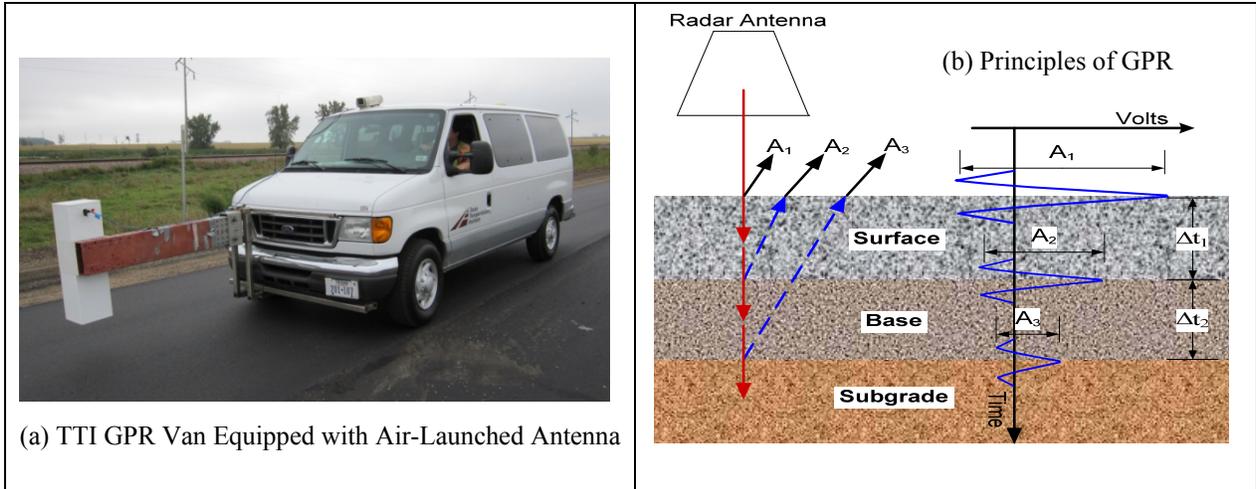
(b) Principles of GPR

(c) One Individual GPR Trace from a Thick HMA Pavement
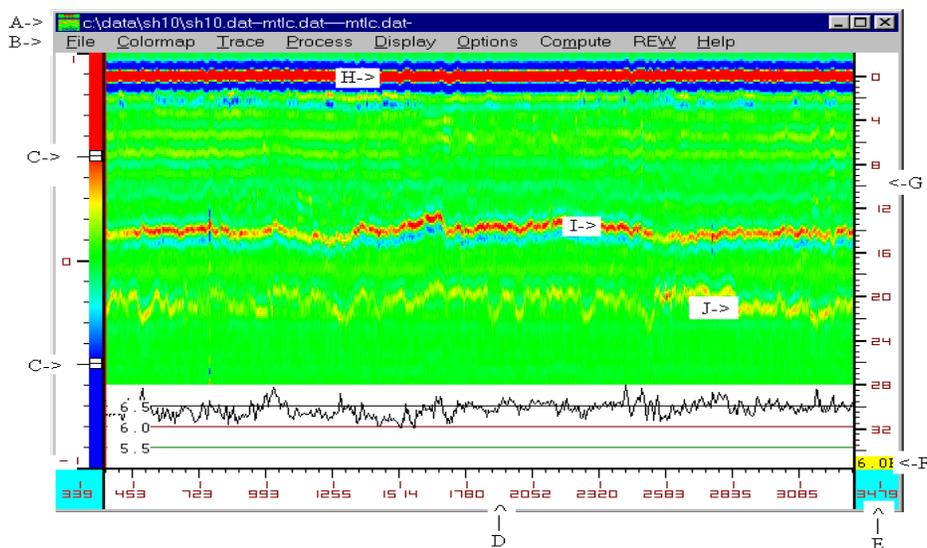
(d) Color-Coded GPR Traces for a Thick Hot Mix Section

Figure 3-1. GPR Equipment and Principles.

Overlay Test

The overlay test, developed at TTI, was employed in this study to evaluate the cracking potential of specimens compacted at different air voids. Overlay tests were conducted on laboratory test specimens following the recommendations by Zhou and Scullion (2003) and the recently adopted TxDOT standard Tex-248-F—"Overlay Test." Figure 3-2(a) depicts the schematic diagram of the overlay apparatus. The overlay tester is comprised of two steel plates; one plate is fixed while the other moves horizontally to simulate the opening and closing of joints or cracks from an existing pavement beneath an overlay. A cyclic load was applied in a triangular waveform at 10 cycles per minute. The overlay test was run at 77°F in a controlled displacement mode with a peak displacement of 0.025 inch until the sample failed. The overlay tester acquires time, displacement, and load data for each load cycle. In addition, the crack length can also be measured manually. Three prismatic specimens (6 inches × 3 inches × 1.5 inches) were sawed from 6-inch diameter field cores. The parameters of interest from this test were the number of load cycles applied to the sample before failure, and the maximum load at the first cycle to initiate cracking. Failure was determined as the point when one continuous crack was visible completely through the exposed portion of the specimen, i.e., cracks visible through two vertical sides and one horizontal (top) surface or when the load reached 8 percent maximum load, whichever occurred first.

Hamburg Test

The Hamburg wheel-tracking (HWT) device is an accelerated loaded wheel tester. This test is commonly used to assess the rutting and moisture susceptibility of asphalt mixtures. Researchers in this study used this test to study the effect of the air void distribution on rutting of asphalt mixtures. The Hamburg test was conducted following TxDOT standard Tex-242-F—"Hamburg Wheel-Tracking Test." In this test, steel wheels are operated on submerged cylindrical HMA specimens (Figure 3-2[b]). The Hamburg test is conducted under water at a constant temperature of 122°F. The steel wheel is 1.85 inches wide and 158 lb-force and travels in a reciprocating motion. The rut depth is measured at several locations along the test sample, including the center where the maximum rut depth occurs. Typically, the test is conducted at 20,000 cycles or until certain rut depth is achieved.

Indirect Tensile Test

The indirect tensile (IDT) test has been used extensively in structural design research for rigid pavements since the 1960s and, to a lesser extent, in HMA mixture design research. However, the indirect tensile test is a popular test for HMA mixture characterization in evaluating pavement structures. The primary reason for its popularity is that cores from thin lifts can be tested directly in the laboratory (Witczak et al. 2002). The indirect tensile method is used to develop tensile stresses along the diametral axis of the test specimen. The test specimen is placed with its axis horizontal between the platens of the testing machine. A compressive load is applied on the diametrically opposite ends of the test specimen. Figure 3-2(c) shows the test setup. The horizontal tensile strength of the mixture was determined from the following equation:

$$\sigma_{max} = \frac{2P_{max}}{\pi t d} \qquad (2)$$

where σ_{max} is the horizontal tensile strength at the center of the test specimen, P_{max} is the maximum load achieved when the specimen is loaded at a rate of 2 inches per minute, d is the diameter of the specimen, and t is the thickness of the specimen.
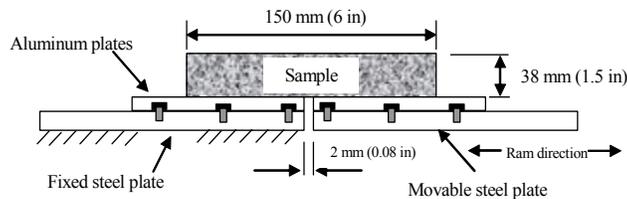
(a) Schematic Diagram of TTI Overlay Tester System (Zhou and Scullion, 2003)

(b) Hamburg Wheel-Tracking Setup

(c) IDT Setup

Figure 3-2. Performance Tests.

GPR MEASUREMENTS

After construction of the test sections was completed, the research team conducted GPR scanning on these test sections. On each test section, the research team drove the GPR van three to five times to measure the dielectric constant values. Each time, the antenna was moved laterally to cover the whole compaction width (7 ft). Typically, the GPR captured the dielectric constant across an 8-inch-wide area during each pass. The GPR data, dielectric constant values, were calibrated with measured bulk densities of a few cores extracted from different locations of the mat. Such calibration is done to convert all the dielectric constant values to density or air voids of compacted mat. Figure 3-3 shows an example of the correlation between measured density and the dielectric constant values. Strong correlations were found between dielectric constant values and percent air voids of recovered cores.

The equation shown on the figure is:

$$y = 172.5e^{-0.513x}$$
$$R^2 = 0.965$$
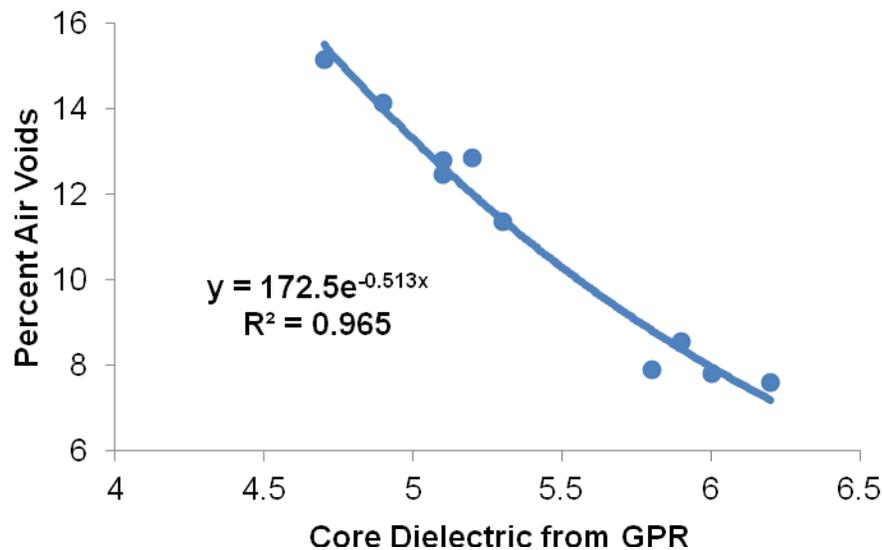
Figure 3-3. Correlation between Dielectric Constant and Percent Air Voids of Recovered Cores.

Each GPR profile contains hundreds of dielectric constant measurements along the test section, and three to five GPR profiles or traces were recorded across the mat. Using a correlation such as the one presented in Figure 3-3 for each test section, the dielectric constant measurements were converted to percent air voids. COLORMAP® software was used to convert these measurements into color maps of air void distribution across the mat width and along the test section length. Figures 3-4 through 3-6 provide examples of such distributions.

65
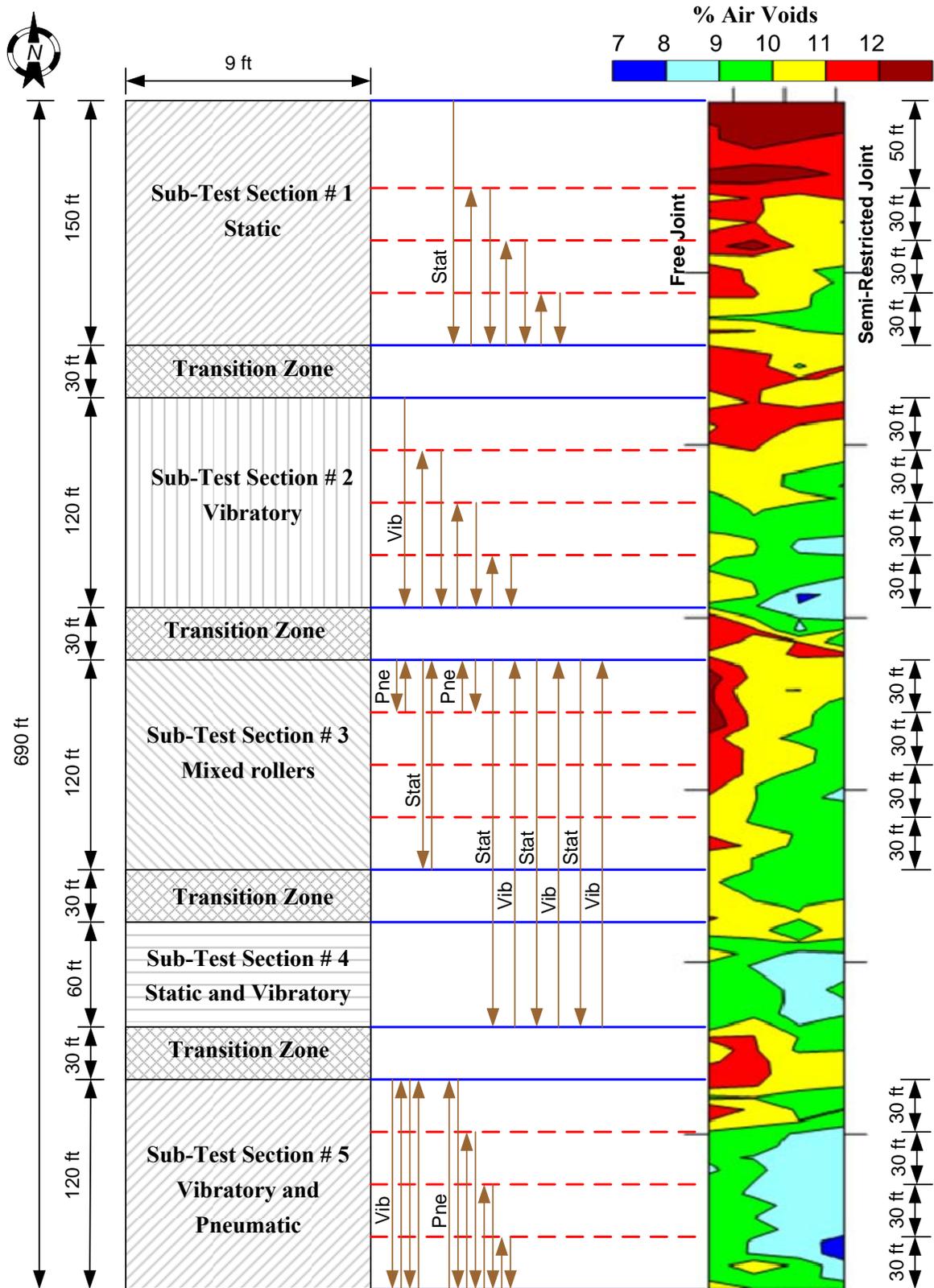
Figure 3-4. Air Void Distribution Maps Using GPR Data: Test Section 1.
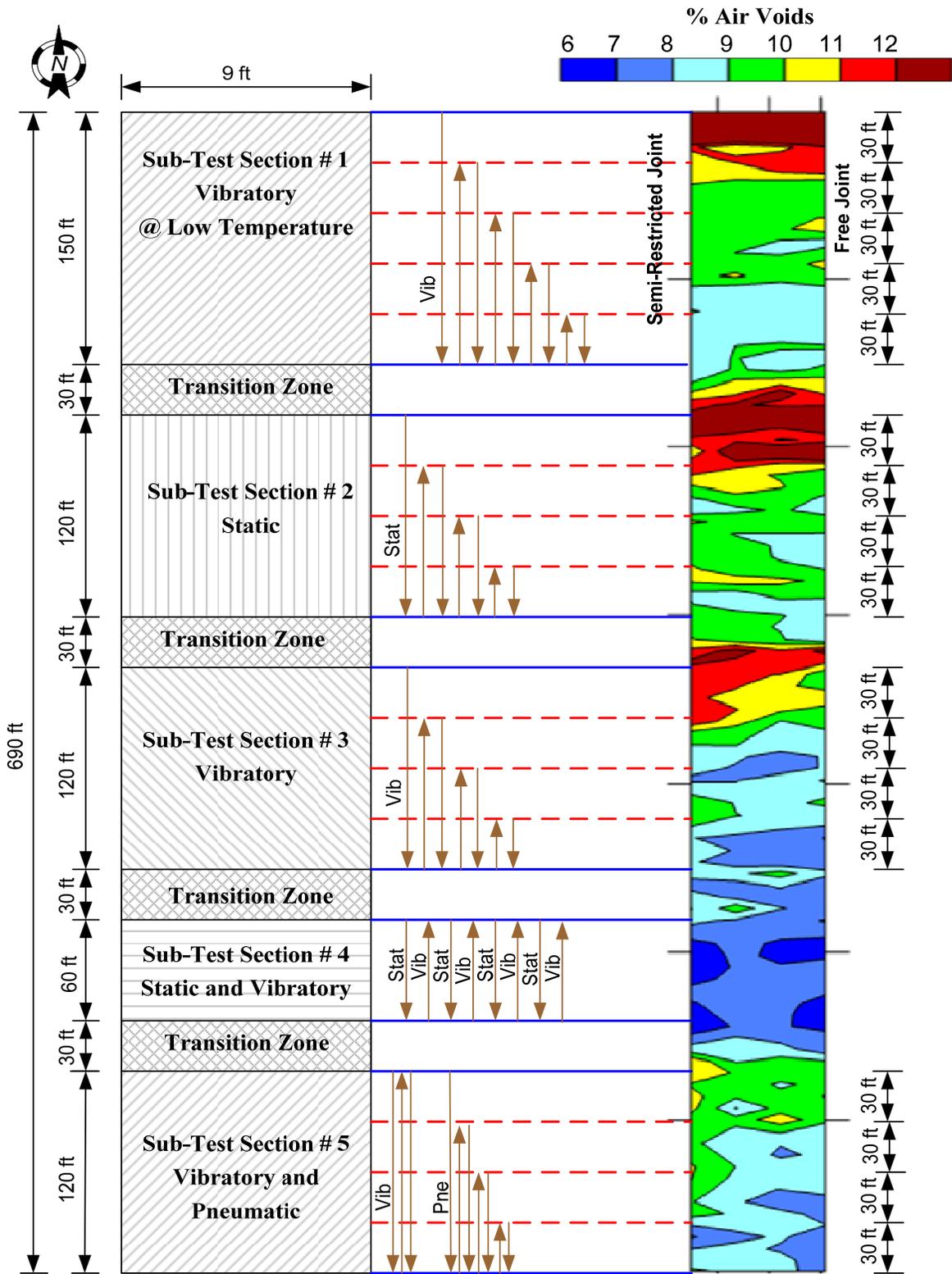
Figure 3-5. Air Void Distribution Maps Using GPR Data: Test Section 2.
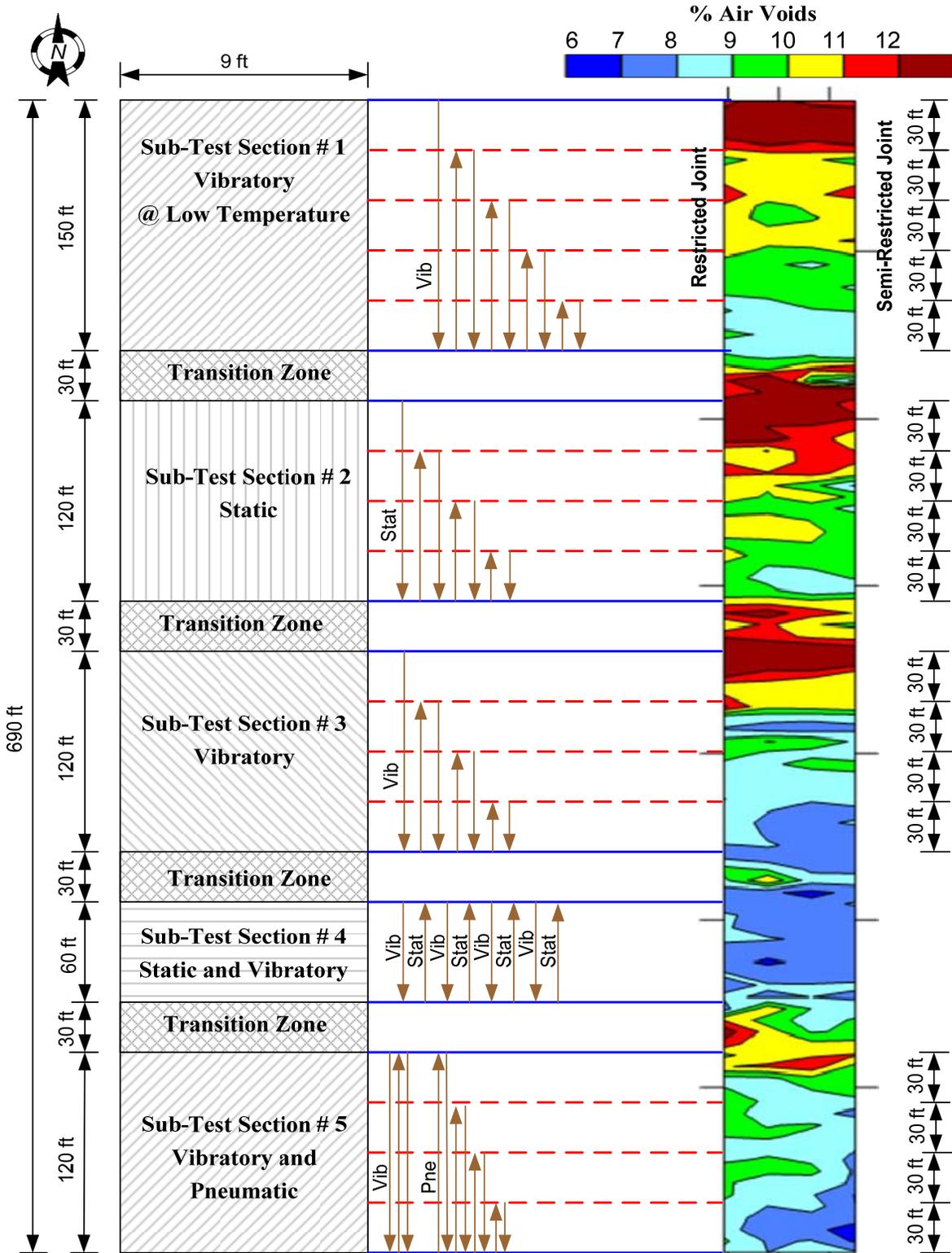
Figure 3-6. Air Void Distribution Maps Using GPR Data: Test Section 3.

AIR VOID DISTRIBUTION USING CORE MEASUREMENTS

As previously discussed in Chapter 2, researchers constructed the test sections with a varying number of roller passes that resulted in varying air voids in smaller test strips within the test sections. Field cores were extracted from different locations across the mat from each strip after the GPR scanning and other non-destructive density measurements. As Figure 2-11 shows, two rows of cores (seven cores in each row) were taken from each strip that was subjected to a varying number of roller passes. The density of the field cores extracted across the mat from each strip was used to generate maps of percent air void distributions by inputting the location of each core and its percent air voids into the Matlab 7.1 software. An interpolation algorithm in Matlab was then used to predict percent air voids in the whole pavement section. Examples of the color-coded air void distribution maps for the test sections are shown in Figures 2-6 through 2-10.

COMPARISON OF AIR VOID DISTRIBUTION MAPS

Comparing the air void distribution maps developed using the GPR data and densities of the recovered cores, researchers made the following observations:

- There is an excellent correlation between GPR void distribution maps and the void maps generated using the extracted field cores (Figure 3-4 versus Figure 2-6, Figure 3-5 versus Figure 2-7, and Figure 3-6 versus Figure 2-8). These results show that GPR is a very good tool for assessing the compaction level in asphalt pavements and in general can be used as a quality control tool in asphalt pavement construction. The advantage of the GPR is that it is a non-destructive tool that operates at the traffic speed. The GPR van can be driven over the mat many times without any interference to the traffic.

- The density increased with the increase in the number of passes, as expected.

- Test sections compacted using vibratory rollers had a higher density than the corresponding ones compacted using static rollers. In addition, sub-test sections compacted at lower temperatures had a lower density than the ones compacted at the designed compaction temperature.

- When comparing the air void distribution maps of HMA test section 2 (Figures 3-5 and 2-7) with WMA test section 3 (Figures 3-6 and 2-8), researchers found that air void distributions were comparable, although WMA was produced and compacted at lower temperatures than HMA. In fact, WMA asphalt was found to improve the compactability

of the asphalt mixtures, as discussed in Chapter 2. The researchers did not observe or experience any compaction problems during the construction of the WMA test section.

PERFORMANCE TEST RESULTS

Indirect Tensile Strength

Thirty-six field cores were tested for indirect tensile strength. Half of the specimens were tested in dry conditions, and the other half were tested in wet conditions following the modified Lottman procedure without the freezing stage (American Association of State Highway and Transportation Officials [AASHTO] T-283-07). A vacuum of 3.38 kPa absolute pressure (736.6 mm Hg. partial pressure) was used to achieve the required saturation level between 70 to 80 percent, as required by AASHTO T-283-07 (AASHTO 2007). This procedure was followed by placing specimens in a 60°C water bath for 24 hours. Then, the test specimens were taken to another 20°C water bath to cool down before testing. Twelve field cores were tested from each asphalt mixture. These cores were collected from strips that were subjected to a different number of roller passes, resulting in different levels of compaction. Three levels of compaction that produced asphalt mixture specimens with different percent of air voids were evaluated. Figure 3-7 presents the results of the IDT test. The results showed that, as expected, the IDT values for dry specimens were much higher than the IDT for wet specimens. Also, the IDT decreased with the increase in percent air voids in both dry and wet conditions (Figure 3-7[a]). This emphasizes the importance of the compaction level on the performance of asphalt mixtures. However, the Type D WMA performed the best in dry conditions and the worst in wet conditions. Figure 3-7(b) shows the percent reduction of IDT. Compared to the Type C HMA and Type D HMA, the Type D WMA mixture had the highest loss of IDT due to moisture conditioning.
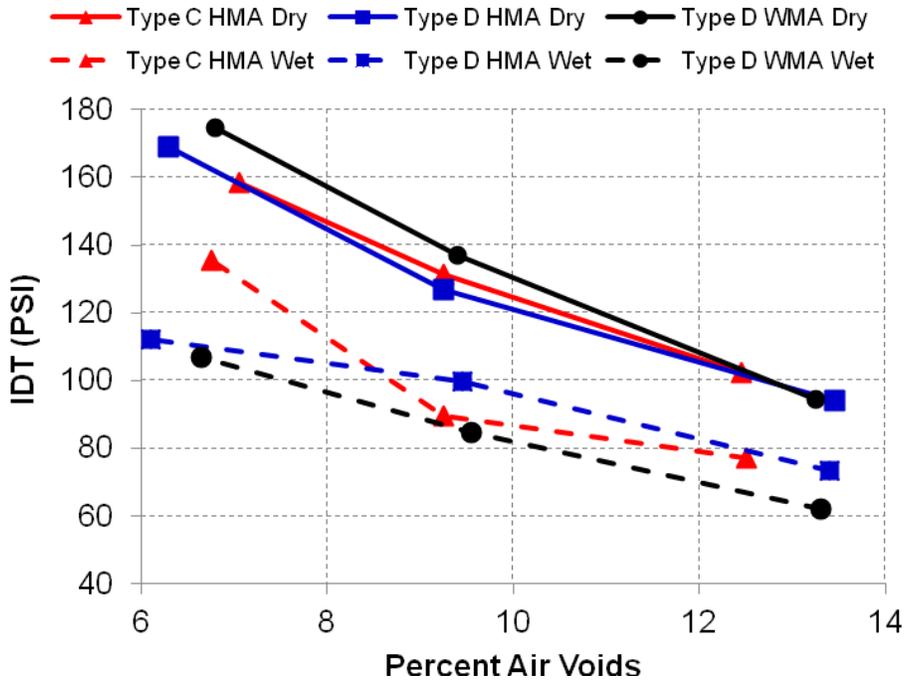
(a) IDT vs. Percent Air Voids
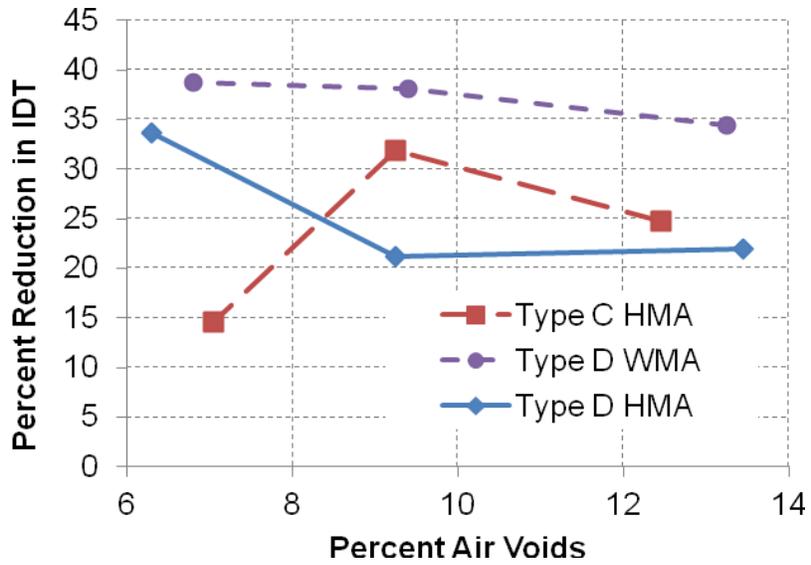
(b) Reduction in Strength vs. Percent Air Voids

Figure 3-7. Indirect Tensile Strength Test Results.

71

Hamburg Wheel-Tracking Test

Similar to IDT testing, researchers tested 36 field cores using the Hamburg wheel-tracking test. Twelve field cores were tested from each asphalt mixture. These cores were taken from strips that were compacted using a different number of roller passes. One set of HWT tests required four field cores—two cores on the left side and two cores on the right side (Figure 3-2[b]). The rut depth was recorded with the number of cycles until failure. The failure criteria depended on the type of binder. TxDOT specifications allow a rut depth less than 0.5 inch (12.5 mm) after 20,000 cycles for mixtures with modified binder and less than 0.5 inch (12.5 mm) rut depth after 10,000 cycles for mixtures with unmodified binder. According to TxDOT specifications, all the tested cores passed the failure criteria. The rut depth and number of cycles displayed in Table 3-1 show that Type C HMA did not rut as much as the other two mixtures—Type D HMA and Type D WMA. Type C HMA had modified binder (PG 76-22), while the other two mixtures had unmodified binders (PG 64-22). The results showed that the compaction level affects the performance of the asphalt mixtures; field cores with higher percent air voids rutted more than field cores with less percent air voids.

Table 3-1. Hamburg Wheel-Tracking Test Results.

Mixture Type	% Air Voids	No. of Cycles	Rut Depth, inch (mm)
Type C HMA	13.1	20,000	0.173 (4.4)
	9.1	20,000	0.158 (4.0)
	7.4	20,000	0.146 (3.7)
Type D HMA	14	10,934	0.579 (14.7)
	9.9	20,000	0.441 (11.2)
	8.6	20,000	0.287 (7.3)
Type D WMA	12.7	16,292	0.539 (13.7)
	9.2	20,000	0.383 (9.7)
	6.1	20,000	0.232 (5.9)

Overlay Test

Specimens with three levels of air voids from each asphalt mixture were tested using the overlay tester. Three replicate specimens were tested at each air void level. Like other performance tests, specimens for overlay testing were also collected from strips that were compacted using a different number of roller passes, resulting in different levels of air voids. Researchers evaluated

two parameters: the maximum load required to initiate crack at first loading cycle and the number of load cycles required to cause specimen failure. Usually, failure is defined when the crack propagates all four faces of specimens or decreases to 7 percent of the maximum load, load measured on first cycle, whichever comes first.

Figure 3-8(a) shows the maximum recorded load needed to initiate the crack in the first cycle for all tested specimens. Figure 3-8(a) shows a fair relationship between the load needed to initiate the crack and the percent air voids in the specimens. Specimens with less percent air voids required higher loads than the specimens with higher percent air voids. The results demonstrated the effect of compaction level on fatigue cracking in asphalt pavements. Figure 3-8(b) shows the number of cycles until failure for different asphalt mixtures. There was no specific trend or relationship between the number of cycles until failure and percent air voids in the specimens. However, the Type C HMA lasted longer than the other two mixtures. This is due to the fact that this mixture, Type C HMA, had modified binder (PG 76-22) while the other two mixtures had unmodified binders (PG 64-22) with 20 percent RAP. Earlier work by Masad et al. (2009a) pointed out the influence of sample air void distribution on cracking life, this being on lab molded samples. The variability of results from these field cores with widely different air void distributions is not surprising. The PG64-22/WMA/RAP samples have the lowest cracking resistance. The cracking life for these samples decreases with increasing air voids, but even at low air voids the overlay tester results are poor at less than 25 cycles to failure (for lab molds samples at 7 percent air voids, the recommended results is more than 300 cycles for good quality surfacings). Air voids is only one factor influencing cracking resistance; the percent binder used, amount of RAP, and aggregate gradation are other factors.
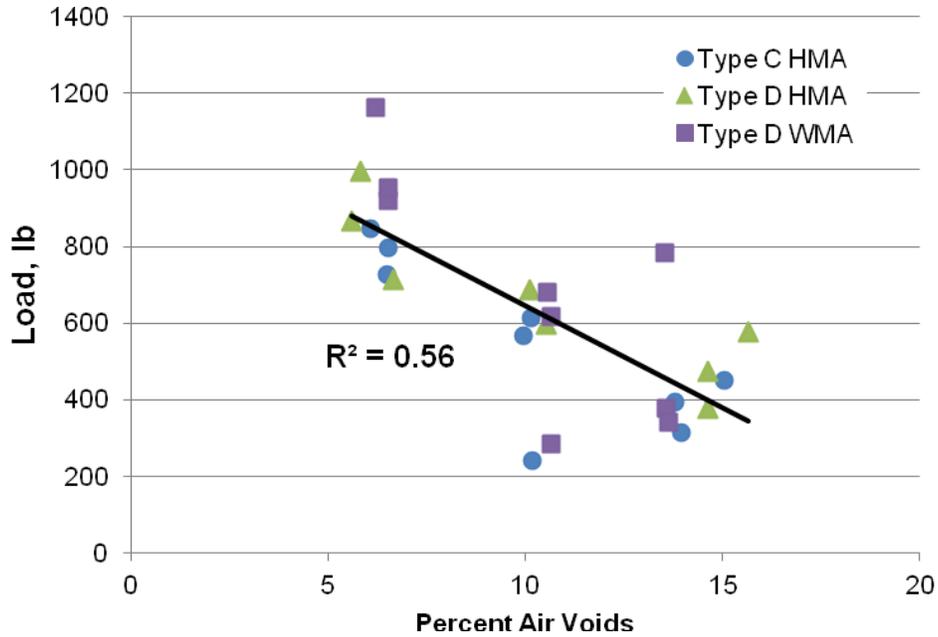
(a) Maximum Load in the First Cycle vs. Percent Air Voids
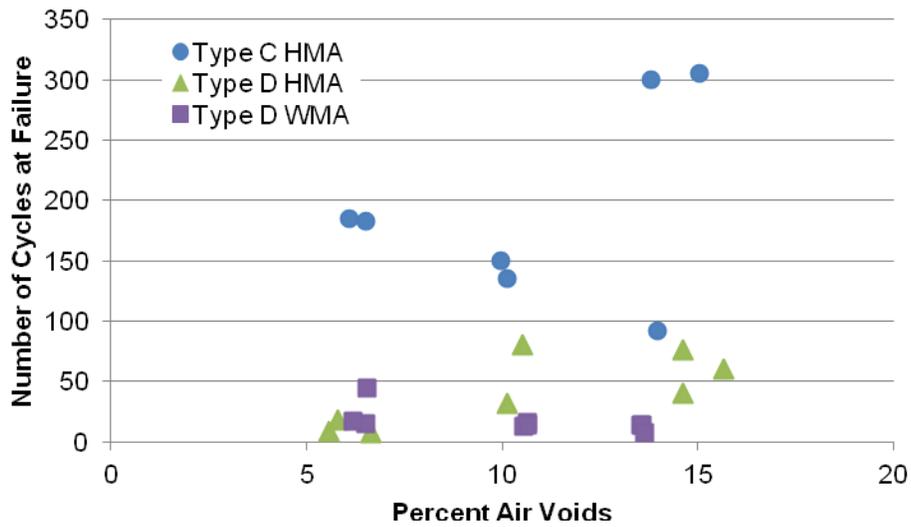
(b) Number of Cycles until Failure vs. Percent Air Voids

Figure 3-8. Overlay Test Results.

CONCLUSIONS

This part of the study assessed the applicability of using the GPR as a non-destructive quality control tool to assess the compaction level in asphalt pavements. In addition, it evaluated the effect of level of compaction on performance of WMA and HMA mixtures. The following are the findings of this study:

- The GPR was found to be an effective tool for rapidly assessing the compaction level in asphalt pavements. There was an excellent correlation between GPR air void distribution maps and the air void maps generated from core measurements. This new application of GPR is useful to obtain maps of air voids in asphalt pavements at a relatively low cost and without causing interference to traffic.

- The compaction level highly affected the performance of asphalt mixtures. Specimens that had less percent air voids performed better in both wet and dry conditions. Specimens with less percent air voids had less rutting in the Hamburg wheel-tracker, higher load in the first cycle of the overlay tester, and a higher strength in the indirect tensile test. These results can be useful to set the quality control limits for percent air voids during construction.

- There were no problems in compacting WMA to the desired density. In fact, the compaction of the WMA mixture was achieved with slightly less compaction effort than with the HMA mixture.

- The IDT results showed that WMA specimens performed better than the corresponding HMA specimens in dry conditions. However, the reduction in strength of the wet WMA mixtures was higher than the wet HMA mixtures.

CHAPTER 4
OVERVIEW OF TTI'S COMPACTION MONITORING SYSTEM

In the second phase of this study, the researchers developed an automated system called the compaction monitoring system (CMS) for monitoring the quality of compaction in real time. The CMS consists of a GPS unit mounted on the roller to track the location of the roller on the mat. Temperature sensors are attached to the sides of the roller to record the mat surface temperature. In addition, an accelerometer sensor is mounted on the roller to determine the mode of operation—static or vibratory. The CMS monitors the location of the roller on the mat and the number of passes across the mat. Each pass is multiplied by the effectiveness factors across the roller's width (Figure 2-14) in order to produce the CI distribution. Such distribution is converted to colored maps in real time. The operator of the roller and the engineers at the site are able to see the colored map on a screen during the compaction. The operator can use the colored maps to adjust the compaction patterns (by changing number of passes, overlapping, and overhanging) needed to achieve a uniform CI in order to obtain the required density uniformly across the mat. In addition, these maps can be converted to predict density distribution if the compaction curves for each compaction method are already known, as discussed later in Chapter 6 as future work.

INTRODUCTION

In TxDOT Project 0-5261, *Application of Imaging Technology to Improve the Laboratory and Field Compaction of HMA*, the researchers recommended developing a setup that can be used on board that records the number of passes and compaction index in real time (Masad et al. 2009a; Masad et al. 2009b). The results of Chapter 2 confirmed the need for such a system to improve and document the compaction process of asphalt mixtures. In this part of this current study, the researchers of TxDOT 0-6992 developed CMS and field tested to measure the uniformity of new HMA overlays. This system uses the latest GPS technologies and various sensors to provide 100 percent coverage of the new mat. The post-processing software system produces color-coded maps showing;

- The number of roller passes on the entire mat.
- The compaction effectiveness (number of passes * effectiveness factor).
- The temperature of the mat on the first pass of the roller.

The complete system was demonstrated on a number of new overlay projects in Texas, and Chapter 5 reveals the typical results. The complete system developed in study 0-6992 is described in detail in report 0-6992-1, which details the system components and data acquisition and processing systems. The system provides a real-time display for the roller operator to determine if all areas of the mat are receiving a similar compaction effort as well as post-processing capabilities to document the uniformity of mat temperatures and compaction effectiveness.

The following items were integrated into TTI's asphalt compaction monitoring system:

- A high-accuracy GPS positioning system.
- Two infrared sensors for measuring the asphalt surface temperature.
- One accelerometer for detecting whether the roller is vibrating.
- A "Toughbook" computer for collecting and viewing the data.
- A battery for the power supply.
- A data acquisition system for converting the analog signals to digital data.

Figure 4-1 shows the operational system.
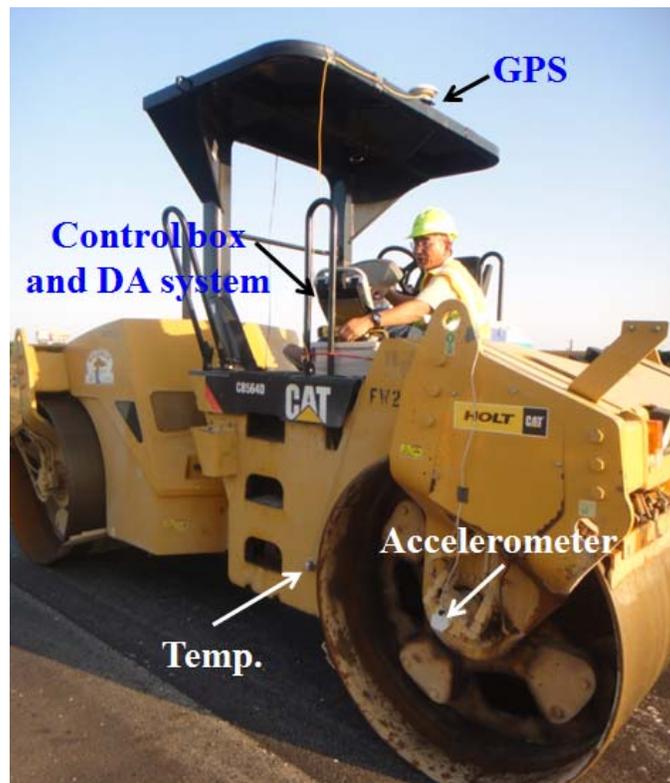
Figure 4-1. TTI's Compaction Monitoring System.

DATA COLLECTION WITH THE ASPHALT COMPACTION MONITORING SYSTEM

The intention of the designers of the compaction monitoring system was that the data would eventually be collected and viewed by the roller operator. The system should take less than 10 minutes to install on any roller, and all of the sensors are attached using magnets that can be easily removed. The data acquisition system uses a rugged computer that can withstand the harsh environment on the roller. The operator can view in real time a color-coded map showing the total mat coverage for the entire mat being compacted. Also, the same data can be saved and post processed to document the effectiveness and uniformity of the compaction process.

As the operator moves back and forward over the new mat, the GPS system accurately tracks the position of the roller and the infrared sensors measure the mat temperatures on either side of the roller. The location and temperature information are displayed in real time for the operator to view. The number of passes and compaction effectiveness displays are continually updated as additional passes are applied to the mat. Figure 4-2 shows a typical compaction effectiveness chart displayed in real time during rolling. By using these icons [icons] provided at the top of this display, the operator can display either number of roller passes or mat temperatures.
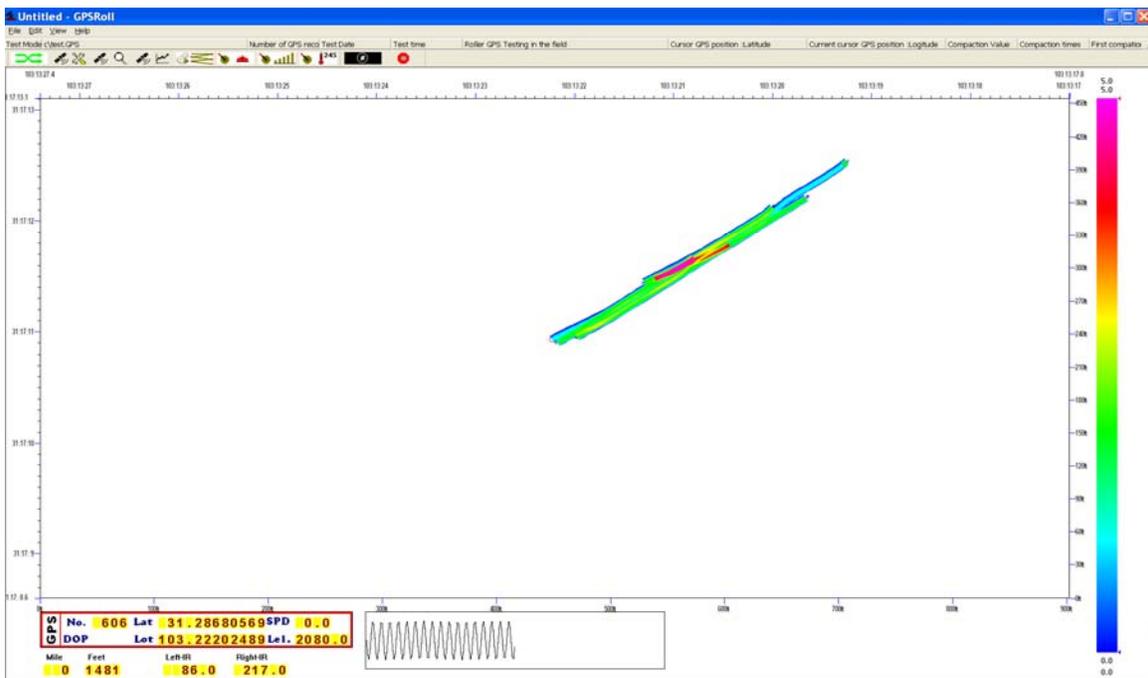

Figure 4-2. Real-Time Display of Compaction Effectiveness.

79

The right side of the screen is the scale for the color display. The numbers at the top and bottom of the scale (5 and zero) are the range of compaction index (# passes * effectiveness factor) values displayed in the figure. Any location with a compaction index of 5 on the effectiveness scale would be colored red, and values close to zero would be blue. On the bottom left of the screen, the user can see all the information from the temperature and displacement sensors and the GPS receiver. This display is shown below in Figure 4-3.
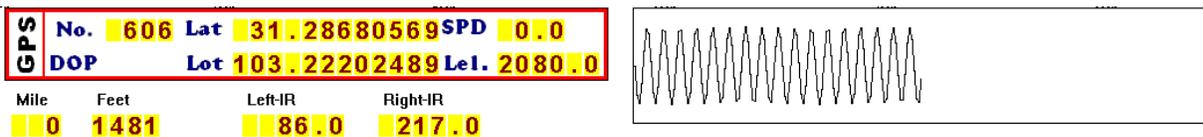

Figure 4-3. Sensor Display from Data Acquisition Screen.

In Figure 4-3, the top box displays the GPS information showing both the latitude and longitude of the current position of the roller. The left- and right-side temperature readings are shown in degrees Fahrenheit. This is a typical first pass of most overlay compaction projects where the left-side reading is 86°F and the right side is 217°F. As with most roller operations, the first pass runs down the edge of the mat, where the left-hand sensor is not on hot asphalt. The analysis/display system takes this into consideration; if there is more than a 30°F temperature difference between the two sensors, then the system assumes that one sensor is off the mat. The high value is therefore used and displayed on the color plot. However, if reasonable readings are found on both sensors, then the system averages these values and saves and reports the value for the entire width of the roller (typically 7 ft) at that location. Under normal operations, a temperature reading is taken for every 8 inches of travel along the mat. It is the temperature on the first pass of the roller that is displayed.

On the right side of Figure 4-3, there is a sine wave showing the current vibration amplitude of the roller. If the operator turns off the vibration, this chart will show a flat line. Currently, accelerometer data are collected and saved to the data file, but with this prototype system, these data are currently not processed or displayed.

Figure 4-4 is a blowup of the compaction effectiveness display from Figure 4-2. This information is displayed in real time for the roller operator to view the coverage on the mat. Displays such as this should be useful to ensure that a uniform effort is being applied to all areas on the mat. The red colors represent a compaction index of 4 to 5, the green 2 to 3 and the blue 1 to 2.

Under ideal conditions the map should be all a similar color, blue areas could be areas where the operator needs to apply more passes.
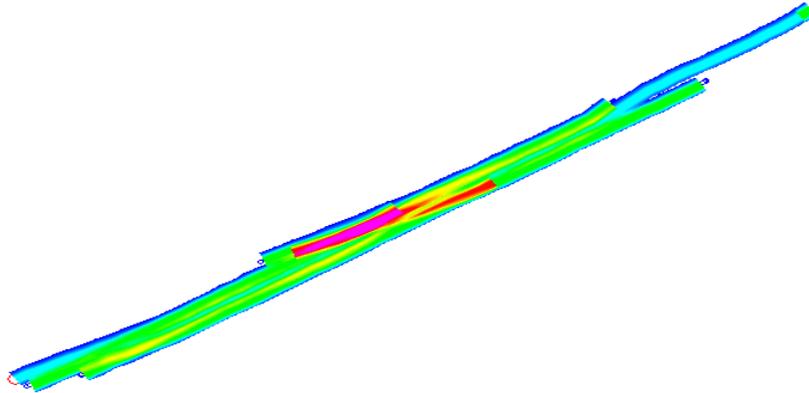
Figure 4-4. Color-Coded Compaction Effort Map Real-Time Displayed.

If the user starts the data acquisition by selecting either the or button, then the real-time display viewed by the roller operator will be either the number of roller passes or mat temperature at the first roller pass.

POST-PROCESSING AND DISPLAY SOFTWARE

This section illustrates the steps required to post process the field data with the CompactView software developed in study 0-6992. Researchers submitted this software as a deliverable to project 0-6992. Figure 4-5 displays the main menu screen in the post-processing mode. Table 4-1 lists the options available for post processing the raw field data.
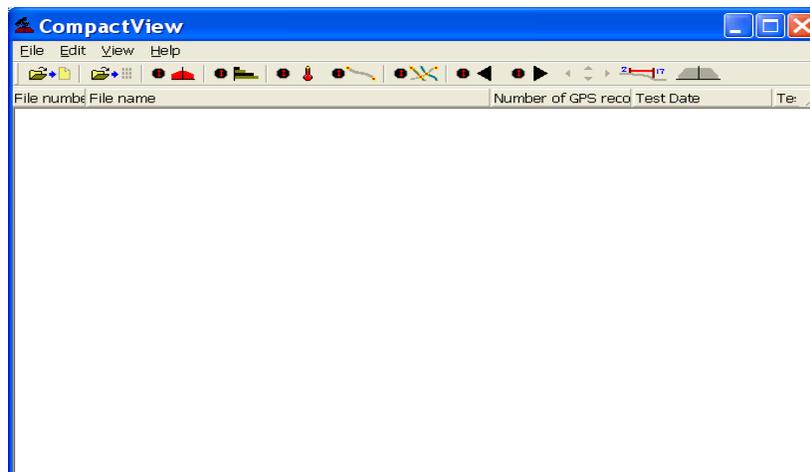
Figure 4-5. Post-Processing Toolbar and Main Interface.

Table 4-1. Explanation of the Post-Processing Tool Bar Buttons.

| Button Image	Explanation of Each Button
	Load the single file to do the single-file processing.
	Load one project folder and do the group-file processing.
	Show the compaction effectiveness color map chart on the display screen.
	Show the number of roller passes color map chart on the display screen.
	Show the temperature at the first roller pass color map chart on the display screen.
	Show a line diagram of all the roller passes over the section.
	Show the rolling path chart for all files in the project folder.
	Show the previous file in the project.
	Show the next file in the project.
	Zoom the data to fit the screen.
	Change the roller compaction effectiveness chart. These relate the compaction effectiveness for different lateral locations on the drum, where the edge is less effective than the center of the drum.

The field studies conducted as part of project 0-6992 and described in Chapter 2 of this report demonstrated that based on controlled field studies and lab-measured cores, the center of the roller has better compaction effectiveness than the edge. This is believed to be based on the lack of confining of the mat at the edge of the roller. This non-uniformity of roller compaction effort will affect the final density of the mat. Pressing the ![icon] icon displays the currently recommended compaction index profiles for steel-wheel rollers. The recommended profile based on this study and earlier studies is the model shown in Figure 4-6. From this profile, for a 7-ft-wide roller drum, 3 ft in the middle part gets full compaction (this value is defined as 1.0). At the edge of the roller drum, the effectiveness factor is only 0.3 or 30 percent of that in the middle of the drum. This is the key calculation made by the CompactView system. The accurate GPS tracks the position of the roller and for each pass calculates the compaction effectiveness for the entire roller width by multiplying the number of passes by the effectiveness factor index from Figure 4-6. Therefore, locations that only receive passes with the edge of the roller will have a computed compaction index much less

than those compacted under the center of the roller. Currently, it is recommended that the TTI distribution shown in Figure 4-6 be used for all data processing.
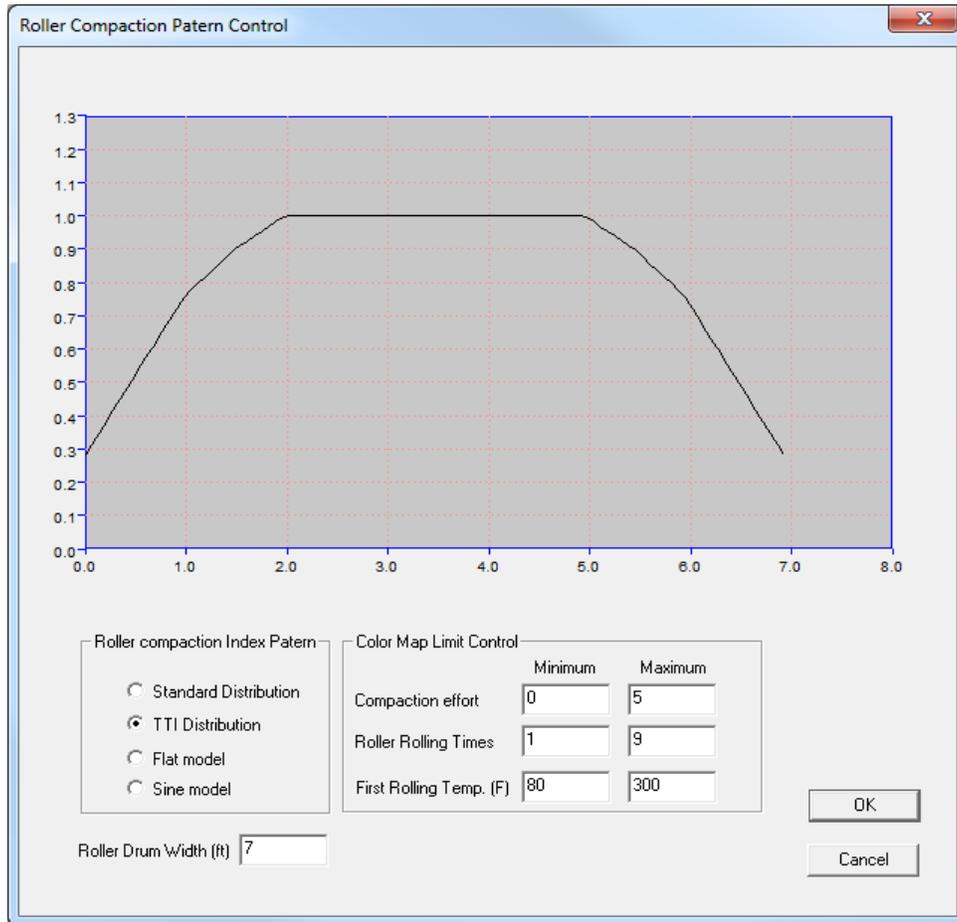
Figure 4-6. Recommended Roller Effectiveness Distribution Based on Study 0-6992.

This dialog box also permits the user to control the graphical display of the color map by changing the max and min limits on each of the color maps. For example, for the temperature map, the lower limit (blue color) is 80°F and the upper limit (red color) is 300°F. These values can be changed in this dialog box.

SINGLE-FILE POST PROCESSING

To process a single file, the user clicks the toolbar button ; then a file open dialog box permits the user to select the raw data file to open and display. All of the files collected have the *.GPS extension. Once selected, the system displays the data for the complete section tested, which in the example shown in Figure 4-7 is over 2300 ft on this section. As described below, the user has the option to zoom into any location in the data set.
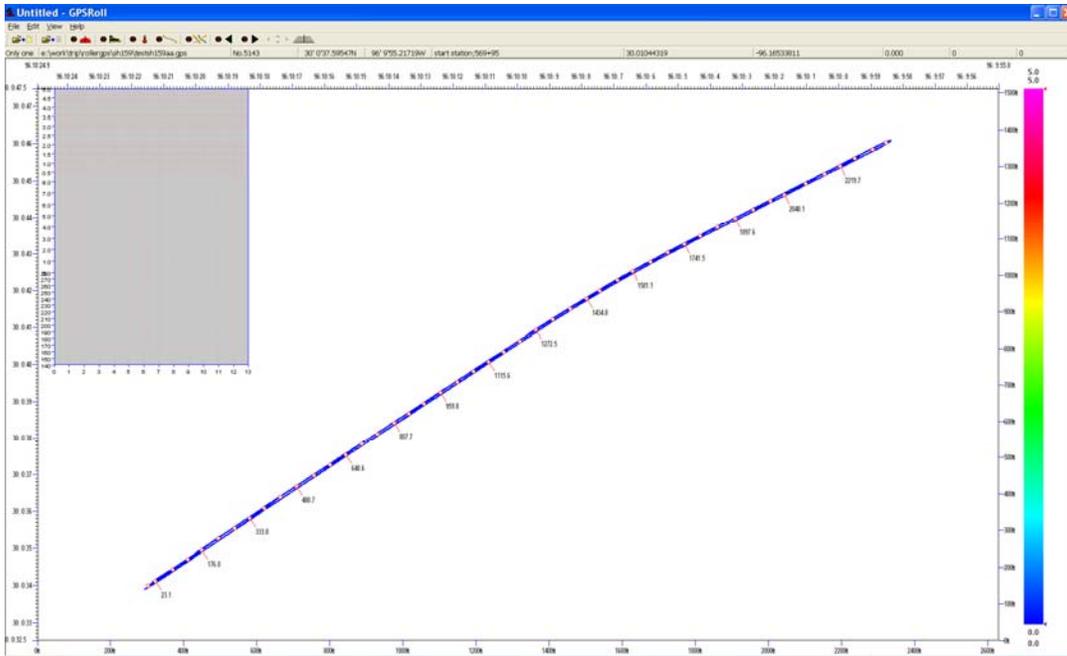
Figure 4-7. First Display Screen Showing the Entire Section Length.

The user can then click any one of the buttons to display the following: ⬤ 🔺 (compaction effectiveness), ⬤ 🟨 (number of passes), or ⬤ 🌡 (first pass temperature). Figure 4-8 displays an example of what the user sees when selecting the ⬤ 🔺 button.
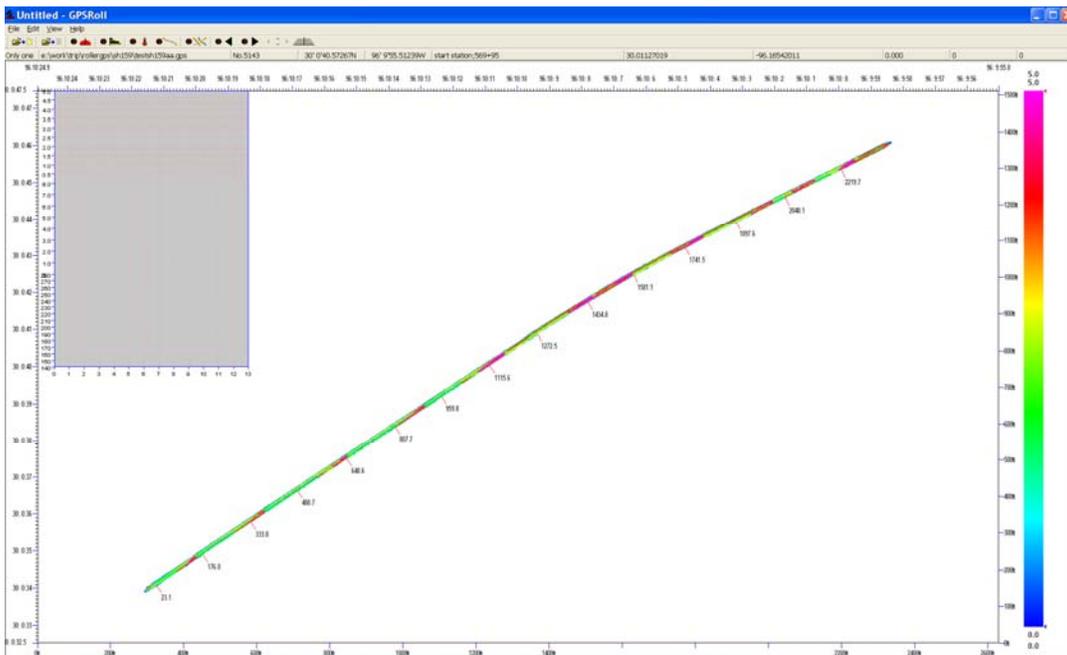
Figure 4-8. Compaction Effort Color Map View of the Loaded Data File.

Since the width of the paved lane is typically 12 ft, this distance is relatively small compared with the length of the section. Therefore, the display of the complete section is very difficult to review to find problem areas. For this reason, an option was included to permit the user to zoom into any part of the project. To zoom in, the user puts the cursor in the required location and while holding down the left mouse button, drags the mouse, as shown in Figure 4-9, as a black rectangle is superimposed on top of the project. When the user releases the mouse button, the information from only the selected section is displayed, as shown in Figure 4-10.
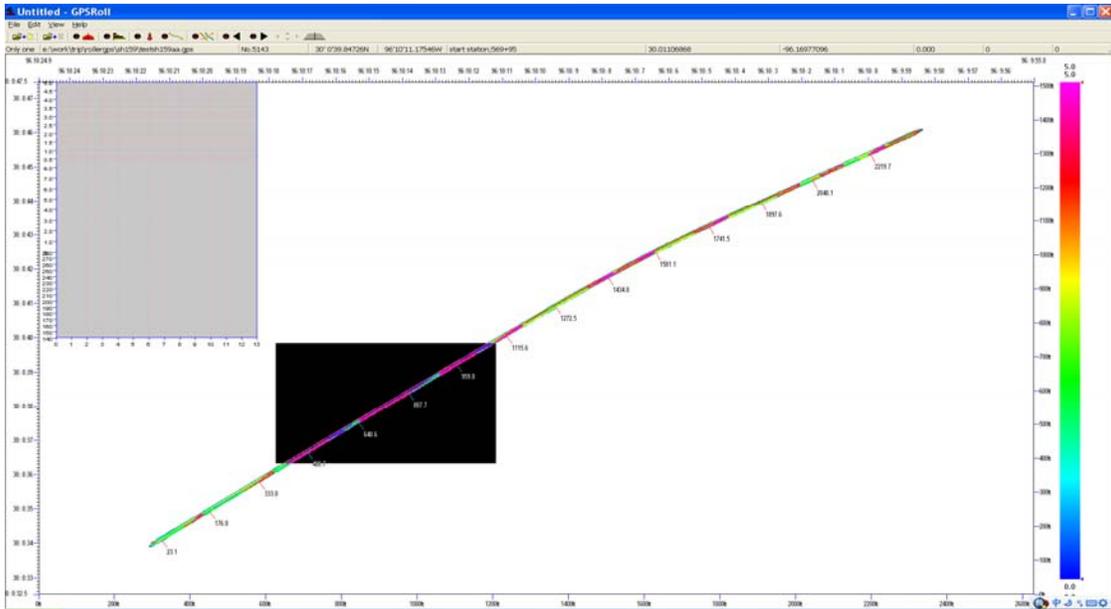
Figure 4-9. Compaction Effort Color Map Selection View.

Figure 4-10. New Zoomed View of Color-Coded Compaction Effort.

85

If the user places the mouse cursor on any location in the zoomed view, some very useful information will be displayed in the upper five boxes of the color plot. As shown in Figure 4-11, placing the cursor at the location of the "X" will result in the following data being shown in the boxes at the top of the screen:

Longitudinal Position from GPS	30.01208
Latitudinal Position from GPS	−96.167853
Compaction Effectiveness	6.32
Number of passes of roller over this location	8
Temperature at the first roller pass	239°F
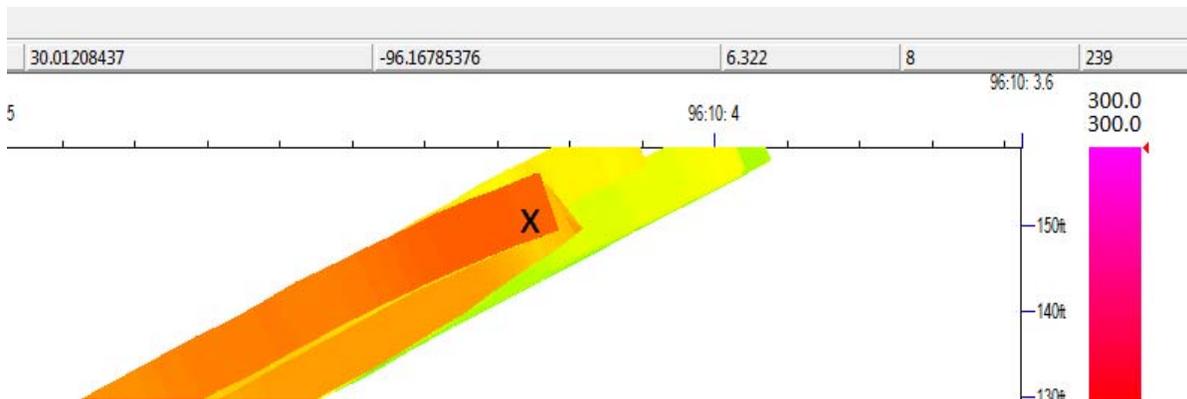
Figure 4-11. Point-Specific Compaction Data.

Also, if the user clicks the mouse at a location of interest, the transverse distribution of compaction and temperature data across the mat will be displayed, as shown in the box in the upper left corner of Figure 4-12 and in detail in Figure 4-13. The upper chart is the compaction effectiveness index, the middle one is the number of passes placed across the mat, and the lower one is the temperature profile during the first pass over the mat. The width shown in Figure 4-13 is 15 ft, but the paving width is only 12 ft. This means that there was at least a 1.5-ft overlap of the roller off each side of the mat.

If there is any uncertainty about the number of passes placed over any section of the mat, then clicking the ⬤ button from the main menu screen will display the path of the roller over that segment. Figure 4-14 shows an example of this. The normal rolling pattern is typically two passes on either side of the mat with a final pass down the center of the mat. Clearly, in this case,

the center pass was not made, and at this location, the effectiveness of compaction in the middle of the mat is in question.
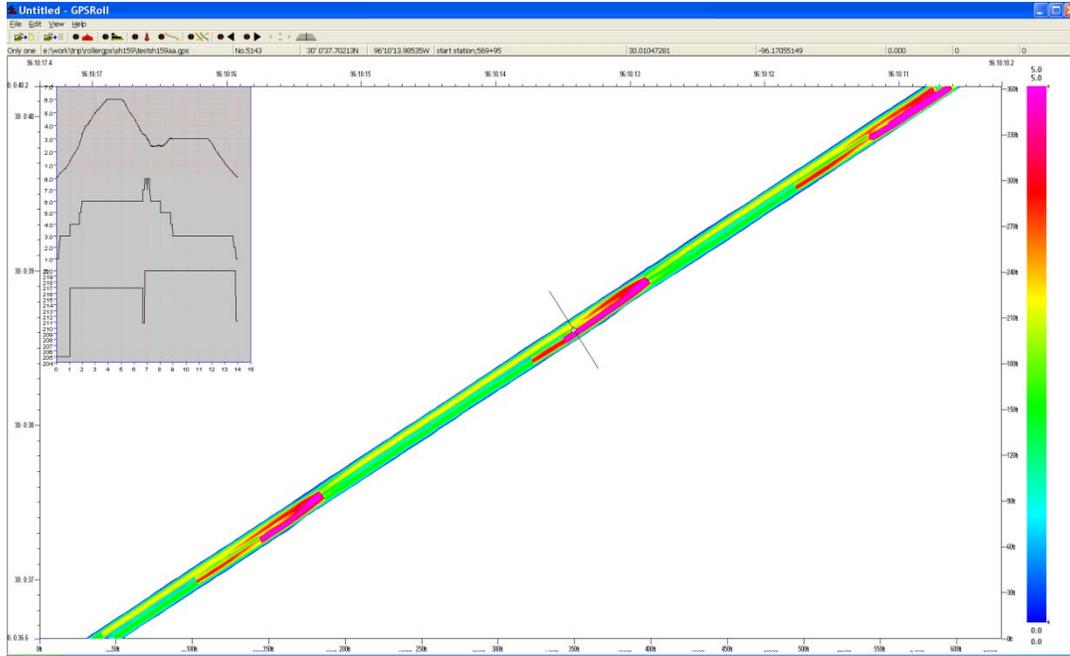
Figure 4-12. Transverse Distribution of Compaction Data at User-Selected Location.
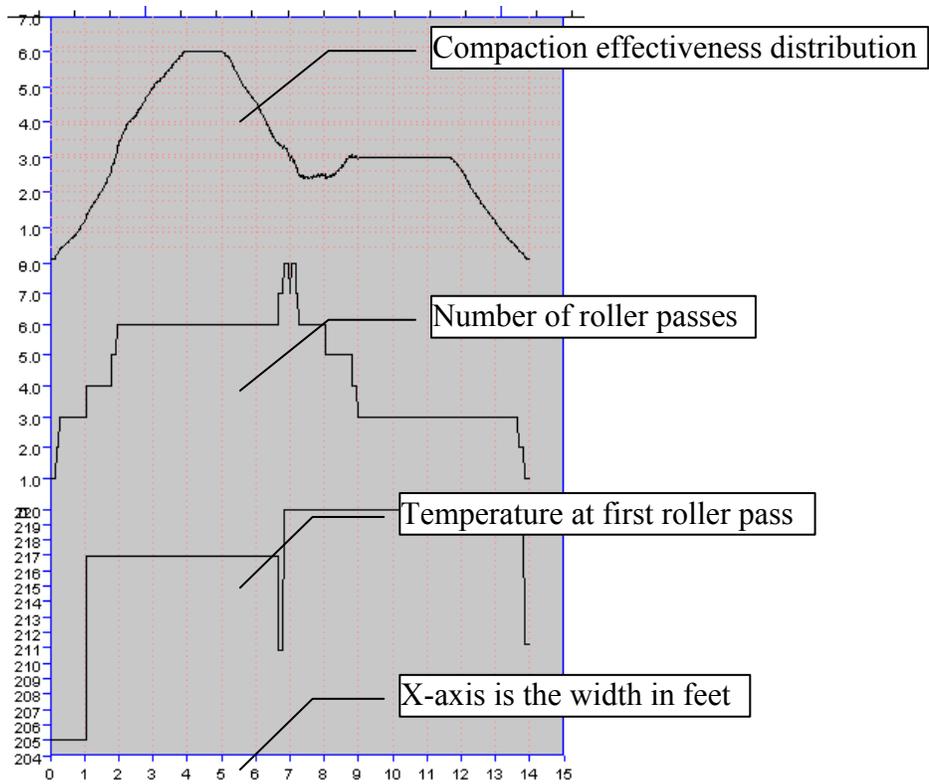
Figure 4-13. Details of the Transverse Distribution Data.
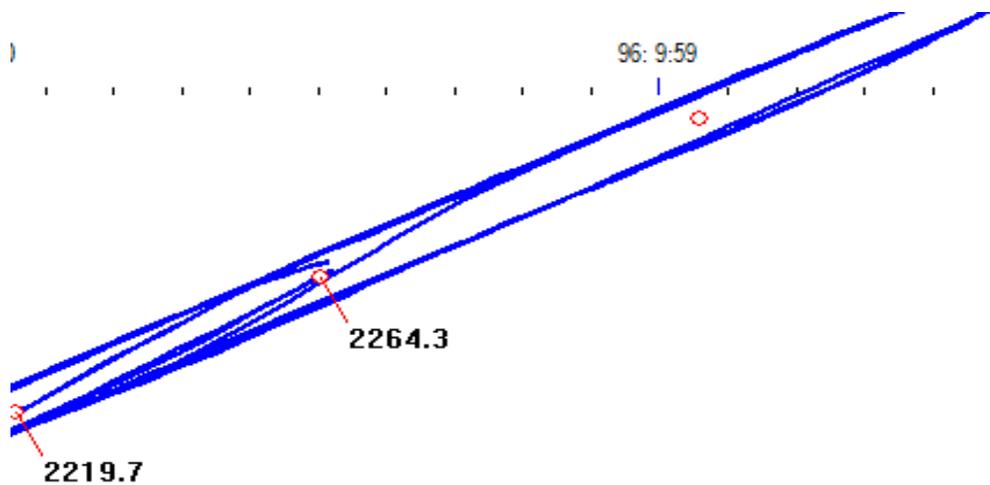
Figure 4-14. Paths Taken by the Roller in the Compaction of This Segment.

88

One last option available to the user is to modify the color display by using the mouse to change the upper limit on the color scale. To do this, the user places the mouse over the red arrow and drags the arrow down to a different level, as Figure 4.15 illustrates. The two numbers at the top of the screen are the maximum values set up in the initial setup menu screen. In this case, the max temperature (300°F) is the surface temperature, at which the display is colored red. By moving the red triangle, the upper level is reset to 260°F, as shown. In this case, the red color will be associated with temperatures at or above 260°F. The color display is automatically changed to reflect the color associated with the new level. The lower end of the temperature scale can also be changed, as can the compaction effectiveness and number of passes charts.

Figure 4-15. Resetting the Color Scale.

CHAPTER 5
FIELD VALIDATION

INTRODUCTION

The research team identified and conducted testing at seven field asphalt mix compaction projects in Texas. The research team made an attempt to find wide ranges of HMA or WMA projects to validate the compaction monitoring system. The primary objective was to find projects with varieties of mixture types and lift thicknesses, as well as roads with different configurations. All of the projects were constructed during the summer of 2011. Some of these mixtures also contained recycled asphalt pavement (RAP) and recycled asphalt shingle (RAS).

DESCRIPTION OF TEST SECTIONS

The research team sought TxDOT districts and contractors to volunteer to participate in this field experiment. Based on the responses from TxDOT districts and contractors, seven projects that also met criteria mentioned earlier were selected. These projects are as follows:

- FM 2854 in the Houston District.
- SL 340 in the Waco District.
- SH 31 in the Waco District.
- SL 111 in the Austin District.
- US 87 in the Austin District.
- US 290 in the Austin District.
- SH 159 in the Yoakum District.

The researchers recorded the compaction patterns and number of passes; conducted tests in the field; obtained field cores and plant mix; and conducted laboratory tests on laboratory-compacted specimens and field cores. In these construction sites, the research team manually recorded the movement or position of each roller at some selected locations. Later, cores were extracted across the mat from those locations. Typically, the research team did not ask to change the rolling pattern. However, in a few instances, contractors were asked to change some rolling pattern for a small length to carry out some mat density testing after each roller pass. Table 5-1 provides a summary of mixtures used in these field projects. Table 5-2 summarizes the equipment used in these

projects for mixture compaction. The following paragraphs briefly describe the research effort at these construction projects.

Table 5-1. Summary of Mixture Designs.

Highway ID	Mixture Type	Date of Field Testing	Aggregate (Major)	Binder Grade (Virgin)	Optimum AC %	Max Rice Sp Gr.	VMA at Op. AC.	Design Air Void, %
FM 2854	Type D	June 2011	Sandstone with RAP	PG 64-22	4.8 (with RAS)	2.570	15.0	3.5
SL 340	Type C	June 2011	Gravel with RAP	PG 64-22	4.8 (with RAS)	2.448	14.0	3.0
SH 31	Type B	July 2011	Limestone with RAP	PG 64-22	5.2 (with RAS)	2.491	15.6	3.0
SL 111	Type C	August 2011	Limestone with RAP	PG 64-22	5.2 (with RAS)	2.392	15.2	3.0
US 87	CMHB-F	August 2011	Sandstone with LS	PG 76-22	6.0	2.395	17.4	3.0
US 290 (detour)	Type C WMA	August 2011	Limestone with RAP	PG 64-22	5.2	2.438	14.9	3.0
SH 159	Type D	August 2011	Limestone with RAP	PG 64-22	5.3 (with RAS)	2.427	15.4	3.5

Table 5-2. Description of Compaction Patterns.

Test Section	Compaction Pattern		
	Breakdown	Intermediate	Finish
FM 2854	Steel-Wheel Vibratory	Pneumatic Tired	None
SL 340	Steel-Wheel Vibratory	Pneumatic Tired	Steel-Wheel Static
SH 31	Steel-Wheel Vibratory	Pneumatic Tired	Steel-Wheel Static
SL 111	Steel-Wheel Vibratory	Pneumatic Tired	Steel-Wheel Static (small)
US 87	Steel-Wheel Vibratory	None	Steel-Wheel Static (small)
US 290 (detour)	Steel-Wheel Vibratory	Pneumatic Tired	Steel-Wheel Static (small)
SH 159	Steel-Wheel Vibratory	Steel-Wheel Static	Steel-Wheel Static

FM 2854 in the Houston District

Testing at the Houston District site was the first field experiment during the summer of 2011. This overlay job was located on FM 2854 near the Conroe area in the Houston District. This project used a Type D mixture with RAP and RAS in it. Unlike other job sites, the vibratory roller operator moved the roller in a curved way from one side of the mat to the other side, which made the manual location tracking very difficult. The width of paving was 16 ft with 2 inches of compacted mat thickness. The longitudinal joint was restrained by overlay already paved on the opposite direction. The other edge of the mat was free.

SL 340 in the Waco District

Testing at this site was conducted on the northbound entrance ramp of SL 340 just north of US 84 in Waco. Type C overlay paving at this site was conducted during the nighttime. Prior to paving, the surface was milled. This site was particularly interesting in that the paving width at some palaces was as high as 20 ft. Since it was a ramp, the paving width was variable along the length of this test section. This variable width provided the opportunity to compare the manual tracking of the roller position with the tracking recorded by CMS. Along with checking the temperature using a handheld laser gun, the researchers collected the mat temperature using the Pave-IR bar. Cores were taken at two rows as well as at low-temperature spots.

SH 31 in the Waco District

This construction site was located on the east side of Waco. This part of the highway is a new construction. The research team conducted testing at two locations on this highway while the contractor was paving a Type B mix on top of a flexible base. The first test section was located on the westbound shoulder of the main roadbed, and the second location was on a side road. The Type B mixture contained limestone aggregate with RAP and RAS. The paving width at the two test locations were 13 and 15 ft, respectively. The thickness of the compacted mat was 4 inches. The first location had one free edge, while the second location had both edges free. Figure 5-1 shows the coring location on the SH 31 test section.

93
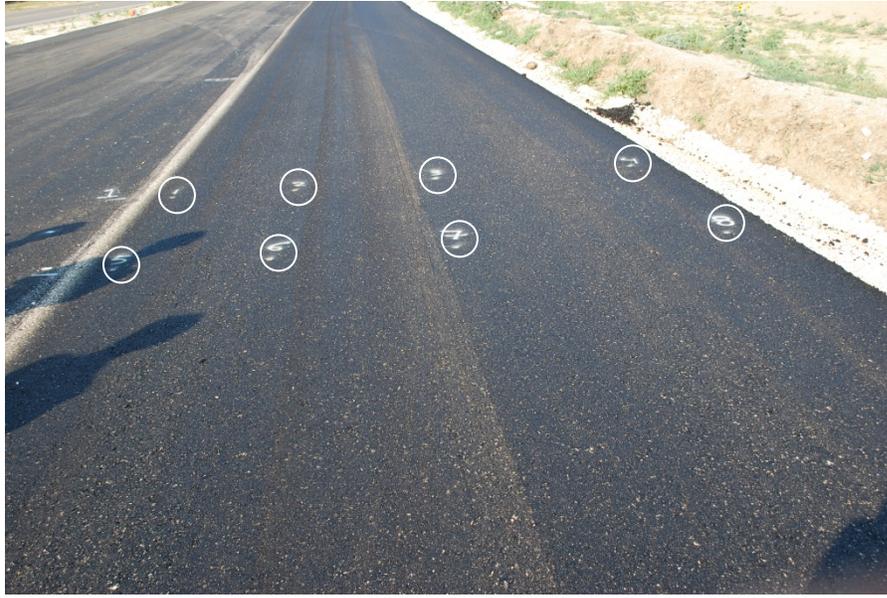
Figure 5-1. Coring Location on SH 31 in the Waco District.

US 87 in the Austin District

The US 87 test section was located just northwest of Fredericksburg in the Austin District. The mixture used at this site was CMHB-F designed with primarily sandstone and PG 76-22 binder. The mat thickness was only 1 inch. The mix was placed on top of a milled HMA layer. Figure 5-2 shows density measurement using a nuclear gauge.

Figure 5-2. Density Measurement on US 87 in the Austin District.

SL 111 in the Austin District

SL 111, or Airport Boulevard, is an urban street located in the city of Austin. It has three lanes in each direction with a turning lane in the middle. The test section was located on the inside lane. The paving width was 12 ft with both edges free or unrestrained. The contractor used a Type C mix with RAP and RAS. The thickness of the compacted mat was 2 inches. This site was paved during night.

US 290 in the Austin District

This test site was located on US 290 near US 183 in the city of Austin. The test was conducted on asphalt overlay construction intended for a traffic detour. The contractor used a Type C WMA mixture that contained limestone with some RAP. Evotherm 3G technology was used to produce this WMA mixture. The paving width was 12 ft with 2 inches of mat thickness. The mat had one free and one restrained edge.

SH 159 in the Yoakum District

This rural highway with one lane in each direction is located just east of Bellville in Austin County under the Yoakum District. A Type D mixture was paved on top of a recently paved level-up course. The mixture used primarily limestone aggregate with some RAP and RAS. PG 64-22 virgin binder was used in this mixture. Both edges of the paving mat were free or unrestrained. During compaction, the contractor used only steel-wheeled vibratory and static rollers.

EVALUATION OF THE DENSITY ACROSS THE MAT

In these field projects, the researchers recorded the number of roller passes and their relative locations during each pass with respect of the edge of the mat. Field cores were obtained from different locations of the paving mat (Figure 5-1). The percent air voids of the extracted field cores were measured using the SSD procedure (AASHTO 2002). Table 5-2 shows the compaction patterns for each test section. The steel-wheel vibratory roller was utilized as a breakdown roller, while the pneumatic and static rollers were used as intermediate and finish rollers, respectively. The pneumatic and static rollers were applied after the mat relatively cooled down. The number of passes of the steel-wheel vibratory roller was plotted along with the percent air voids across the test sections. The percent air voids represents the average percent of air voids of at least two cores taken

longitudinally at a given distance from the pavement section edge, as Figure 5-1 illustrates. In addition, the CI, which is the summation of the number of passes of the steel-wheel vibratory roller multiplied by the effectiveness factor corresponding to each pass, was plotted against the percent air voids for each test section. As discussed in Chapter 2, the efficiency of compaction (reducing air voids) at a given point on a paving mat was found to be a function of the location of this point with respect to the roller width. The effectiveness factor describes the efficiency of compaction across the roller width. The efficiency distribution of the compactive effort across the roller width was presented in Figure 2-4.

Figures 5-3 and 5-4 show examples of the distributions of the average percent air voids and compaction index across the mat, correlation between the average percent air voids and number of passes, and correlation between the average percent air voids and compaction index. The results of the remaining test sections are presented in Figures A-21 through A-25 in the appendix. The results show that the CI correlated very well with the percent air voids for the test sections. Low CI resulted in higher air voids across the mat and vice versa. The correlation between the CI and percent air voids is better than the correlation between number of passes and percent air voids for most of the test sections, which confirms the findings in Chapter 2. Table 5-3 presents the R-squared values between percent air voids, number of passes, and compaction index for the field test sections. Strong correlation was found between compaction index and percent air voids except for in two test sections: US 87 and SL 111. The researchers noted that in the SL 111 test section, two passes of the steel-wheel vibratory roller were applied as breakdown, while 10 passes of the pneumatic roller were applied as intermediate rolling while the mat was still hot. The researchers believe that the compaction was accomplished mainly using the pneumatic roller in this project. The mixture used in the US 87 test section was CMHB-F; however, it had higher average percent air voids, about 15 percent. This particular mixture was found to be comparable to fine PFC. The density of PFC mixtures does not change much with the increase in the number of roller passes.
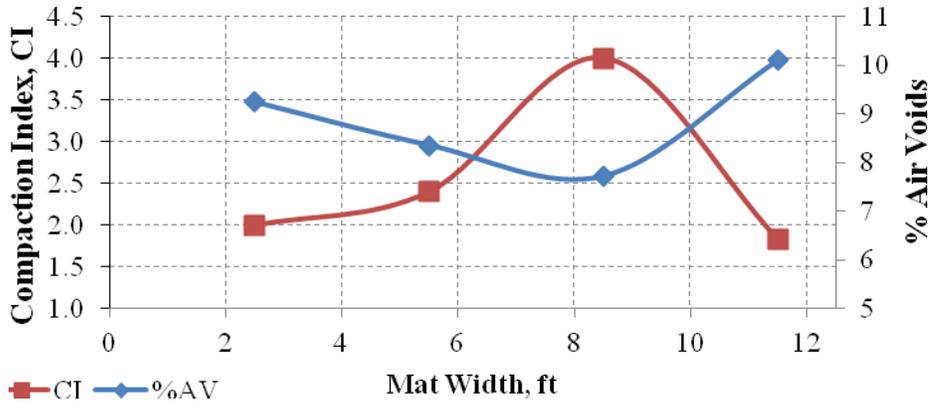
CI and Percent of Air Voids Distributions across the Mat
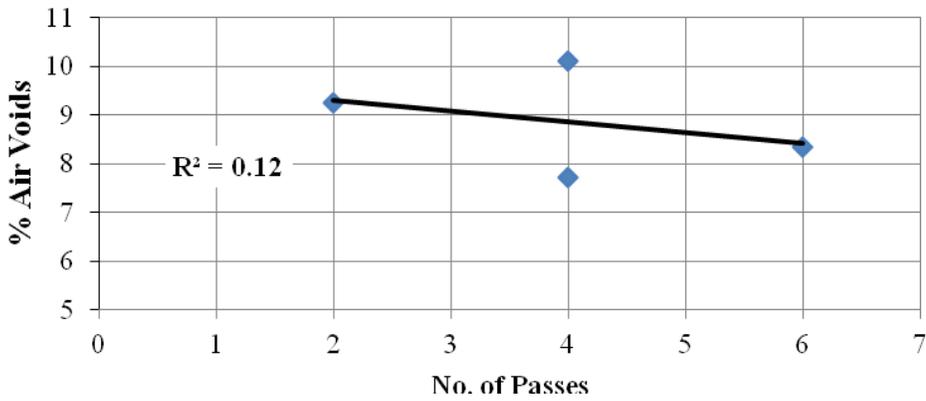
Number of Passes versus the Percent of Air Voids
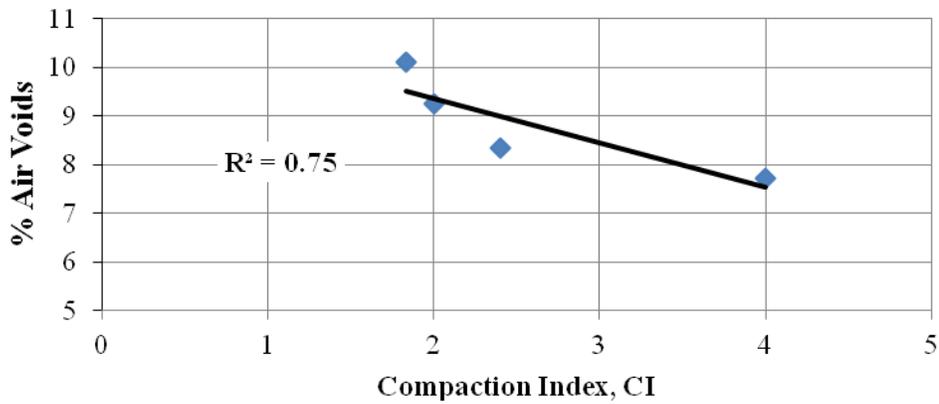
Compaction Index versus the Percent of Air Voids

Figure 5-3. Test Section US 290.
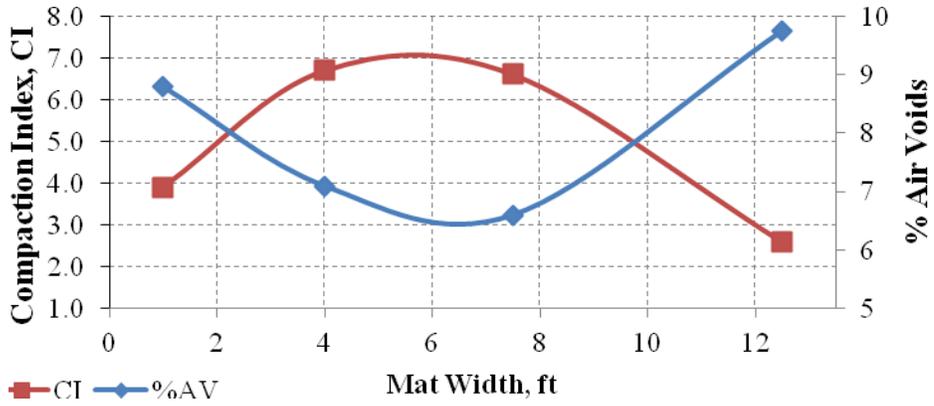
CI and Percent of Air Voids Distributions across the Mat
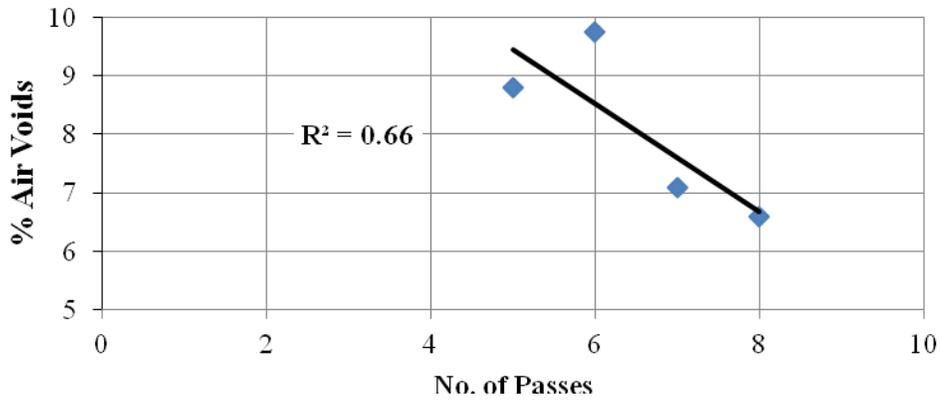
Number of Passes versus the Percent of Air Voids
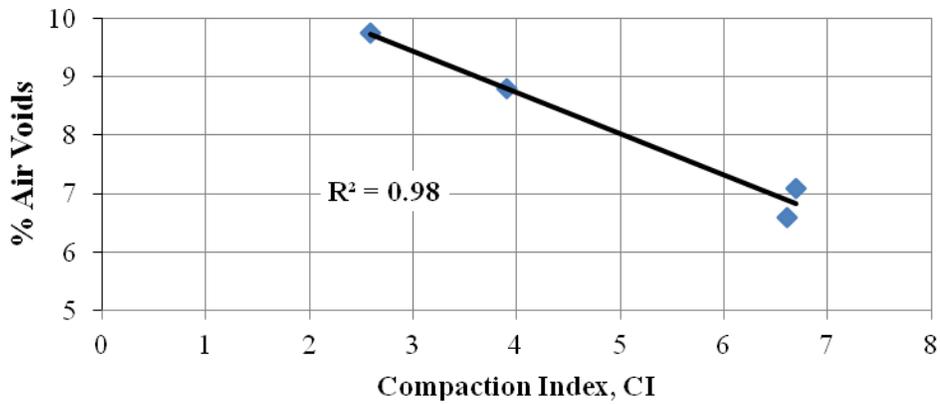
Compaction Index versus the Percent of Air Voids

Figure 5-4. Test Section SH 31 (Test Section 1).

Table 5-3. R-Squared Values between Air Voids, Number of Passes, and Compaction Index for the Field Test Sections.

Project	Section No.	R-squared	
		% AV vs. No. of Passes	% AV vs. CI
US 290	1	0.12	0.75
SH 31	1	0.66	0.98
	2	0.78	0.85
FM 2854	1	0.75	0.85
	2	0.59	0.95
SL 340	1	0.54	0.71
US 87	1	*	*
SL 111	1	0.28	0.33
SH 159	1	*	0.69

* No correlation was found

PREDICTION OF FIELD DENSITY

In this section, the researchers verified the proposed method in Chapter 2 to predict the density in several test sections: FM 2854, SH 31, US 159, and US 290. The researchers obtained the compaction curves—compaction index versus percent air voids for the breakdown rollers used in these test sections. They recorded the change in density at two locations with the number of breakdown roller passes. These two spots were chosen to be within 2 to 5 ft from the edge of the roller during compaction, where the efficiency of the compaction effort is uniform (Figure 2-4). Figure 5-5 shows an example of the recorded field compaction curves. These field compaction curves were used to estimate the density at different locations in the mat based on the recorded CI. Field cores were extracted from different locations in the mat (Figure 5-1) after the compaction. The predicted densities for the recovered field cores were compared to those measured in the laboratory (Figure 5-6). Good correlation between the predicted densities and the measured ones was found. This verifies the applicability of the proposed method in Chapter 2 to predict the density in real time during compaction.

$$y = 11.64x^{-0.32}$$
$$R^2 = 0.93$$
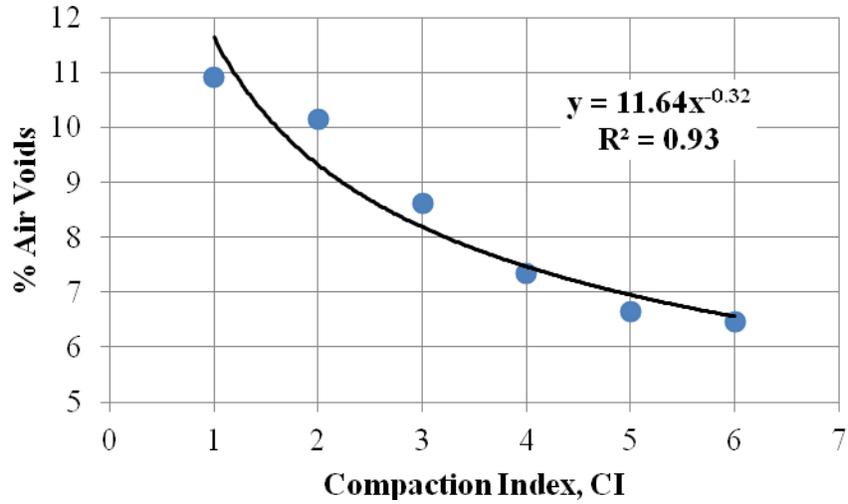
Figure 5-5. Recorded Compaction Curve for Steel-Wheel Roller in Test Section SH 31.

$$R^2 = 0.82$$

■ FM 2854 ▲ SH 31 ◆ US 159 ● US 290
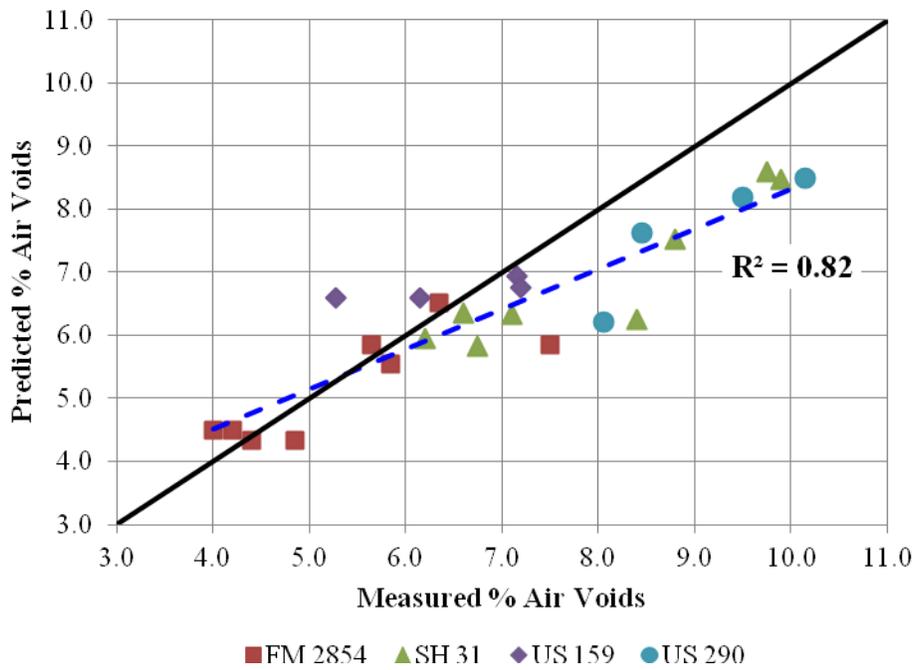
Figure 5-6. Measured vs. Predicted Percent Air Voids.

LABORATORY AND FIELD COMPACTABILITY OF ASPHALT MIXTURES

The researchers at TTI and University of Texas San Antonio (UTSA) worked separately to develop indices that can be used to assess field compactability based on laboratory measurements. Loose mixtures were collected from the field from all the mixtures evaluated in this study and previously described in Tables 2-1 and 5-1. There were 10 different asphalt mixtures evaluated in this study. In addition, the researchers added 10 more mixtures; seven of these mixtures were evaluated in a previous TxDOT project, 0-5261 (Masad et al. 2009a, 2009b), and three were evaluated in project 0-6132 at UTSA. Table 5-4 gives a summary of these mixtures.

Table 5-4. Summary of the Asphalt Mixtures.

Mixture #	Project ID	Mixture Type	Compaction Index	LCI	WEI	PI
1	Riverside 1	HMA Type C	5.45	24.21	4.93	5.34
2	Riverside 2	HMA Type D	7.4	23.85	3.19	4.69
3	Riverside 3	WMA Type D	4	25.98	6.87	5.59
4	SL 111	HMA Type C	4	27.14	5.40	5.32
5	SH 31	HMA Type B	5.5	24.75	3.90	4.54
6	Loop 340	HMA Type C	4.8	22.03	4.28	4.54
7	FM 2854	HMA Type D	1	29.69	7.53	6.22
8	US 87	HMA CMHB-F	*	18.90	1.18	3.61
9	US 290	WMA Type C	3.6	21.90	2.57	4.68
10	US 159	HMA Type D	1	28.21	7.01	6.87
11	LAREDO	HMA Type C	5	20.13	3.36	4.61
12	LA-modified	HMA Type C	2.5	24.09	7.29	6.14
13	LA-control	HMA Type C	3.5	23.12	6.14	5.53
14	IH 35	HMA SMA	1.4	27.92	5.32	4.16
15	HW 6	HMA SMA	2	26.24	4.44	4.12
16	SH 44	HMA Type B	3	25.19	5.13	5.89
17	SH 36	HMA Type D	2.1	24.83	4.21	5.05
18	US 259	HMA Type C	3.8	27.13	5.79	5.46
19	SH 21	HMA Type C	4.4	21.59	2.72	4.89
20	US 87	HMA Type C	6.1	22.74	3.65	5.44

* Could not achieve 8 percent air voids in the field

At TTI, the researchers molded two laboratory SGC specimens (6-inch diameter and approximately 2.5 inches in height) at a 1.25° gyration angle from each mixture. They recorded the SGC compaction curves, as shown in Figure 5-6. The intercept (a) and the slope (b) of percent air voids to number of gyrations in logarithmic scale were calculated for each mixture, as shown in Figure 5-7. The slope was calculated from the initial compaction point to the point of 8 percent air voids.
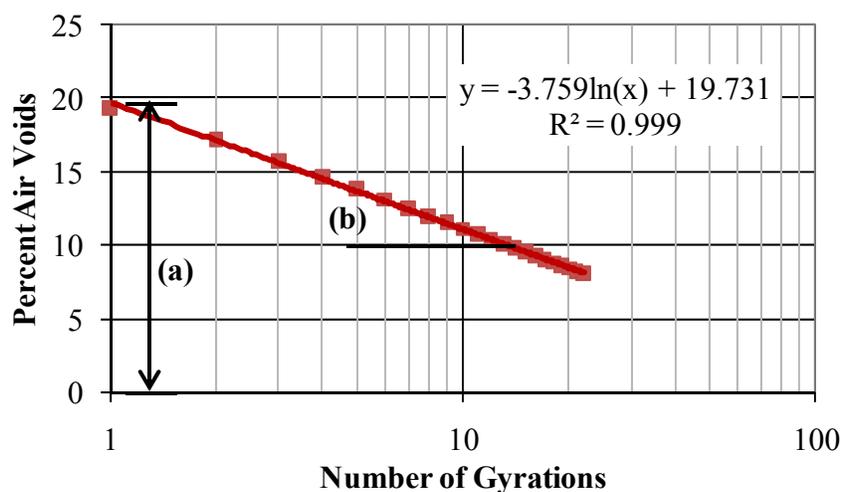
Figure 5-7. Example of SGC Compaction Curves.

Researchers at TTI developed an index called the laboratory compaction index (LCI) to quantify the laboratory compaction effort, and it was correlated to the field compaction index needed to achieve the same percent air voids (8 percent). The LCI is calculated using the following formula:

$$LCI = 100 * \frac{b^{1.2}}{a} \qquad (3)$$

where a is the intercept and b is the slope of the compaction curves (absolute value). The LCI index was found to have fair correlation with the CI. Figure 5-8(a) shows the correlation for all the mixtures evaluated at TTI, while Figure 5-8(b) shows the correlation for all the mixtures, including the three mixtures (11, 12, and 13) from UTSA. UTSA provided TTI with the laboratory compaction curves for these three mixtures. This correlation is considered a good correlation since there are many factors that affect the compactability of the mixtures. These factors are not related to the characteristics of the mixtures, and they include compaction temperature, compaction method, weight of the rollers, mode of the operation (static vs. vibratory), base conditions, ambient temperature, wind speed, etc. Researchers believe that such correlation is very useful in assessing the compactability of asphalt mixtures while in the mixture design stage. Mixtures with higher slope and lower intercept in the laboratory needed less CI in the field (less compaction effort). Higher slope means that there is a steep reduction in percent air voids with number of gyrations, while mixtures with lower intercept means

that these mixtures have low percent air voids after the first gyration. Mixtures with high LCI are preferred since they need low CI or a few number of roller passes to achieve the target air voids.
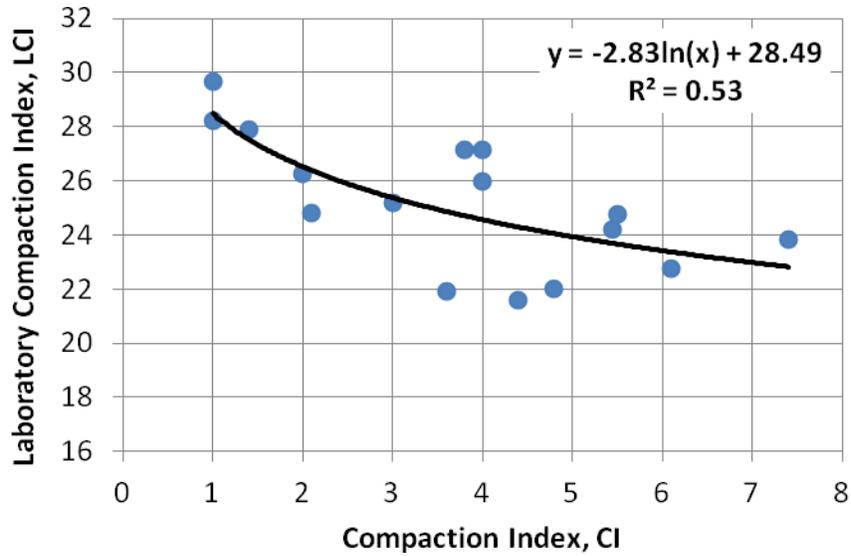
(a) For all the Mixtures in Table 5-4 except Mixtures 11, 12, 13
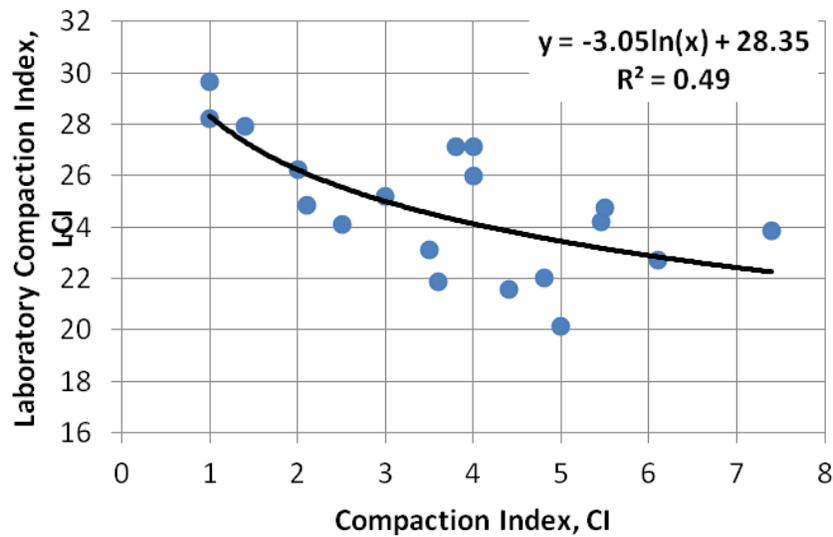
(b) For all the Mixtures in Table 5-4

Figure 5-8. Correlation between LCI and CI.

Researchers at UTSA utilized two workability indices—workability energy index (WEI) and porosity index (PI)—to evaluate the compactability of asphalt mixtures. The workability index is determined using a distinct zone in the compaction curve, as shown in Figure 5-9.
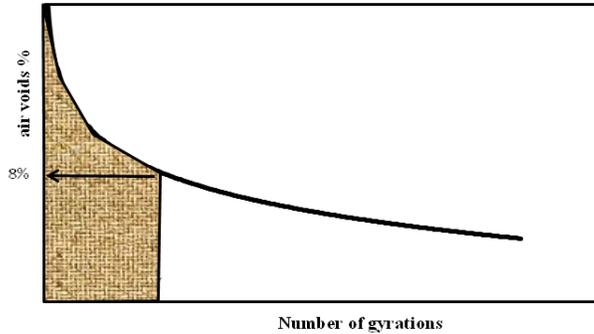
Figure 5-9. The Distinct Areas Used to Determine the Workability Index.

The area from the loose (non-compacted) phase until 8 percent air voids (92 percent density) reflects the mix workability in the field. The workability index can be defined as:

$$WEI = \frac{\pi d^2 / 4 * P * \sum_{N=1}^{N_{92}} \Delta h}{N_{92\%}} \quad (N/m) \qquad (4)$$

where d is the mix diameter and is equal to 6 inches [150 mm]; P is the compaction pressure, which equals 600 kPa; h is the mix height during compaction; N is the number of gyrations; and N_{92} corresponds to 92 percent Gmm (8 percent air voids).

The numerator reflects the energy imposed to the mix, and the denominator reflects the number of gyrations needed to achieve the target density. Mixes with difficulty compacting from a loose state to 92 percent Gmm will need more numbers of gyrations, resulting in higher WEI values. Mixes that achieve higher WEI are desirable, as they take less energy and/or rolling passes to compact to target density. Higher WEI values are associated with simpler and faster mat compaction during construction.

The second index, PI, is defined as follows (Cabrera and Dixon 1994):

$$PI = \frac{100}{A} \qquad (5)$$

where *A* is the intercept of the Gmm-N compaction curve plotted in a logarithmic magnitude. The index correlates the workability of the mix to its initial air voids obtained from the placement prior to the rolling compaction.

Researchers at UTSA evaluated the first 13 mixtures in Table 5-4 in their lab while, TTI provided them with the laboratory compaction curves for the last seven mixtures. The TTI research team used Servopac SGC, while the UTSA team used Pine® SGC compactor. A good correlation was found between the WEI and the CI for the mixtures that were evaluated at UTSA (Figure 5-10),

while poor correlation was found when all the mixtures were included (Figure 5-11). Similarly, there was a good correlation between the PI and CI for the mixtures that were evaluated at UTSA (Figure 5-12), while no correlation was found when all the mixtures were included (Figure 5-13). This could be due to the effect of combining two different laboratory compaction methods—Servopac SGC and Pine® compactor. In summary, the WEI and PI were correlated to the CI if one compaction method was considered. These indices can be used to identify the number of passes needed to achieve desirable air voids in the field. For instance, a WEI and PI of five or more is equivalent to four roller passes or less in the field. A series of similar relationships can be developed at various target air voids, and the equivalent roller passes can then be predicted for a particular mix.

The equation shown on the plot:
$$y = -0.70x + 7.99$$
$$R^2 = 0.55$$
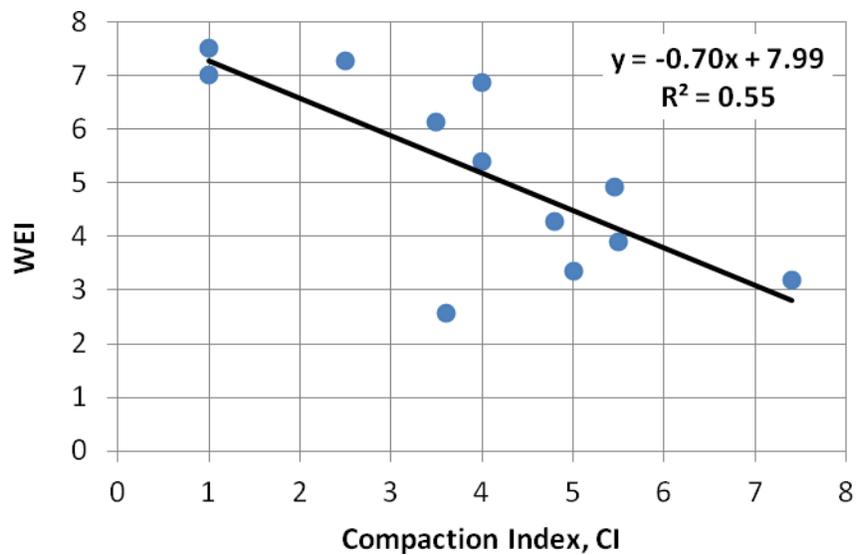
Figure 5-10. Correlation between WEI and CI (for the First 13 Mixtures in Table 5-4).
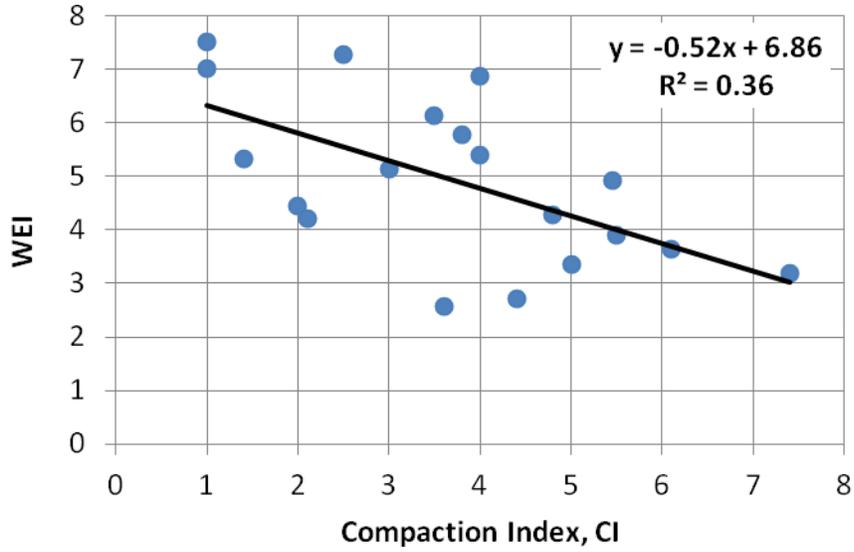
Figure 5-11. Correlation between WEI and CI (for All the Mixtures in Table 5-4).
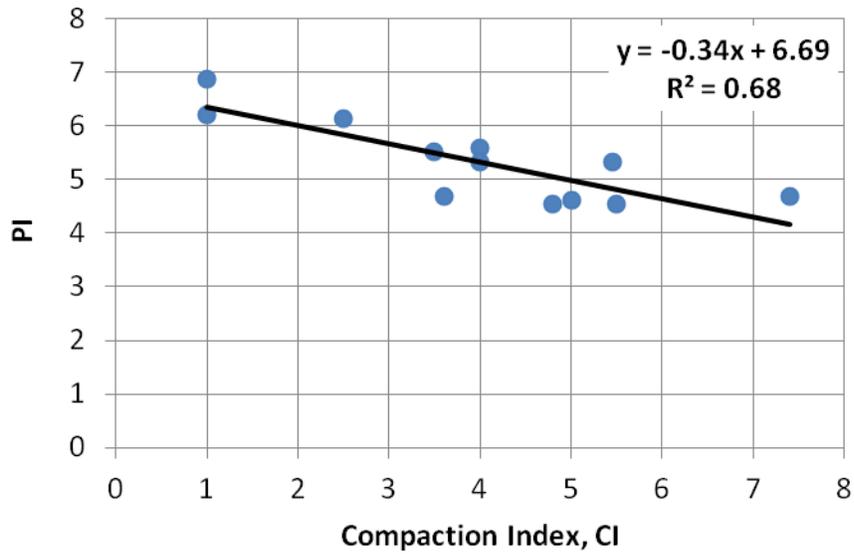
Figure 5-12. Correlation between PI and CI (for the First 13 Mixtures in Table 5-4).

106
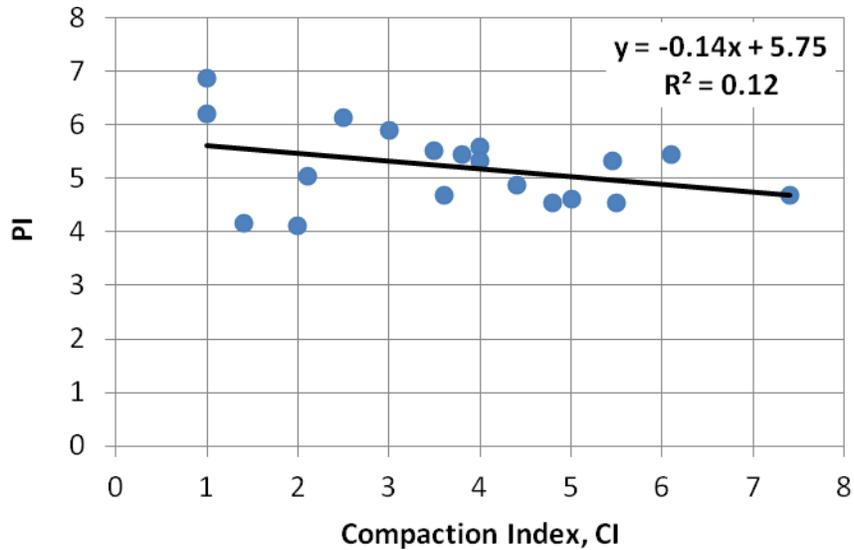
Figure 5-13. Correlation between PI and CI (for All the Mixtures in Table 5-4).

UTILIZING THE COMPACTION MONITORING SYSTEM IN THE FIELD

The researchers tested the compaction monitoring system, described in Chapter 4, in the field on a number of experimental projects around Texas. The first testing of the system occurred at the Pecos test track construction site where six 1000-ft-long experimental thin pavement layers were placed. Figure 5-14 shows the use of the system at Pecos.

Figure 5-14. Compaction of the SMA.

Figure 5-15 shows typical data from the Pecos test section. The upper plot shows the roller paths. In the middle area, the data show two passes down the edge of the mat and one pass down the middle. The second and third plots show the compaction index and number of passes from approximately the same locations. The number of passes may be significantly different in 4, 5, and 9, but the compaction effectiveness may be very similar in 3.9, 4.6, and 4.3, with the difference being associated with the non-uniform compaction index applied across the width of the roller. The lower graphs show the temperatures recorded at the first pass of the roller. The compaction effort and roller passes were judged as good in the compaction of the SMA layer at Pecos.
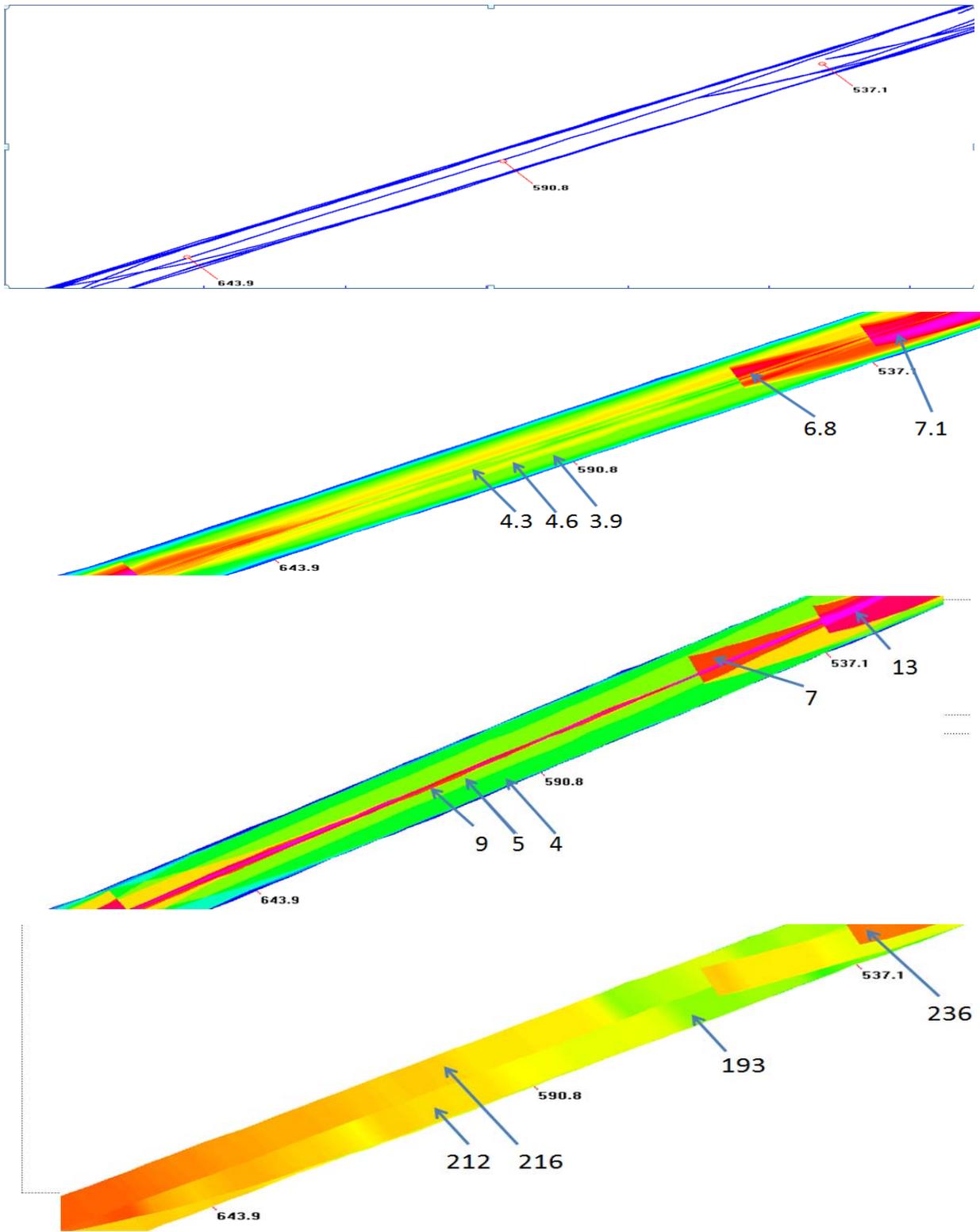
Figure 5-15. Complete Data for a 140-ft Section from the SMA at the Pecos Test Track.

Figure 5-16 shows the transverse distribution plots (compaction effectiveness, number of passes, and mat temperatures) from the approximately 593-ft location. The number of passes in the middle was close to nine, but since many of these were under the edge of the roller, the compaction effectiveness was reasonably uniform across the mat.
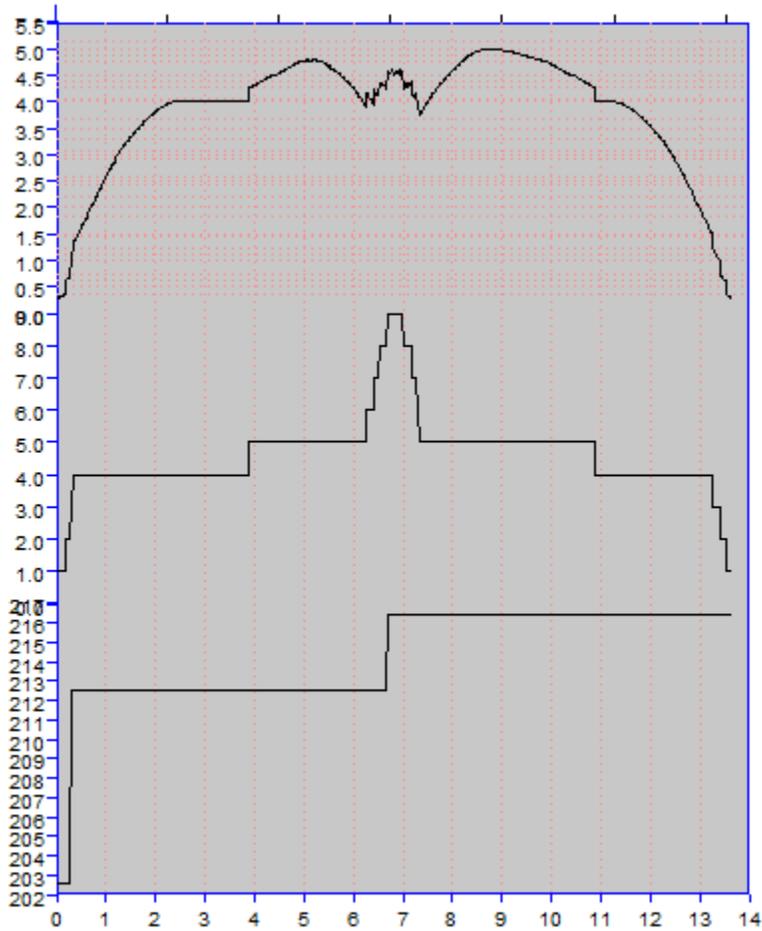
Figure 5-16. Transverse Distribution Plots from 593-ft Location.

The CMS was also utilized in several field projects in this study. Typical data sets are shown in the following sections.

US 87 in the Austin District

The mix used on this project was the thin-lift CMHB Type F mix designed by the Austin District. The nominal lift thickness for this lift is 1.0 inch. Figure 5-17 shows the placement operation. This project was conducted in the middle of summer 2011, when ambient temperatures were over 100°F. Figure 5-18 shows the data from this project.

Figure 5-17. Placement of the CMHB-F on US 87.
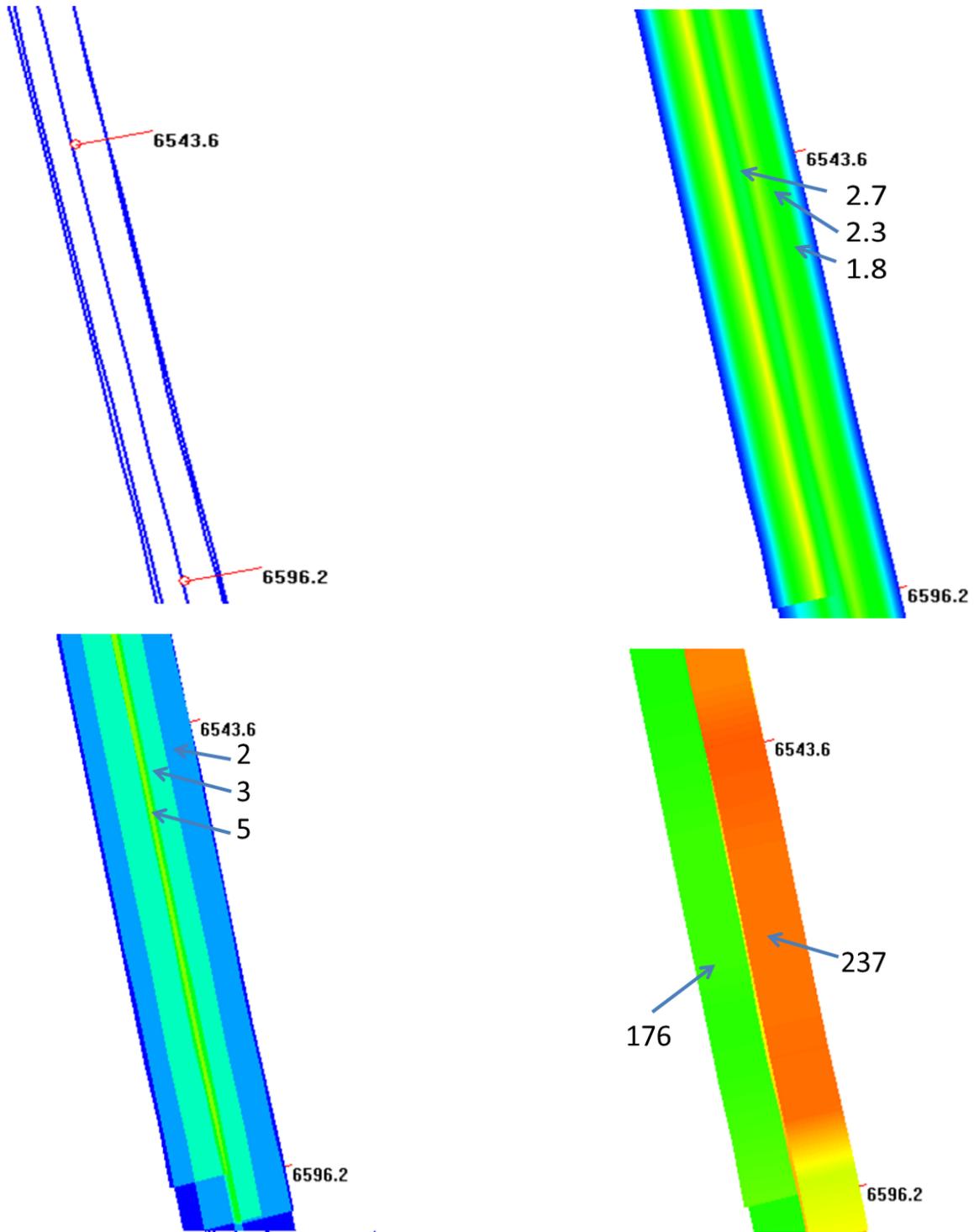
Figure 5-18. Compaction Data from US 87. Top Left Clockwise: (a) Roller Paths, (b) Compaction Effectiveness, (c) Mat Temperatures, and (d) Number of Passes.

The rolling pattern for US 87 was the traditional two passes along each side of the mat with a final pass down the middle of the mat. The most significant feature of this plot was the large drop in temperatures experienced while compacting both sides of the mat. In the first pass on the right of the mat, the lift temperature, as indicated in Figure 5-18, was 237°F. For the next passes on the left of the mat, the mat temperature dropped to 176°F. This clearly points out a construction issue with these thin mats, specifically the rapid drop in temperature. For a typical 2-inch mat, temperature drops of around 20° were found for similar passes. For US 87, a drop of 50°F plus was found. This clearly points to the need to modify construction practices with these thin lifts. For future projects, TxDOT should consider either the use of warm mix additives as compaction aid or the use of two steel-wheel rollers working in tandem (or both). It must be remembered that US 87 was placed under ideal conditions and that lacing these mixes in the cooler parts of the year could lead to compaction problems.

Cores were taken from US 87, and very low densities were found in some areas, air void contents as high as 15 percent were found, and the mix was very open, as Figure 5-19 shows.

Figure 5-19. Typical Core from US 87.

The researchers verified the number of passes recorded using the CMS by manually recording the location of the roller during construction. Figure 5-20(a) shows color maps for the number of passes in a section of US 87. Figure 5-20(b) and (c) show the number of passes across the mat recorded manually and using the CMS, respectively. It is obvious that both distributions match each other. In fact, the CMS provided better accuracy.
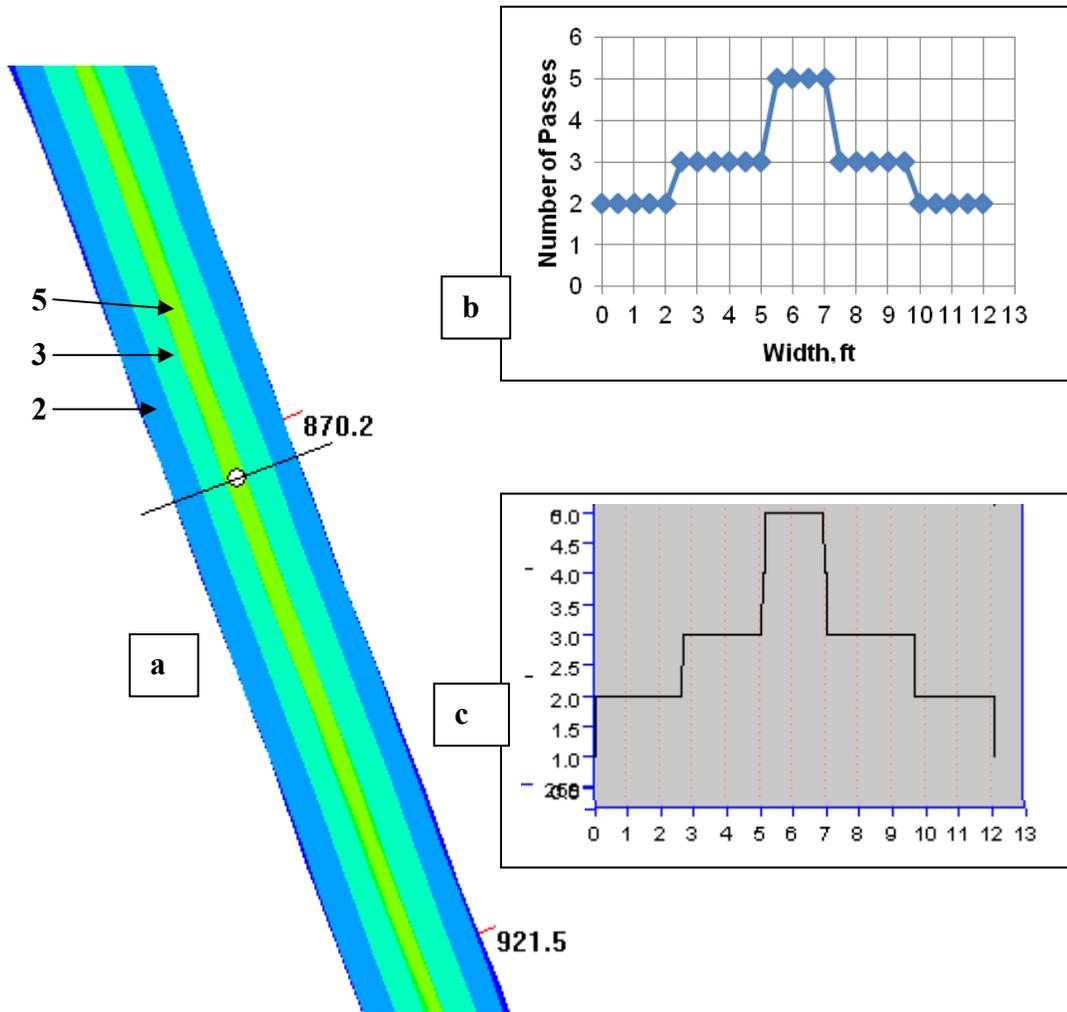
Figure 5-20. Verification of Number of Passes.

US 84 in the Waco District

On several of the projects, the Pave-IR was attached to the laydown machine to measure the temperature at placement. Figure 5-21 shows the Pave-IR output for one problem location on US 84 in Waco. At this location, the paver stopped and the temperature of the mat at placement in the blue areas was between 217°F and 229°F. Figure 5-22 shows the same location in the compaction monitoring system. By the time the roller first got to the cold spot, the mat surface temperature had dropped to below 160°F.
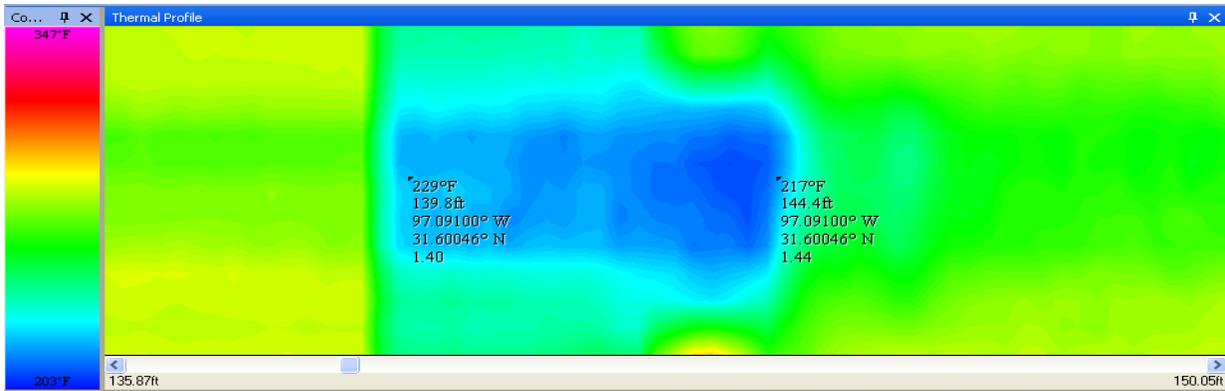
Figure 5-21. Pave-IR Output from US 84 in Waco District—Cold Spot Caused by Paver Stop.
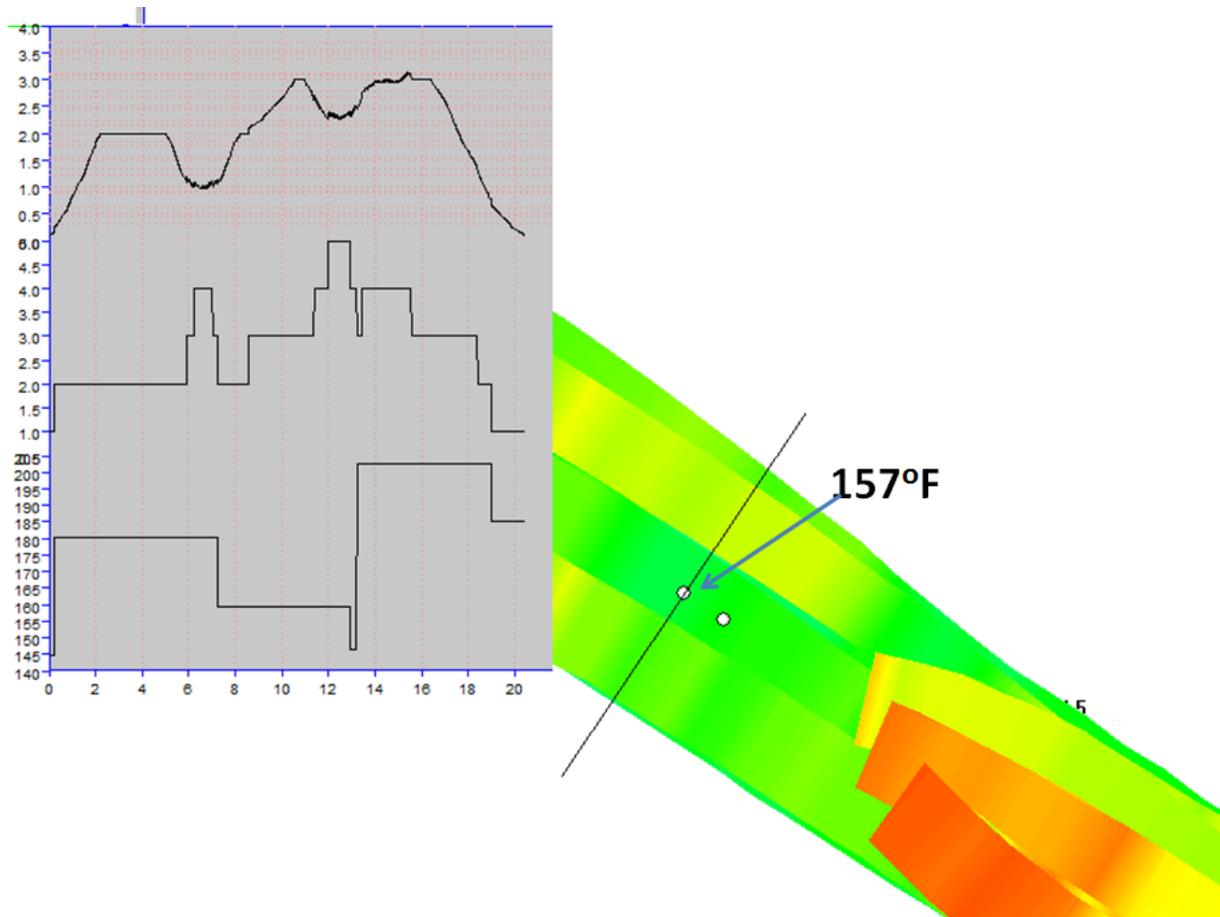
Figure 5-22. Temperature at Time of Compaction for Cold Spot in Figure 5-21.

CHAPTER 6
CONCLUSIONS AND FUTURE WORK

CONCLUSIONS

Chapter 1 of this study presented a literature search on compaction of hot and warm asphalt mixtures; a previous comprehensive literature search was conducted in TxDOT 0-5261 (Masad et al. 2009a, 2009b). The search included recent technologies in field compaction of asphalt mixtures. The intelligent compaction was found to be a promising technology; however, its applicability in monitoring the compaction of thin lifts of asphalt pavement is still questionable, especially in Texas where the HMA surface layers are relatively thin and the deflections measured on the surface will be strongly related to base and subgrade strengths. Recent studies have found that the correlation between the IC stiffness measurements and HMA density was poor. The relatively small thickness of the asphalt layer could hinder the IC roller from using its intelligent features of applying more compactive effort when it is needed. New intelligent rollers are equipped with GPS systems that track the location of the roller during compaction and produce color maps of coverage in real time. This is very useful information; however, it is not sufficient, as previous studies (Masad et al. 2009a, 2009b) showed that the efficiency of the compactive effort under rollers is not equally uniform. Moreover, there is a need to develop a practical approach for density prediction in the field during compaction.

Chapter 2 reported the findings of a field study that the researchers conducted at the Riverside Campus of Texas A&M University. They constructed several test sections for comprehensive evaluation of important factors that influence the compaction of both HMA and WMA. The researchers found that the efficiency of the compactive effort across the steel rollers was non-uniform. A point on the mat closer to the center of the roller was subjected to more compaction than a point closer to the edge of the roller. The cores compacted close to restricted or semi-restricted joints had more density than cores near free or unrestricted joints. The compaction temperature was found to have a great effect on compaction irrespective of mixture type—HMA or WMA. On average, there was a 10 percent increase in the measured percent air voids per 30°F reduction in the compaction temperature. The WMA was relatively easier to compact when compared to the HMA in spite of the fact that the WMA was laid and compacted at lower temperatures than the HMA. The researchers noticed that incorporating RAP in asphalt mixtures could require increasing the compaction effort to achieve the desired density compared to mixtures without RAP. However,

117

several other factors besides the use of RAP may affect the compactability of HMA, such as aggregate gradation, VMA, aggregate characteristics, etc. In addition, the results showed that the HMA compacted on the top of a rigid base had a higher density than the mixture compacted on a flexible base. The researchers presented a method for predicting the density of asphalt pavement compacted using both static and vibratory rollers. This method utilizes the location of the roller on the mat and the compaction curves for each roller to predict the density. The predicted density was close to the measured one. This approach can be used to set up the compaction pattern that is needed to achieve the desired asphalt pavement density.

Chapter 3 described the researchers' use of the GPR as a non-destructive quality control tool to assess the compaction level in asphalt pavements. In addition, the researchers evaluated the effect of level of compaction on performance of WMA and HMA mixtures. The GPR was found to be an effective tool for assessing the compaction level in asphalt pavements. There was an excellent correlation between the GPR predicted air void distribution maps and the air void maps generated from core measurements. This application of the GPR is useful to obtain maps of air voids in asphalt pavements at a relatively low cost, without the need for mass coring, and without causing interference to traffic. The results showed that the compaction level highly affected the performance of asphalt mixtures. Specimens that had less percent air voids performed better in both wet and dry conditions. Specimens with less percent air voids had less rutting in the Hamburg wheel-tracker, higher load in the first cycle of the overlay tester, and a higher strength in the indirect tensile test. These results can be useful to set the quality control limits for percent air voids during construction. Researchers found no problems in compacting WMA to the desired density. In fact, the compaction of WMA mixtures was achieved with slightly less compaction effort than HMA mixtures. The performance IDT results showed that WMA specimens performed better than the corresponding HMA specimens in dry conditions. However, the reduction in strength of the wet WMA mixtures was higher than the wet HMA mixtures.

Chapter 4 discussed the development of the compaction monitoring system. This system uses the latest GPS technologies and various sensors to provide full coverage of the newly constructed mat. The post-processing software system produces color-coded maps that show the following in real time: (a) the number of roller passes on the entire mat, (b) the compaction index (number of passes multiplied by the effectiveness factors), and (c) the temperature of the mat for the first pass of the roller. The developed system has several components that include a high-accuracy

GPS positioning system, two infrared sensors for measuring the asphalt surface temperature, one accelerometer for detecting whether the roller is vibrating, a Toughbook computer for collecting and viewing the data, a battery for the power supply, and a data acquisition system for converting the analog signals to digital data. The CMS documents the compaction process for the whole project, and the data are saved on the computer. The data can be opened using the same software for reviewing the whole compaction process. The system was found to be simple and easy to use.

Chapter 5 described the field testing that the researchers conducted on several test sections to validate the findings of Chapter 2 and 3 and to test the developed software for monitoring field compaction in real time. The researchers monitored and documented the compaction process on seven field projects in Texas. These projects used hot and warm asphalt mixtures, and some of these mixtures also contained RAP and RAS. The density of the received field cores had better correlation with the compaction index than the number of passes. Asphalt mixtures near the center of the roller were subjected to more compactive efforts that the mixtures near the edges of the roller. The researchers verified the proposed method presented in Chapter 2 for density prediction. They verified this method to predict the density in several test sections, and the results showed good correlation between the predicted densities and the measured ones. The researchers also developed several indices that correlate the laboratory compaction characteristics to the compaction effort needed in the field to achieve certain percent air voids. The developed indices had good correlation with the compaction index, and these indices have the potential to be used to estimate the CI required for field compaction of asphalt mixtures. In addition, the researchers field tested the compaction monitoring system described in Chapter 4 on a number of experimental projects around Texas. The CMS was found to be simple to install and use. The results of the CMS were very useful in monitoring the compaction process. The CMS maps showed coverage, compaction index, and temperature in real time. The CMS was able to document some inconsistencies in the compaction process, for example, unequal converges across the mat, non-uniform temperature, significant delay in compaction after placement of the mixtures, etc.

FUTURE WORK

The researchers presented two practical tools for improving the uniformity of HMA compaction as follows:

- A compaction monitoring system (CMS) to monitor in real time the HMA compaction process. At the basic level, the roller operator can see a color-coded display of the number of passes and compaction index that each area of the mat has received. The agency can also monitor coverage and temperature profiles to determine if the field operation is providing satisfactory results.

- A new method was proposed for predicting the density of asphalt pavements during field compaction in real time. This was partially verified in several field test sections where the predicted densities using the proposed method correlated well with the measured ones.

The TxDOT should consider an additional implementation study to proceed with the implementation of both of these products of their research program.

Implementation of the CMS

The benefits of the CMS system were clearly identified in this project, especially with the work on US 87 where rapid cooling of the HMA lead to significant compaction concerns. Providing the roller operator with a simple color map showing compactive effort will also be a great help, as shown in some of the field testing in some locations the mat only receive a single roller pass where as other adjacent areas the mat received 6 or more passes. Implementation of this new technology should take the same approach as the Pave-IR system which was proposed and field tested in a TxDOT research study and successfully developed into a robust field system by a commercial company (MOBA). The research agencies (TTI) have the capability to develop and pilot test new systems but full implementation and product support is best handled by commercial companies.

It is proposed that TTI contact several companies such as roller manufacturers and equipment developers such as MOBA to determine their interested in developing a commercial system based on the CMS system developed in this study.

Further Development and Implementation of the Automated Field Density Prediction

This method requires having the compaction curves for each roller, the compaction pattern (sequence of rollers), and efficiency distribution of the compactive effort across the roller. There is also a need for integrating this method into the CMS software in order to predict the field density in real time. This can be achieved through a number of steps, as shown in Figure 6-1 and explained below:

- Step 1: Record the compaction curve of each compaction method in the field. The compaction curve—change in percent air voids with number of passes—should be obtained for each roller. The initial step in the development of these curves will be to calibrate the nuclear density gauge for the mix being compacted. This will require a test strip where cores are taken and densities measured in the laboratory and correlated to nuclear density gauge (NDG) measurements. After calibration the compaction curves will be simple to generate on a test strip where density measurements are taken with an NDG after every pass of the roller. Compaction curves will need to be developed for both static and vibratory modes. The temperature at the time of compaction will also need to be recorded. The density should be recorded toward the middle of the roller where the efficiency distribution of the compactive effort is uniform. This step needs to be integrated into the CMS software.

- Step 2: Measure temperature distribution using the CMS. The temperature has a significant effect on the compactability of asphalt mixtures. Currently, the CMS is capable of recording temperatures across the mat in real time, as Figure 6-1 (Step 2) illustrates. The temperature measured by the CMS is a surface temperature; however, the internal temperature should be higher than the surface temperature. The difference between the surface and internal temperature depends on many factors, which include the ambient temperature, thickness of the mat, wind speed, etc. There is a need for further research to better correlate the surface and internal temperatures.

- Step 3: Determine the modified compaction curve. The researchers found that on average, there was a 10 percent increase in the measured percent air voids per 30°F reduction in the compaction temperature; hence, the original compaction curves obtained in Step 1 need to be revised at different compaction temperatures. This step needs to be automated and integrated in the CMS software so that the CMS can use the correct compaction

121

curves at a given compaction temperature. Figure 6-1 (Step 3) shows an example of the compaction curves at different temperatures for given mixtures.

- Step 4: Record the number of passes distribution using the CMS. The CMS records the number of passes across the mat in real time. Each pass is then multiplied by the efficiency factor to produce the compaction index distribution, as presented in Step 5 in Figure 6-1.

- Step 5: Determine the CI distribution using the CMS. Currently, the CMS shows the compaction index distribution in real time, which can be converted to density distribution upon obtaining the proper compaction curves. It would be possible to convert the compaction index to density measurements in real time upon integrating Step 3 into the CMS software. The CMS is currently capable of defining the mode at which the roller operates, whether static or vibratory. The CMS utilizes the correct compaction index based on the type, mode, and type of roller.

- Step 6: Determine the predicted density distribution using the CMS. The CMS can produce density distribution maps in real time that can be used by the operator of the roller to adjust the number of passes and the location of the roller to achieve the target density across the mat, which is the ultimate goal of the compaction process in the field.

In addition to recommending the further development of the CMS, the authors suggest evaluating other laboratory equipment (procedures) for assessing the compactability of asphalt mixtures. In this study, the researchers developed several laboratory compaction indices, based on the SGC measurements, which have acceptable correlation with the compaction index required in the field. However, the researchers believe that other equipment, such as the linear kneading compactor or the small walk-behind roller compactor, may better simulate the field roller compactors.
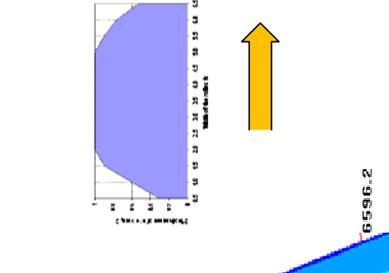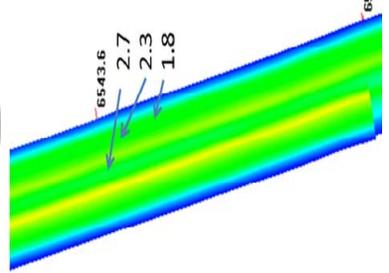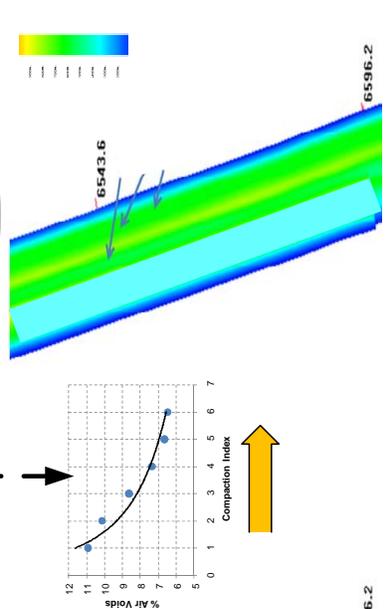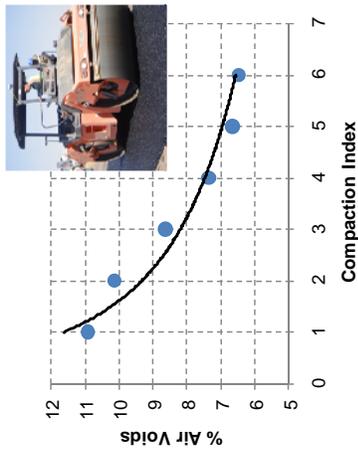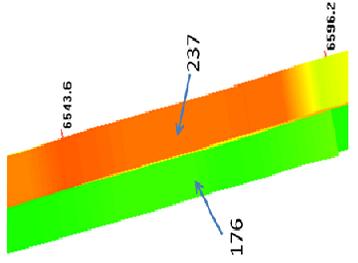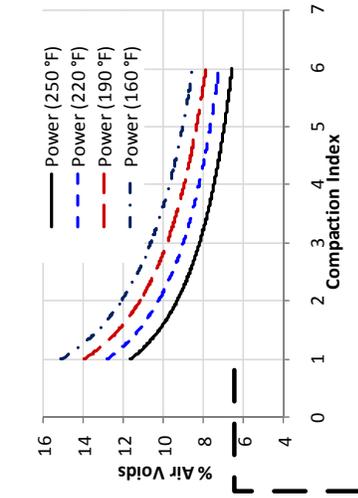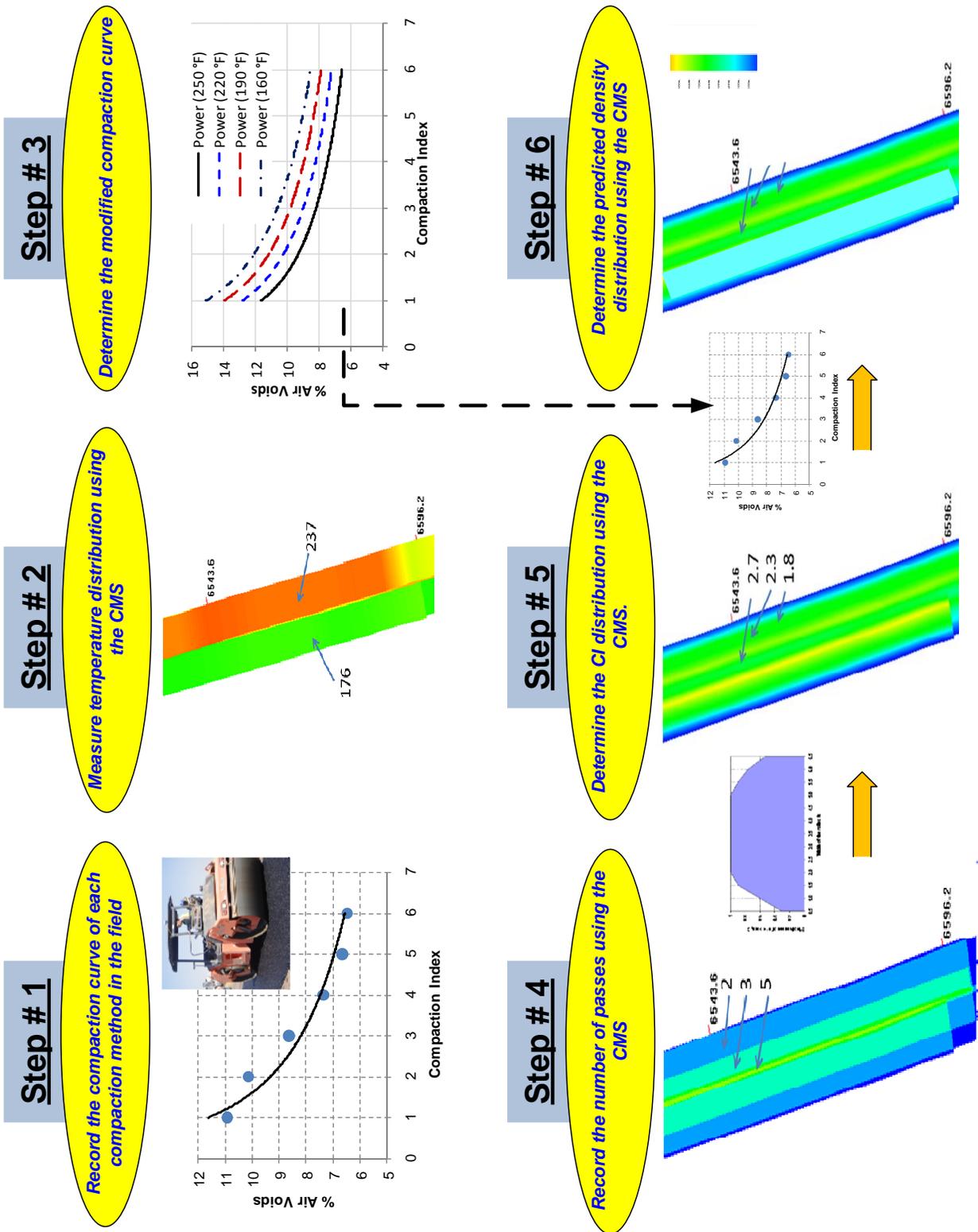
Figure 6-1. Further Development of the CMS.

REFERENCES

American Association of State Highway and Transportation Officials (AASHTO). (2002). "Bulk Specific Gravity of Compacted Asphalt Mixtures Using Saturated Surface-Dry Specimens." T166. Standard Specifications for Transportation Materials and Methods Sampling and Testing, American Association of State Highway and Transportation Officials, Washington, D.C.

American Association of State Highway and Transportation Officials (AASHTO). (2007). Standard Method of Test for Resistance of Compacted Asphalt Mixtures to Moisture-Induced Damage. T 283. Standard Specifications for Transportation Materials and Methods Sampling and Testing, American Association of State Highway and Transportation Officials, Washington, D.C.

Anderegg, R. (2000). "ACE Ammann Compaction Expert—Automatic Control of the Compaction." Proceedings, European Workshop on Compaction of Soils and Granular Materials, Paris, 229–236.

Asphalt Institute. (2010). "Intelligent Compaction: A Smart Innovation." Webinar organized by Asphalt Institute. http://www.asphaltinstitute.org/public/asphalt_academy/Webinars/PDFs/ICWebinar_Combined_Presentations_032610.pdf , accessed March 2010.

Cabrera, J.G. and Dixon, J.R. (1994). Performance and Durability of Bituminous Material. Proceeding of Symposium, University of Leeds, Leeds, United Kingdom.

Commuri, S., Mai, Anh T., and Zaman, M. (2011). "Neural Network-Based Intelligent Compaction Analyzer for Estimating Compaction Quality of Hot Asphalt Mixes." *ASCE Journal of Construction Engineering and Management,* doi:10.1061/(ASCE)CO.1943-7862.0000343

Consuegra, A., Little, D.N., Quintus, H.V., and Burati, J. (1989). "Comparative Evaluation of Laboratory Compaction Devices Based on Their Ability to Produce Mixtures with Engineering Properties Similar to those Produced in the Field." *Transportation Research* Record 1228, TRB, National Research Council, Washington, D.C., 80–87.

Corps of Engineers. (2000). Hot-Mix Asphalt Paving Handbook 2000, AC 150/5370-14A, U.S. Army Corps of Engineers, Washington, D.C.

Chowdhury, A., and Button, J. (2009). A Review of Warm Mix Asphalt. Report No. SWUTC/09/473700-1, Texas Transportation Institute, College Station, TX.

D'Angelo, J., Harm, E., Bartoszek, J., Baumgardner, G., Corrigan, M., Cowsert, J., Harman, T., Jamshidi, M., Jones, W., Newcomb, D., Prowell, B., Sines, R., and Yea-Ton, B. (2008). Warm-Mix Asphalt: European Practice. Report No. FHWA-PL-08-007, American Trade Initiatives, Alexandria, VA.

FHWA (2009). Intelligent Compaction for Asphalt Materials. www.fhwa.dot.gov/pavement/ic/techbriefs/ic_hma.cfm , accessed on Dec. 2009.

Forssblad, L. (1992). "Control of Bearing Capacity by Means of Compaction Meter." Proceedings of International Symposium on Bearing Capacity of Roads and Airfields, Trondheim, Norway, 912–921.

Harris, R., and McNaught, E. (1978). "A Direct Reading Instrument for Measurement of Resultant Particle Velocity of Ground Vibration." *Australian Road Research*, 8(1), 17–24.

Harvey, J., and Monismith, C.L. (1993). "Effects of Laboratory Asphalt Concrete Specimen Preparation Variables on Fatigue and Permanent Deformation Test Results Using Strategic Highway Research Program A-003A Proposed Testing Equipment." *Transportation Research Record 1417*, TRB, National Research Council, Washington, D.C., 38–57.

James Informational Media. (1987). "CONEXPO report: Part II." Better Roads, 57(5), 46–52.

Jaselskis, E.J., Han, H.C., Grigas, J., Tan, L., and Fahrion, D. (2001). "Status of Roller Mountable Microwave Asphalt Pavement Density Sensor." *Journal of Construction Engineering and Management*, ASCE, 127(1), 46–52.

Kassem, E., Masad, E., Chowdhury, A., and Claros, G. (2008). "Influence of Field Compaction Pattern on Asphalt Pavement Uniformity." *Journal of the Association of Asphalt Paving Technologists,* AAPT, 77, 257–298

Kloubert, H-J, Thiele, R., and Dietl, F. (2007). Testing the Unbound Layer on the South Runway and Taxiways Using SCCC" Bomag®. Job report, Boppard, Germany, http://www.intelligentcompaction.com/downloads/PapersReports/Bomag_JobReport_2007.pdf , accessed May 2010.

Koenders, B.G., Stoker, D.A., Robertus, C., Larsen, O., and Johansen, J. (2002). "WAM-Foam, Asphalt Production at Lower Operating Temperatures." Proceedings, 9th Conference of International Society for Asphalt Pavements, Copenhagen, Denmark.

Komandi, G. (1999). "An evaluation of the Concept of Rolling Resistance." *Journal of Terramechanics,* 36, 159–166.

Krishnamurthy, B.K., Tserng, H.P., Schmitt, R.L., Russell, J.S., Bahia, H.U., and Hanna, A.S. (1998). "AutoPave: Towards an Automated Paving System for Asphalt Pavement Compaction Operations." *Automation in Construction*, 8(2), 165–180.

Leiva, F., and West, R. C. (2008). "Relationship between Laboratory Measured Characteristics of HMA and Field Compactability." *Journal of the Association of Asphalt Paving Technologists,* AAPT, 77, 183–219.

Li, C., Oloufa, A. A., and Thomas, H. R. (1996). "A GIS-based System for Pavement Compaction." *Automation in Construction*, 5(1), 51–59.

Lu, M., Chen, W., Shen, X., Lam, H., and Liu, J. (2007) "Positioning and Tracking Construction Vehicles in Highly Dense Urban Areas and Building Construction Sites." *Automation in Construction,* 16(5), 647–656.

Masad, E. A., Muhunthan, B., Shashidhar, N., and Harman, T. (1999). "Quantifying Laboratory Compaction Effects on the Internal Structure of Asphalt Concrete." *Transportation Research Record 1681*, TRB. Washington, D.C., 179–184.

Masad, E., Kassem, E., Chowdhury, A. (2009a). Application of Imaging Technology to Improve the Laboratory and Field Compaction of HMA. Report No. 0-5261-1. Texas Transportation Institute, College Station, TX.

Masad, E., Kassem, E., Chowdhury, A., and Zhanping, Y. (2009b). A Method for Predicting Asphalt Mixture Compactability and Its Influence on Mechanical Properties. Report No. 0-5261-2. Texas Transportation Institute, College Station, TX.

Mattos, P.G. (2003). High Sensitivity GNSS Techniques to Allow Indoor Navigation with GPS and with Galileo. GNSS 2003, European Navigation Conference, Graz, Austria, 11, 22–25.

Maupin, G. W. (2007). Preliminary Field Investigation of Intelligent Compaction of Hot-Mix Asphalt. Report No. VTRC 08-R7, Virginia Transportation Research Council, Charlottesville, VA.

Minchin, R. E., and Thomas, H. R. (2003). "Validation of a Vibration-based Onboard Asphalt Density Measuring System." *Journal of Construction Engineering and Management*, 129(1), 1–7.

Muras, A. (2010). Prediction of Asphalt Compactability from Mixture and Aggregate Properties. M.S. Thesis, Civil Engineering, Texas A&M University, College Station, TX.

Muro, T., and O'Brien, J. (2004). Terramechanics, A.A. Balkema Publishers, Exton, Pennsylvania.

Newcomb, D. (2010). An Introduction to Warm Mix Asphalt. National Asphalt Pavement Association, Lanham, MD, http://fs1.hotmix.org/mbc/Introduction_to_Warm-mix_Asphalt.pdf , accessed May 2010.

Oloufa, A. A. (2002). "Quality Control of Asphalt Compaction using GPS-based System Architecture." IEEE Robotics & Automation Magazine, 29–35.

Peterson, B., Mahboub, K., Anderson, M., Masad, E., and Tashman, L. (2004). "Comparing Superpave Gyratory Compactor Data to Field Cores." *Journal of Materials in Civil Engineering*, ASCE, 16(1), 78–83.

Peyret, F., Betaille, D., and Hintzy, G. (2000). "High-precision Application of GPS in the Field of Real-time Equipment Positioning." *Automation in Construction* 9, 299–314.

Rinehart, R., and Mooney M. (2008). "Instrumentation of a Roller Compactor to Monitor Vibration Behavior during Earthwork Compaction." *Automation in Construction* 17, 144–150.

Roberts, F.L., Kandhal, P.S., Brown, E.R., Lee D., and Kennedy, T. W. (1996). Hot Mix Asphalt Materials, Mixture Design and Construction. National Asphalt Pavement Association, Research and Education Foundation, Lanham, MD.

Roberts, G.W., Dodson, A.H., and Ashkenazi, V. (1999). "Global Positioning System Aided Autonomous Construction Plant Control and Guidance." *Automation in Construction,* 8, 589–595.

Romier, A., Audeon, M., Jac, D., and Martineau, Y. (2004). "Low-Energy Asphalt (LEA) with the Performance of Hot Mix Asphalt." Europeanroads Review, ISSN 1763-3087, Paris, France, 20–29, (http://cat.inist.fr/?aModele=afficheN&cpsidt=17303194).

Saarenketo, T. (1997). Using Ground-Penetrating Radar and Dielectric Probe Measurements in Pavement Density Quality Control. *Transportation Research Record 1575*, Transportation Research Board, Washington, D.C., 34–41.

Scullion, T., and Chen, Y. (1999). COLORMAP Version 2, User's Manual with Help Menus. Texas Transportation Institute, Report No. FHWA/TX-00/1702-4, College Station, TX.

Scullion, T., Sebesta, S.D., Rich, D.J., and Liu, W. (2006). Field Evaluation of New Technologies for Measuring Pavement Quality. Report No. 0-4774-2. Texas Transportation Institute, College Station, TX.

Seamon, D. (1988). "Dynamic Testing: Density on the Run." *Transportation Research Record 1178*, Transportation Research Board, Washington, D.C., 16–22.

Sebaaly, P. E., Fernandez, G., and Hoffman, B. (2008). "Evaluation of Construction Techniques for Longitudinal Joints in HMA Pavements." *Journal of the Association of Asphalt Paving Technologists*, AAPT, 77, 143–182.

Sebesta, S. D., Estakhri, C. K., Scullion, T., and Liu, W. (2006). New Technologies for Evaluating Flexible Pavement Construction: Year 1 Report. Report No. 0-4774-1. Texas Transportation Institute, College Station, TX.

Stakston, A., Bahia, H., and Bushek, J. (2002). "Effect of Fine Aggregate Angularity on Compaction and Shearing Resistance of Asphalt Mixtures." Transportation Research Record 1789, TRB. Washington, D.C., 14–24.

Tashman, L., Masad, E., Peterson, B., and Saleh, H. (2001). "Internal Structure Analysis of Asphalt Mixes to Improve the Simulation of Superpave Gyratory Compaction to Field Conditions." *Journal of the Association of Asphalt Paving Technologists*, 70, 605–645.

Tateyama, K., Nakajima, S., and Fujiyama, T. (1995). "The Evaluation of Ground Properties and Its Application to the Automatic Control of Vibratory Soil Compactors." Proceedings of the 12th International Symposium on Automation and Robotics in Construction, International Association for Automation and Robotics in Construction, Warsaw, Poland, 563–570.

Texas Department of Transportation. (2004). Standard Specifications for Construction and Maintenance of Highways, Streets, and Bridges. TxDOT, Austin, TX.

Thurner, H. (1998). "Continuous Compaction Control of Asphalt Pavements." Proceedings of the 3rd International Symposium, Road Construction Systems and Technologies, München, Germany, 129–134.

Tserng, H.P., and Russell, J.S. (1997). "Instantaneous Motion Planning and Controlling Tool (Impact) For Construction Equipment." Proceedings of Construction Congress, ASCE, New York, 1020–1029.

Veeramani D., Tserng, H.P., and Russell. J.S. (1998) "Computer-Integrated Collaborative Design and Operation in the Construction Industry." *Automation in Construction,* 7, 485–492.

White, D. J., Jaselskis, E. J., Schaefer, V. R., and Cackler, E. T. (2005). "Real-Time Compaction Monitoring in Cohesive Soils from Machine Response." *Transportation Research Record 1936*, Transportation Research Board, Washington, D.C., 173–180.

White, D., Thompson, M., and Vennapusa, P. (2007). Field Validation of Intelligent Compaction Monitoring Technology for Unbound Materials. Report No. MN/RC-2007-10, Iowa State University, Ames, IA.

Witczak, M.W., Kaloush, K., Pellinen, T., Basyouny, M.E., and Quintus, H.V. (2002). Simple Performance Test for Superpave Mix Design. NCHRP Report No. 465. National Research Council, Washington, D.C.

Zhou, F., and Scullion, T. (2003). Upgraded Overlay Tester and Its Application to Characterize Reflection Cracking Resistance of Asphalt Mixtures. Report No. FHWA/TX-04/4467-1, TTI, College Station, TX.

APPENDIX

HMACP MIXTURE DESIGN : COMBINED GRADATION

Refresh Workbook   File Version: 04/17/08 08:13:09

SAMPLE ID:	KRHC03-J76	SAMPLE DATE:	
LOT NUMBER:		LETTING DATE:	
SAMPLE STATUS:		CONTROLLING CSJ:	
COUNTY:		SPEC YEAR:	2004
SAMPLED BY:		SPEC ITEM:	
SAMPLE LOCATION:		SPECIAL PROVISION:	
MATERIAL CODE:		MIX TYPE:	ITEM341_C_Coarse_Surface
MATERIAL NAME:			
PRODUCER:			
AREA ENGINEER:		PROJECT MANAGER:	
COURSE\LIFT:		STATION:		DIST. FROM CL:		CONTRACTOR DESIGN # :	

7ь·ϽϽС

BIN FRACTIONS

	Bin No.1	Bin No.2	Bin No.3	Bin No.4	Bin No.5	Bin No.6	Bin No.7		
Aggregate Source:									
Aggregate Pit:	Hanson	Hanson	Hanson	Hanson	Scamardo	Austin White			
Aggregate Number:	C ROCK	D ROCK	F ROCK	Washed Screening	Sand	Lime			
Sample ID:	New Braunsfels	New Braunsfels	New Braunfel	New Braunfel					Combined Gradation
Rap?:								Total Bin	

Individual Bin (%):	17.0	Percent	17.0	Percent	26.0	Percent	25.0	Percent	14.0	Percent	1.0	Percent		Percent	100.0%	Lower & Upper Specification Limits			
Sieve Size:	Cum.% Passing	Wtd Cum. %	Cum.% Passing	Wtd Cum. %	Cum.% Passing	Wtd Cum. %	Cum.% Passing	Wtd Cum. %	Cum.% Passing	Wtd Cum. %	Cum.% Passing	Wtd Cum. %	Cum.% Passing	Wtd Cum. %	Cum. % Passing	Lower	Upper	Within Spec's	
1"	100.0	17.0	100.0	17.0	100.0	26.0	100.0	25.0	100.0	14.0	100.0	1.0			100.0	100.0	100.0	Yes	
3/4"	98.7	16.8	100.0	17.0	100.0	26.0	100.0	25.0	100.0	14.0	100.0	1.0			99.8	95.0	100.0	Yes	
3/8"	24.6	4.2	86.8	14.8	100.0	26.0	100.0	25.0	100.0	14.0	100.0	1.0			84.9	70.0	85.0	Yes	
No. 4	4.0	0.7	18.2	3.1	52.3	13.6	96.4	24.1	96.3	13.5	100.0	1.0			56.0	43.0	63.0	Yes	
No. 8	1.4	0.2	2.7	0.5	8.2	2.1	75.2	18.8	91.4	12.8	100.0	1.0			35.4	32.0	44.0	Yes	
No. 30	1.3	0.2	2.0	0.3	3.8	1.0	38.5	9.6	70.2	9.8	100.0	1.0			22.0	14.0	28.0	Yes	
No. 50	1.3	0.2	1.7	0.3	1.7	0.4	22.6	5.7	33.5	4.7	100.0	1.0			12.3	7.0	21.0	Yes	
No. 200	1.0	0.2	1.6	0.3	1.6	0.4	6.2	1.6	4.1	0.6	100.0	1.0			4.0	2.0	7.0	Yes	

Not within specifications   # Not cumulative

Asphalt Source & Grade:	JEBRO PG 76-22		Binder Percent, (%):	4.8	Asphalt Spec. Grav.:	1.035
Antistripping Agent:	LIME		Percent, (%):	5		

Remarks:

Test Method: Tested By: Tested Date:

TX207		
TX226		
TX227		
TX235		
TX242		
TX530		

Test Stamp Code: Omit Test: Completed Date: Reviewed By:

Locked By: TxDOT: District: Area:

Authorized By: Authorized Date:

Figure A-1. Mixture Design of HMA Type C with PG 76-22 Binder.

132

HMACP MIXTURE DESIGN : COMBINED GRADATION

Refresh Workbook

File Version: 07/15/08 13:33:34

SAMPLE ID:		SAMPLE DATE:	10/31/08
LOT NUMBER:		LETTING DATE:	
SAMPLE STATUS:	DESIGN	CONTROLLING CSJ:	
COUNTY:	BRAZOS	SPEC YEAR:	2004
SAMPLED BY:	Jerry Groves	SPEC ITEM:	341
SAMPLE LOCATION:	PLANT	SPECIAL PROVISION:	
MATERIAL CODE:		MIX TYPE:	ITEM341_D_Fine_Surface
MATERIAL NAME:	DENSE GRADED D MIX		
PRODUCER:	KNIFE RIVER CORPORATION		
AREA ENGINEER:	KARL NELSON, P.E.	PROJECT MANAGER:	

64-22 Warm

COURSE\LIFT:		STATION:		DIST. FROM CL.:		CONTRACTOR DESIGN # :	KRHD01-J64-R-W

BIN FRACTIONS

	Bin No.1	Bin No.2	Bin No.3	Bin No.4	Bin No.5	Bin No.6	Bin No.7	
Aggregate Source:	HANSON	HANSON	HANSON	KNIFE RIVER	AUSTIN	RAP		
Aggregate Pit:	New Braunsfels	New Braunsels	New Braunsels	SCAMARDO				
Aggregate Number:								
Sample ID:	D ROCK	F ROCK	SCREENINGS	SAND	LIME	-1/2 FRACTIONATED		Combined Gradation
Rap?:						Yes		
Asphalt%:						5.2		Total Bin

Individual Bin (%):	29.5	Percent	16.6	Percent	25.4	Percent	7.5	Percent	1.0	Percent	20.0	Percent		Percent	100.0%	Lower & Upper Specification Limits		
Sieve Size:	Cum.% Passing	Wtd Cum. %	Cum.% Passing	Wtd Cum. %	Cum.% Passing	Wtd Cum. %	Cum.% Passing	Wtd Cum. %	Cum.% Passing	Wtd Cum. %	Cum.% Passing	Wtd Cum. %	Cum.% Passing	Wtd Cum. %	Cum.% Passing	Lower	Upper	Within Spec's
3/4"	100.0	29.5	100.0	16.6	100.0	25.4	100.0	7.5	100.0	1.0	100.0	20.0			100.0	100.0	100.0	Yes
1/2"	100.0	29.5	100.0	16.6	100.0	25.4	100.0	7.5	100.0	1.0	100.0	20.0			100.0	98.0	100.0	Yes
3/8"	89.4	26.4	100.0	16.6	100.0	25.4	100.0	7.5	100.0	1.0	95.2	19.0			95.9	85.0	100.0	Yes
No. 4	17.9	5.3	79.1	13.1	94.5	24.0	96.4	7.2	100.0	1.0	63.4	12.7			63.3	50.0	70.0	Yes
No. 8	2.3	0.7	8.8	1.5	89.5	22.7	84.0	6.3	100.0	1.0	53.7	10.7			42.9	35.0	46.0	Yes
No. 30	1.1	0.3	2.0	0.3	36.0	9.1	59.7	4.4	100.0	1.0	46.5	9.3			24.5	15.0	29.0	Yes
No. 50	1.0	0.3	1.5	0.2	20.6	5.2	26.3	2.0	100.0	1.0	25.1	5.0			13.8	7.0	20.0	Yes
No. 200	1.0	0.3	1.0	0.2	6.0	1.5	2.0	0.2	100.0	1.0	12.3	2.5			5.6	2.0	7.0	Yes

Not within specifications   # Not cumulative

Lift Thickness, in:	2.00

| Asphalt Source & Grade:	JEBRO PG 64-22	Binder Percent, (%):	5.2	Asphalt Spec. Grav.:	1.033
Antistripping Agent:	HYDRATED LIME	Percent, (%):	1		

Remarks:

Test Method:	Tested By:	Tested Date:
TX207		
TX226		
TX227		
TX235		
TX242		
TX530		

Test Stamp Code:		Omit Test:	Completed Date:	Reviewed By:

Locked By:	TxDOT:	District:	Area:

Authorized By:		Authorized Date:

Figure A-2. Mixture Design of WMA Type D with PG 64-22 Binder.

HMACP MIXTURE DESIGN : COMBINED GRADATION

Refresh Workbook   File Version: 07/15/08 13:33:34

SAMPLE ID:		SAMPLE DATE:	10/31/08
LOT NUMBER:		LETTING DATE:	
SAMPLE STATUS:	DESIGN	CONTROLLING CSJ:	
COUNTY:	BRAZOS	SPEC YEAR:	2004
SAMPLED BY:	Jerry Groves	SPEC ITEM:	341
SAMPLE LOCATION:	PLANT	SPECIAL PROVISION:	
MATERIAL CODE:		MIX TYPE:	ITEM341_D_Fine_Surface
MATERIAL NAME:	DENSE GRADED D MIX		
PRODUCER:	KNIFE RIVER CORPORATION		
AREA ENGINEER:	KARL NELSON, P.E.	PROJECT MANAGER:	

64-22 Hot

COURSE\LIFT:		STATION:		DIST. FROM CL:		CONTRACTOR DESIGN # :	KRHD01-J64-R

BIN FRACTIONS

	Bin No.1		Bin No.2		Bin No.3		Bin No.4		Bin No.5		Bin No.6		Bin No.7		Total Bin	Combined Gradation		
Aggregate Source:	HANSON		HANSON		HANSON		KNIFE RIVER		AUSTIN		RAP							
Aggregate Pit:	New Braunsfels		New Braunsels		New Braunsels		SCAMARDO											
Aggregate Number:																		
Sample ID:	D ROCK		F ROCK		SCREENINGS		SAND		LIME		-1/2 FRACTIONATED							
Rap?:											Yes							
Asphalt%:												5.2						

Individual Bin (%):	29.5	Percent	16.6	Percent	25.4	Percent	7.5	Percent	1.0	Percent	20.0	Percent		Percent	100.0%	Lower & Upper Specification Limits		

Sieve Size:	Cum.% Passing	Wtd Cum. %	Cum.% Passing	Wtd Cum. %	Cum.% Passing	Wtd Cum. %	Cum.% Passing	Wtd Cum. %	Cum.% Passing	Wtd Cum. %	Cum.% Passing	Wtd Cum. %	Cum.% Passing	Wtd Cum. %	Cum. % Passing	Lower	Upper	Within Spec's
3/4"	100.0	29.5	100.0	16.6	100.0	25.4	100.0	7.5	100.0	1.0	100.0	20.0			100.0	100.0	100.0	Yes
1/2"	100.0	29.5	100.0	16.6	100.0	25.4	100.0	7.5	100.0	1.0	100.0	20.0			100.0	98.0	100.0	Yes
3/8"	89.4	26.4	100.0	16.6	100.0	25.4	100.0	7.5	100.0	1.0	95.2	19.0			95.9	85.0	100.0	Yes
No. 4	17.9	5.3	79.1	13.1	94.5	24.0	96.4	7.2	100.0	1.0	63.4	12.7			63.3	50.0	70.0	Yes
No. 8	2.3	0.7	8.8	1.5	89.5	22.7	84.0	6.3	100.0	1.0	53.7	10.7			42.9	35.0	46.0	Yes
No. 30	1.1	0.3	2.0	0.3	36.0	9.1	58.7	4.4	100.0	1.0	46.5	9.3			24.5	15.0	29.0	Yes
No. 50	1.0	0.3	1.5	0.2	20.6	5.2	26.3	2.0	100.0	1.0	25.1	5.0			13.8	7.0	20.0	Yes
No. 200	1.0	0.3	1.0	0.2	6.0	1.5	2.0	0.2	100.0	1.0	12.3	2.5			5.6	2.0	7.0	Yes

Not within specifications   # Not cumulative

Lift Thickness, in:	2.00

Asphalt Source & Grade:	JEBRO PG 64-22	Binder Percent, (%):	5.2	Asphalt Spec. Grav.:	1.033

Antistripping Agent:	HYDRATED LIME	Percent, (%):	1

Remarks:

Test Method:	Tested By:	Tested Date:
TX207		
TX226		
TX227		
TX235		
TX242		
TX530		

Test Stamp Code:	Omit Test:	Completed Date:	Reviewed By:

Locked By:	TxDOT:	District:	Area:

Authorized By:		Authorized Date:

Figure A-3. Mixture Design of HMA Type D with PG 64-22 Binder.

134
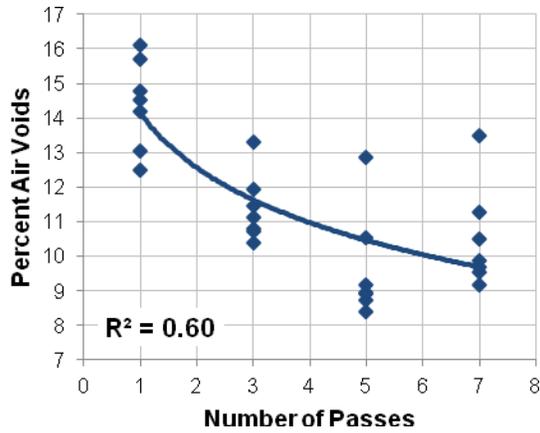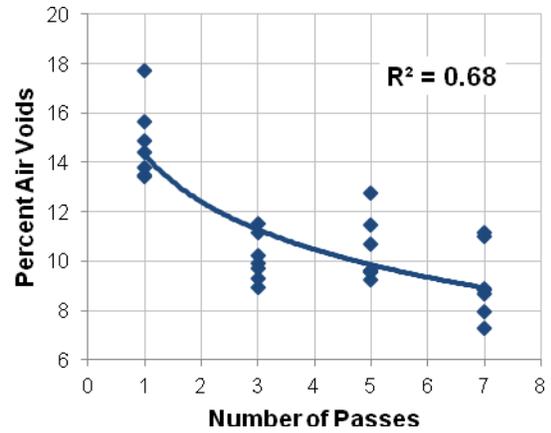
(a) Test Section 2 (Static Roller)   (b) Test Section 2 (Vibratory Roller)

**Figure A-4. Percent Air Voids versus Number of Passes for Test Section 2.**
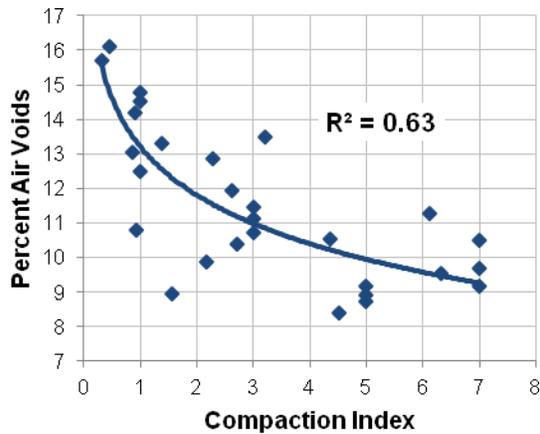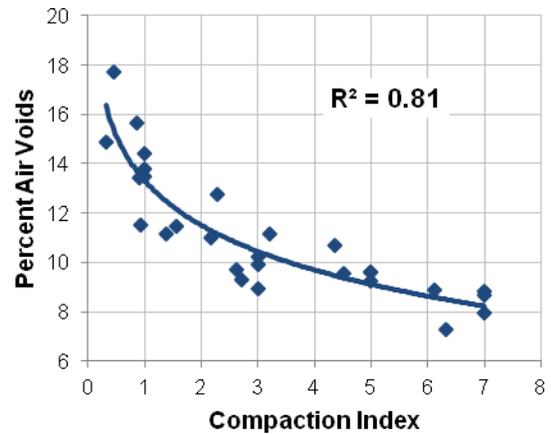

(a) Test Section 2 (Static Roller)   (b) Test Section 2 (Vibratory Roller)

**Figure A-5. Percent Air Voids versus Compaction Index for Test Section 2.**
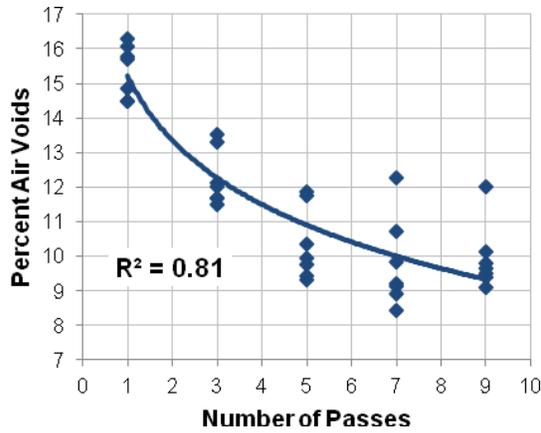
(a) Test Section 2 (Vibratory Roller)   (b) Test Section 2 (Vibratory Roller)
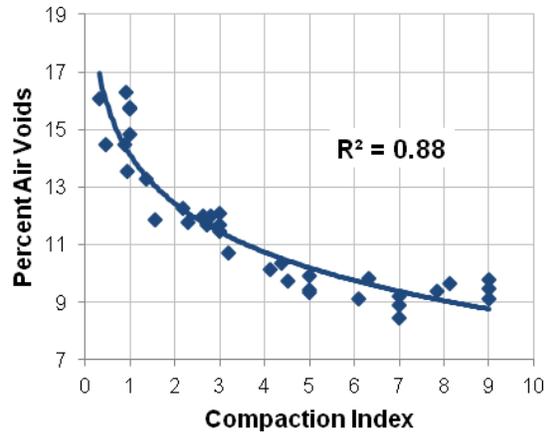
Note: Sub-test section was compacted at lower temperature.

Figure A-6. Percent Air Voids versus Number of Passes and Compaction Index for Test Section 2.
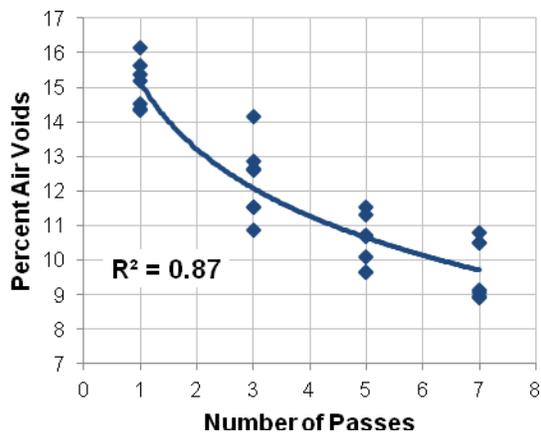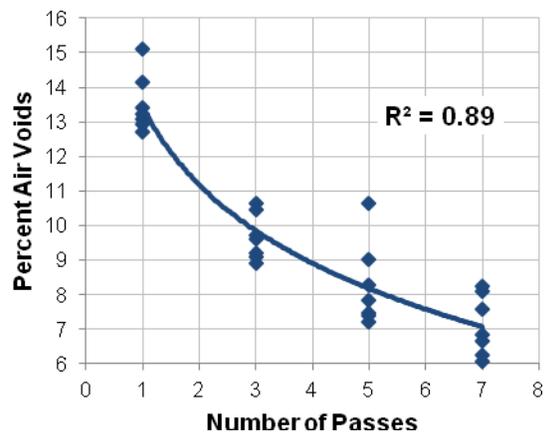
(a) Test Section 3 (Static Roller)   (b) Test Section 3 (Vibratory Roller)

Figure A-7. Percent Air Voids versus Number of Passes for Test Section 3.

136
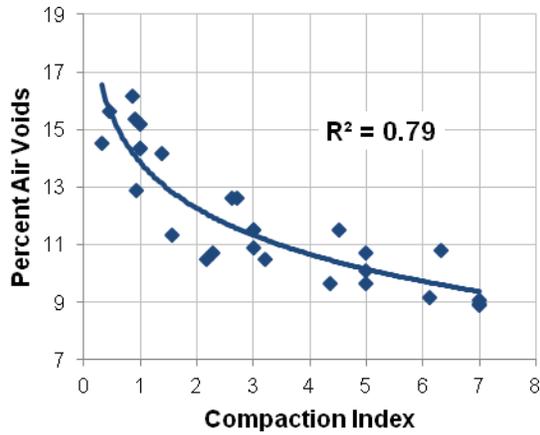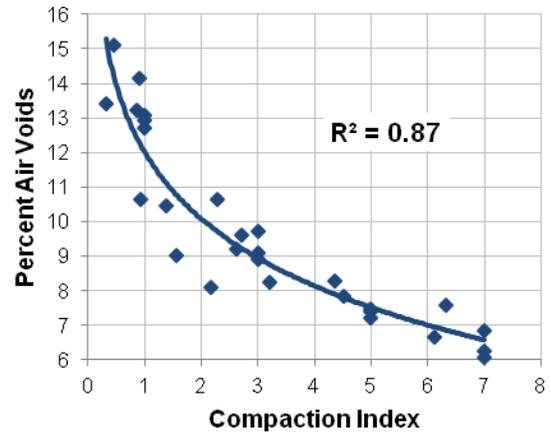
(a) Test Section 3 (Static Roller) (b) Test Section 3 (Vibratory Roller)

Figure A-8. Percent Air Voids versus Compaction Index for Test Section 3.
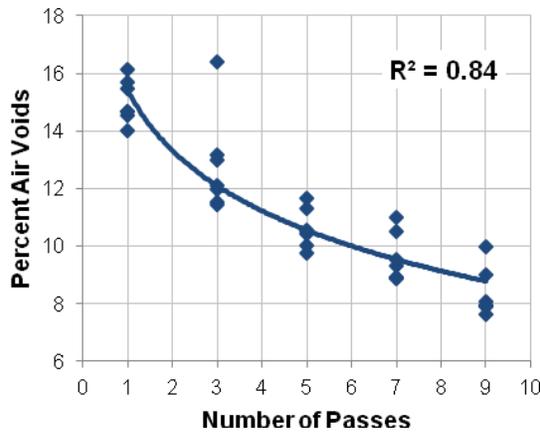
(a) Test Section 3 (Vibratory Roller) (b) Test Section 3 (Vibratory Roller)
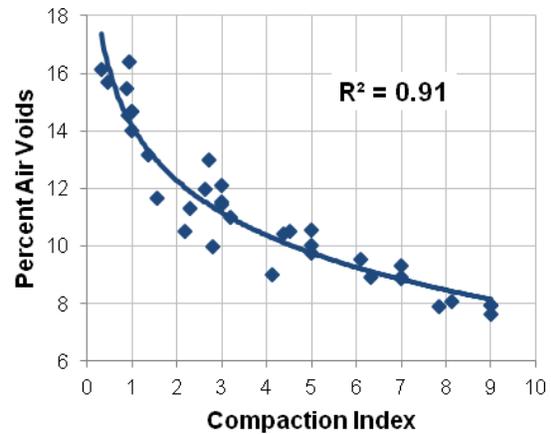
Note: Sub-test section was compacted at lower temperature.

Figure A-9. Percent Air Voids versus Number of Passes and Compaction Index for Test Section 3.
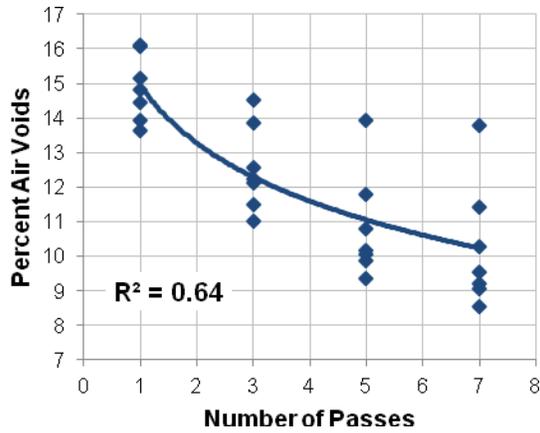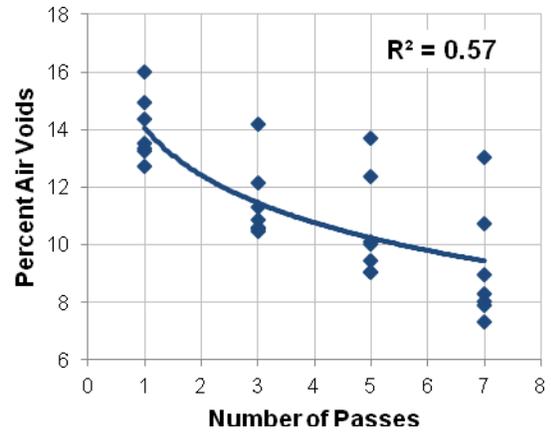
(a) Test Section 4 (Static Roller)   (b) Test Section 4 (Vibratory Roller)

Figure A-10. Percent Air Voids versus Number of Passes for Test Section 4.
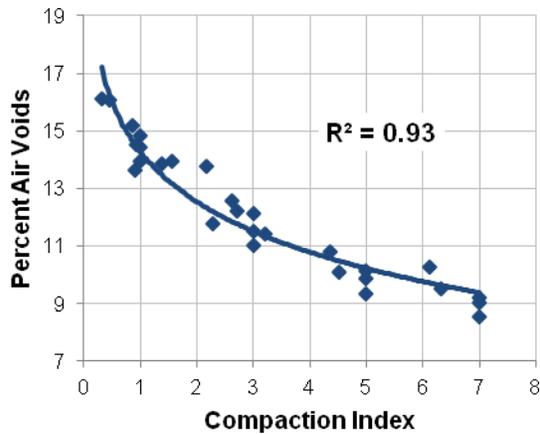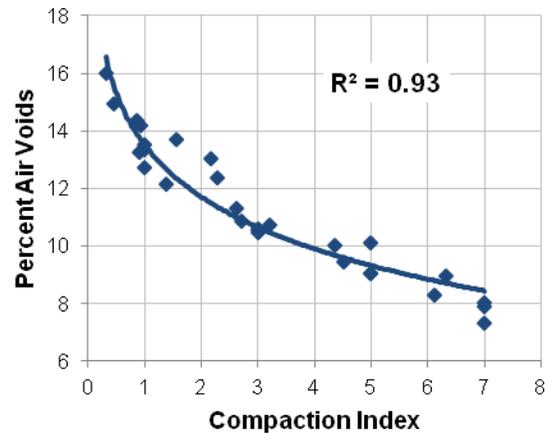
(a) Test Section 4 (Static Roller)   (b) Test Section 4 (Vibratory Roller)

Figure A-11. Percent Air Voids versus Compaction Index for Test Section 4.

138
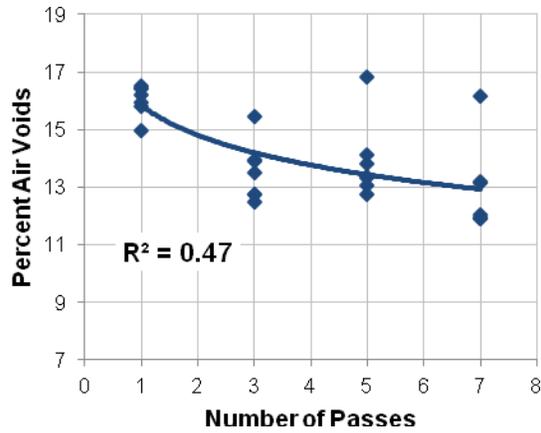
(a) Test Section 4 (Vibratory Roller)   (b) Test Section 4 (Vibratory Roller)
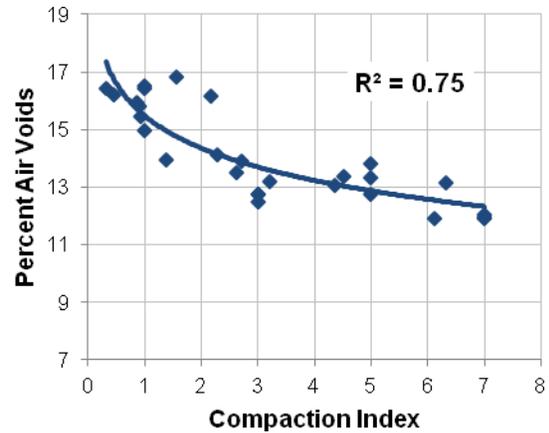
Note: Sub-test section was compacted at lower temperature.

Figure A-12. Percent Air Voids versus Number of Passes and Compaction Index for Test Section 4.
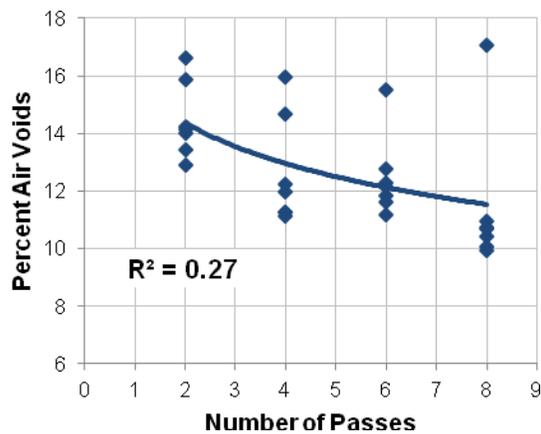
(a) Test Section 5 (Vibratory Roller)   (b) Test Section 5 (Vibratory Roller)
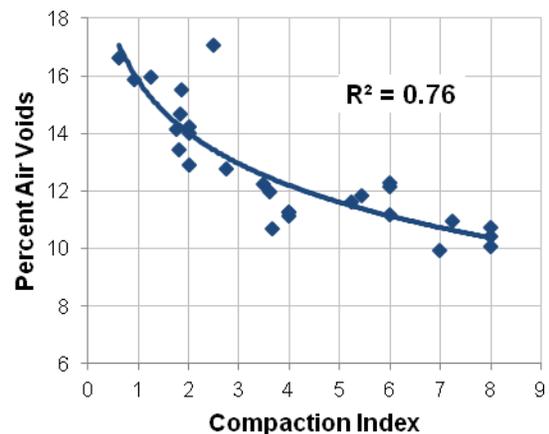
Note: Sub-test section was compacted at lower temperature.

Figure A-13. Percent Air Voids versus Number of Passes and Compaction Index for Test Section 5.
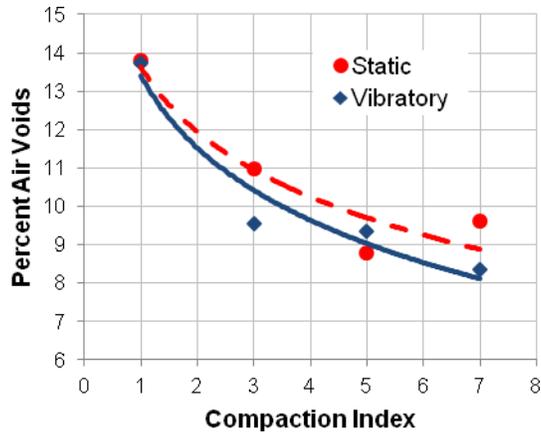
(a) Test Section 2
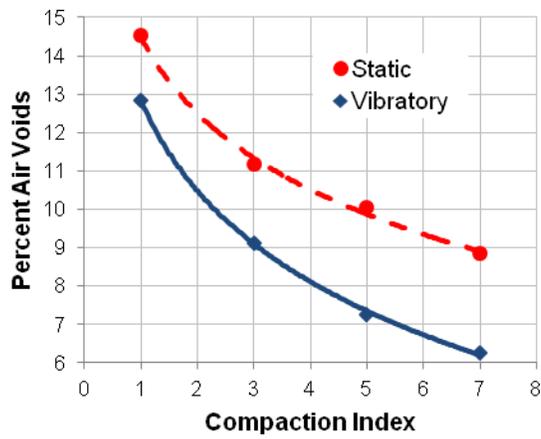
(b) Test Section 3
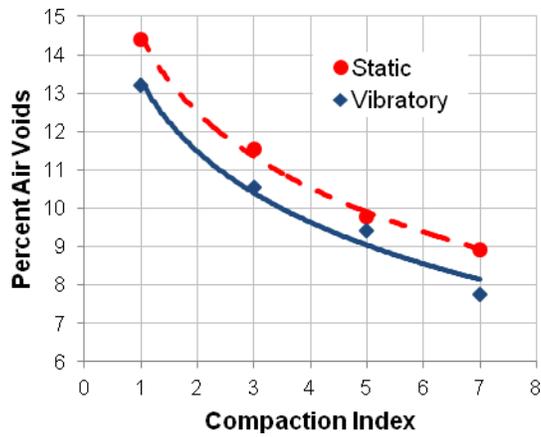
(c) Test Section 4

Figure A-14. Percent Air Voids versus Compaction Index for Different Rollers.
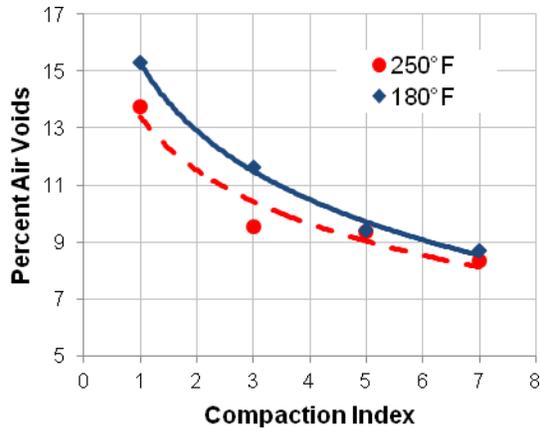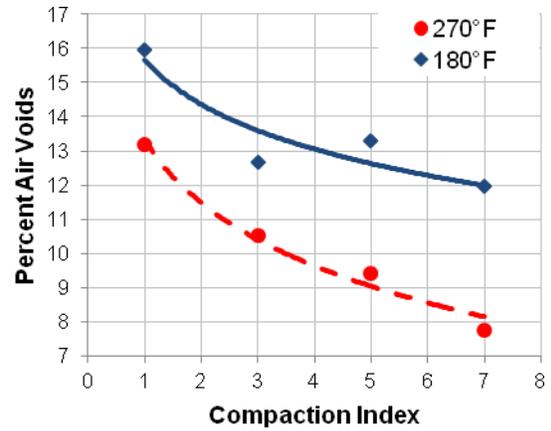
(a) Test Section 2   (b) Test Section 4

Figure A-15. Percent Air Voids versus Compaction Index at Different Compaction Temperatures.
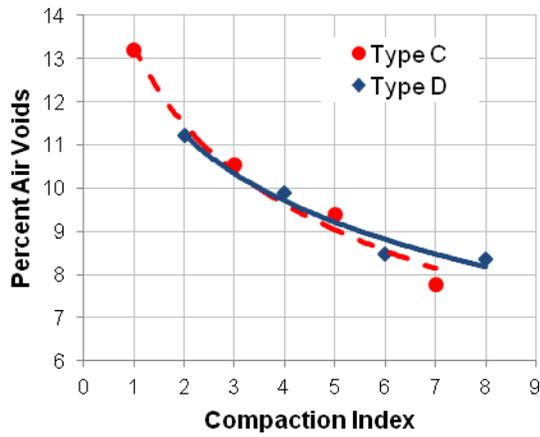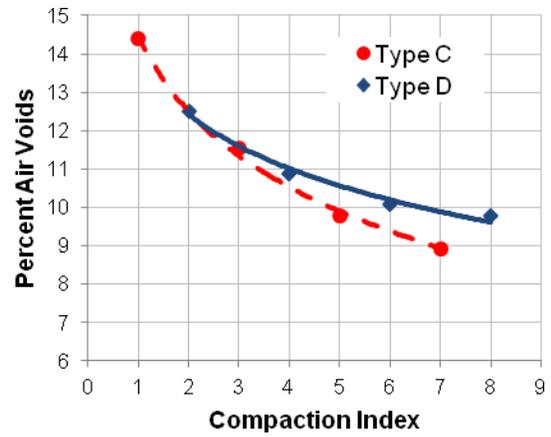
(a) Vibratory Roller   (b) Static Roller

**Figure A-16. Influence of Mixture Design on Density:
Test Section 4 vs. Test Section 5.**

(a) Vibratory Roller   (b) Static Roller
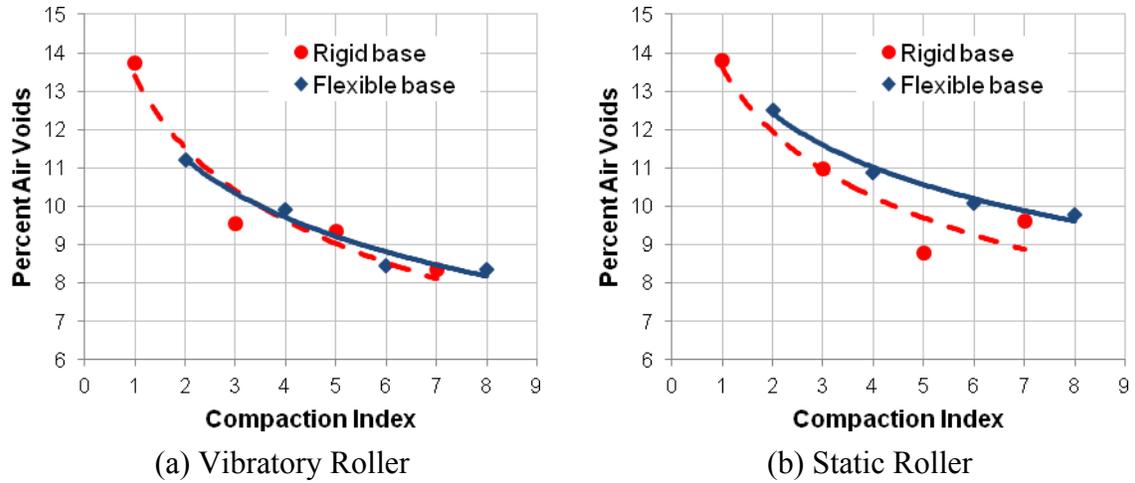
Figure A-17. Influence of Base Support Type on Compactability:
Test Section 2 vs. Test Section 5.
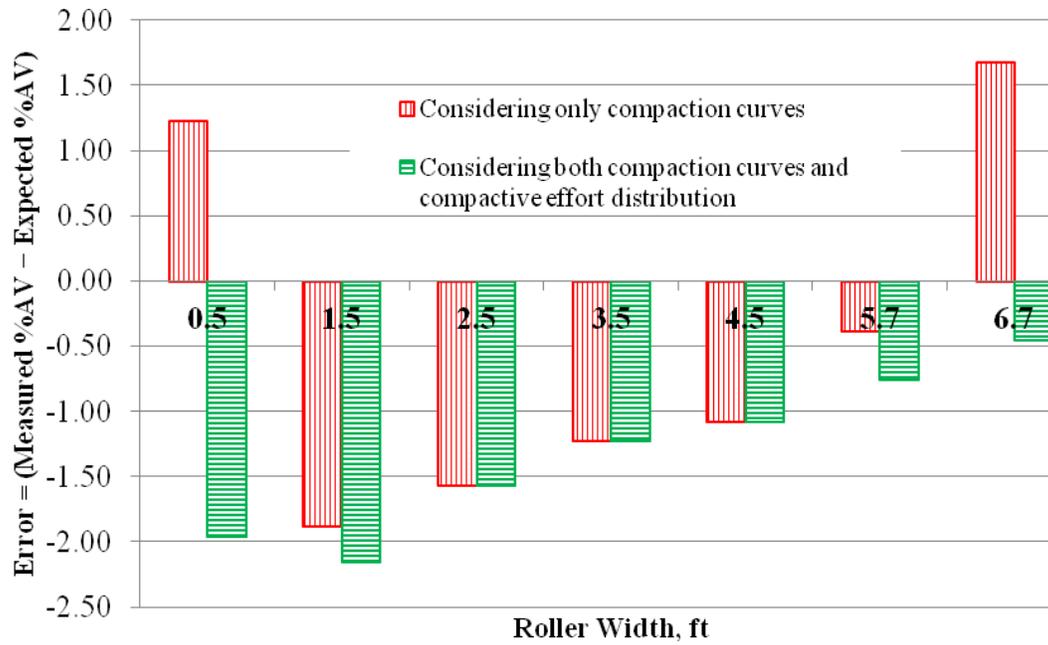
Figure A-18. Error in Predicting Density Level for Test Section 2.
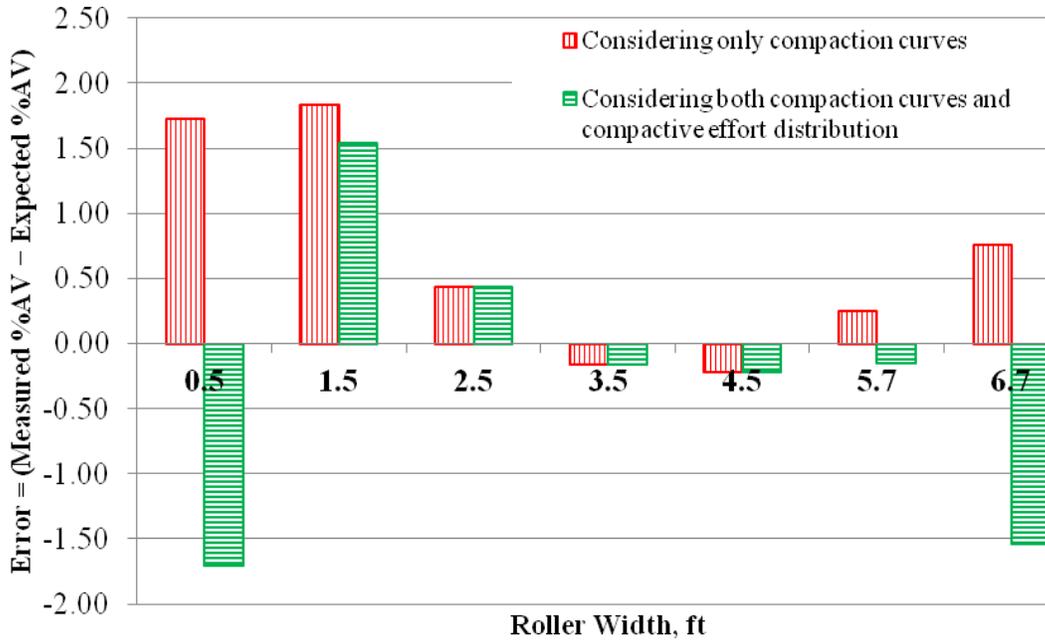
Figure A-19. Error in Predicting Density Level for Test Section 3.
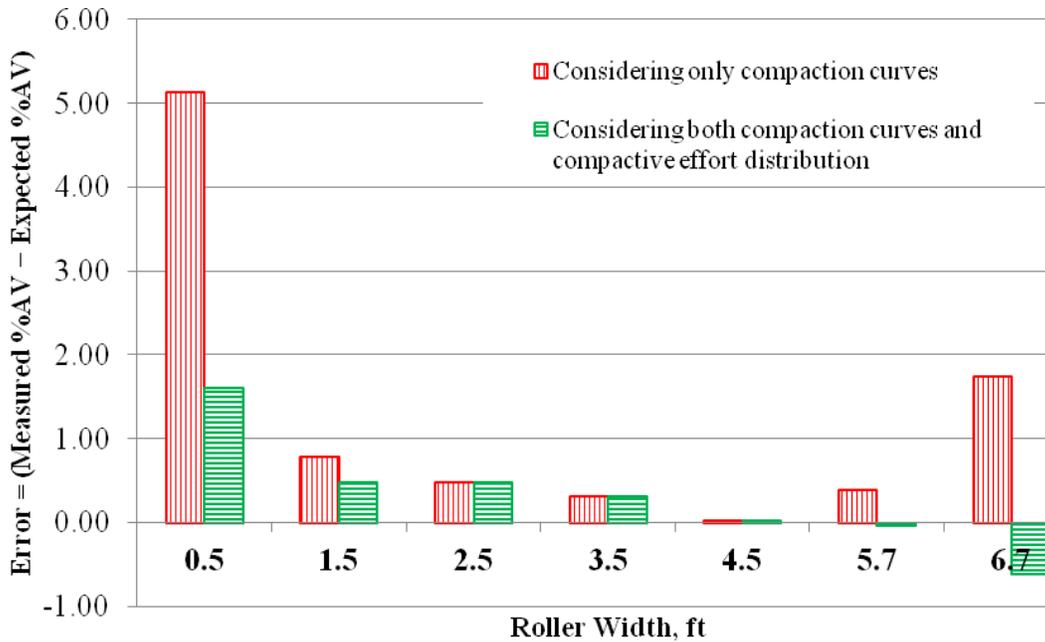
Figure A-20. Error in Predicting Density Level for Test Section 4.
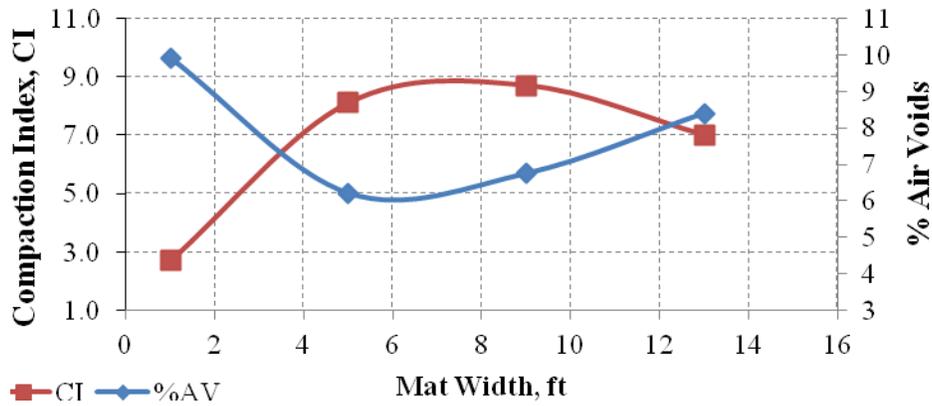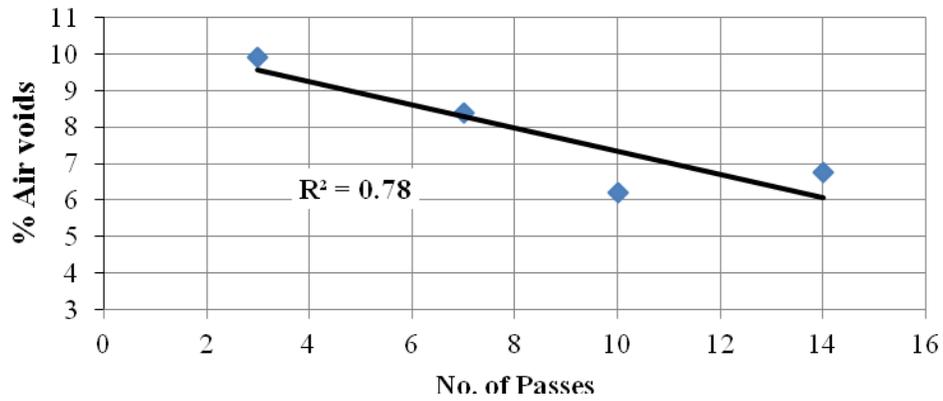
143

(a) CI and Percent of Air Voids Distributions across the Mat


(b) Number of Passes versus the Percent of Air Voids
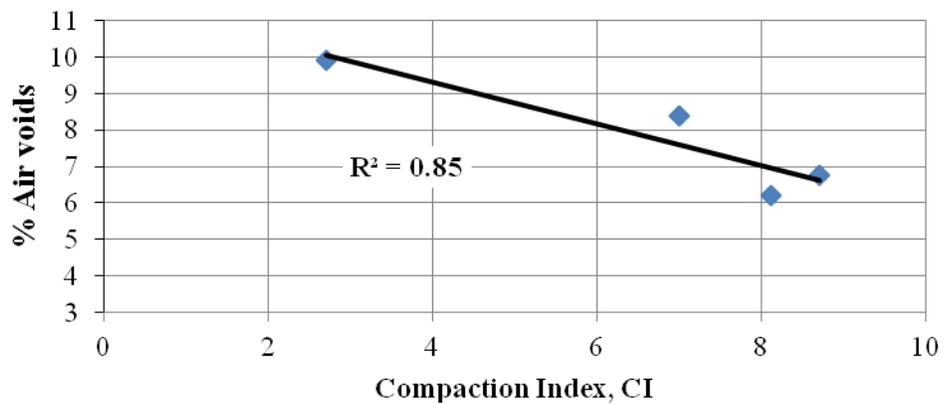
(c) Compaction Index versus the Percent of Air Voids

Figure A-21. Test Section SH 31 (Test Section 2).
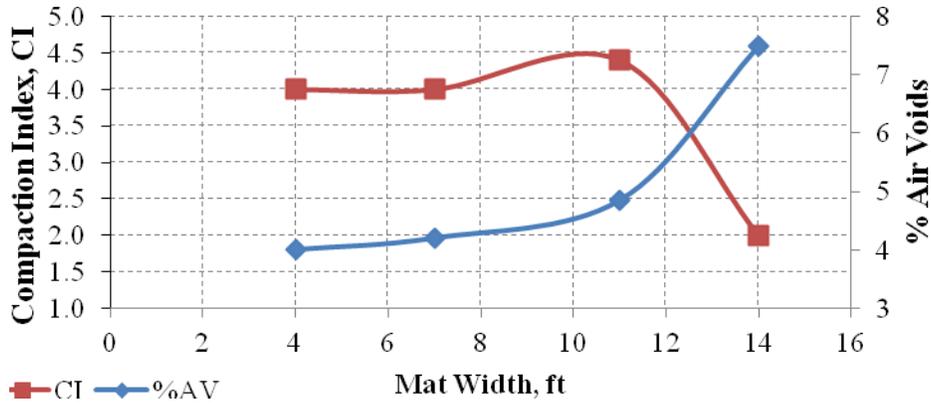
(a) CI and Percent of Air Voids Distributions across the Mat
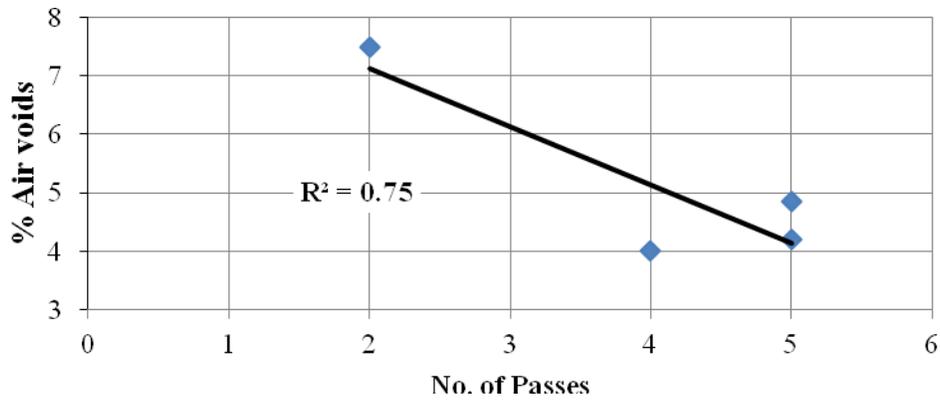

(b) Number of Passes versus the Percent of Air Voids
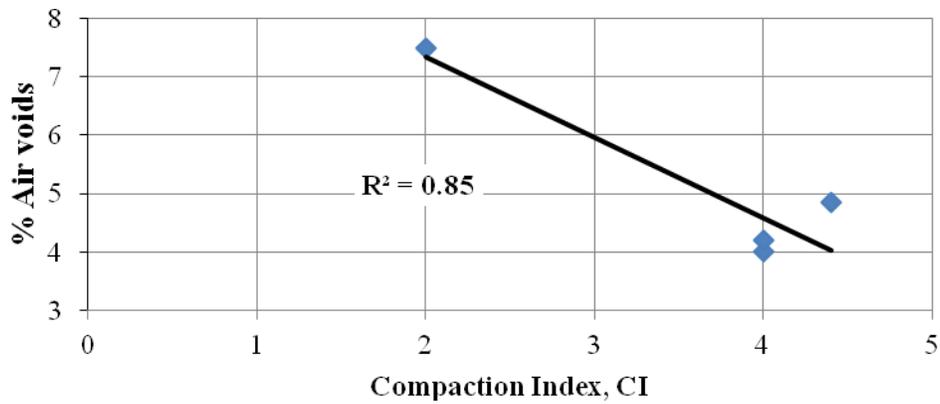
(c) Compaction Index versus the Percent of Air Voids

Figure A-22. Test Section FM 2854 (Test Section 1).
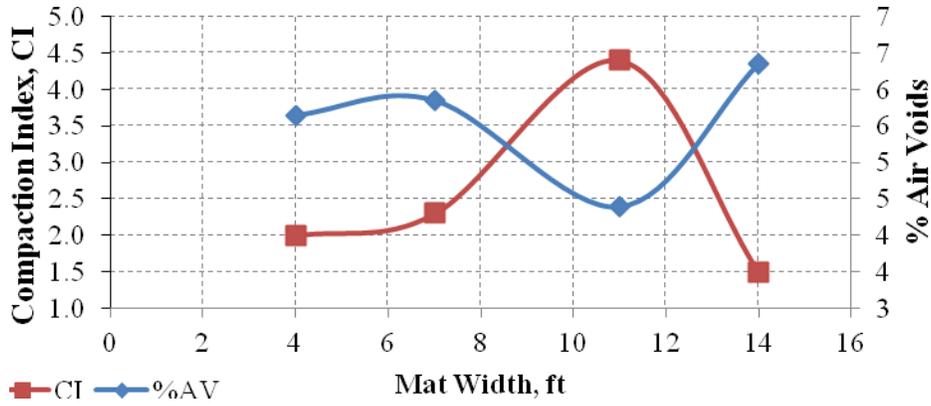
(a) CI and Percent of Air Voids Distributions across the Mat
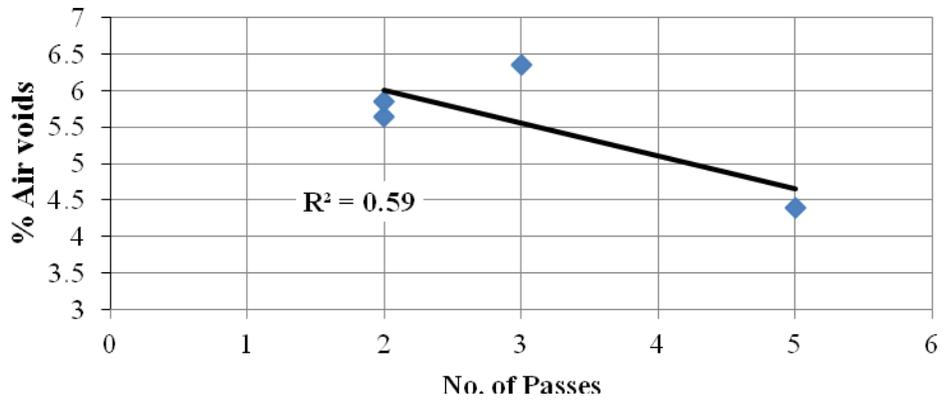
(b) Number of Passes versus the Percent of Air Voids
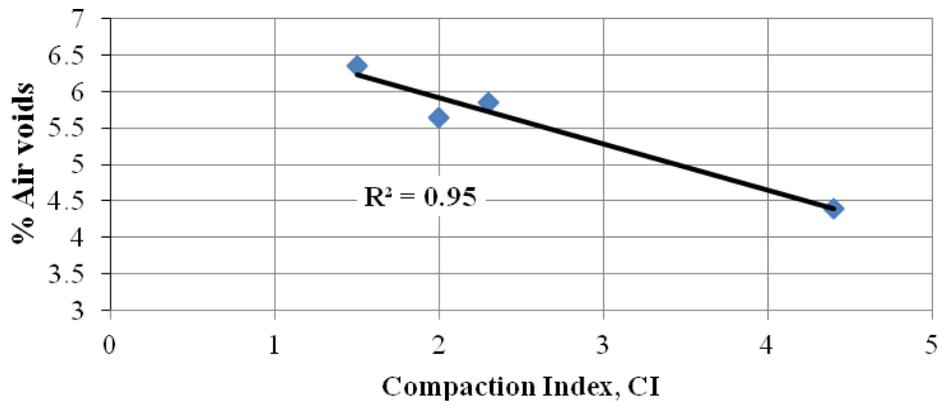
(c) Compaction Index versus the Percent of Air Voids

Figure A-23. Test Section FM 2854 (Test Section 2).
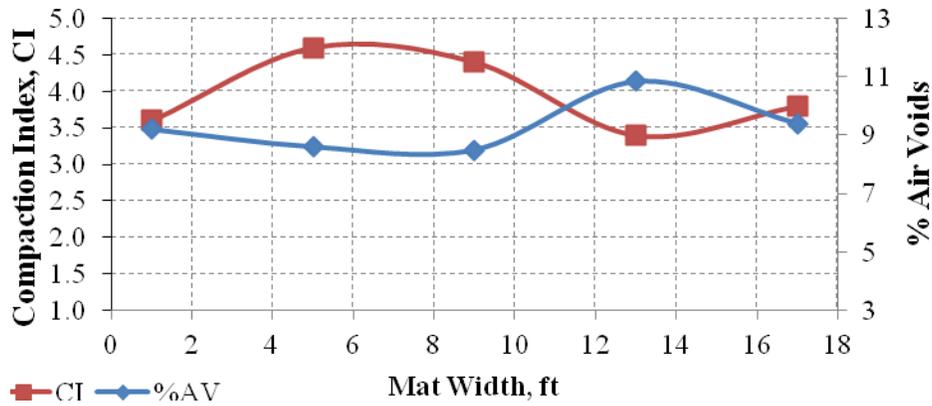
(a) CI and Percent of Air Voids Distributions across the Mat
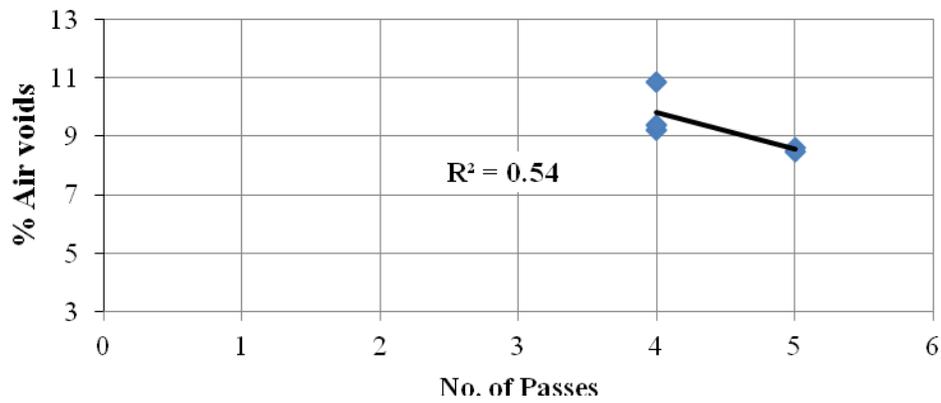

(b) Number of Passes versus the Percent of Air Voids
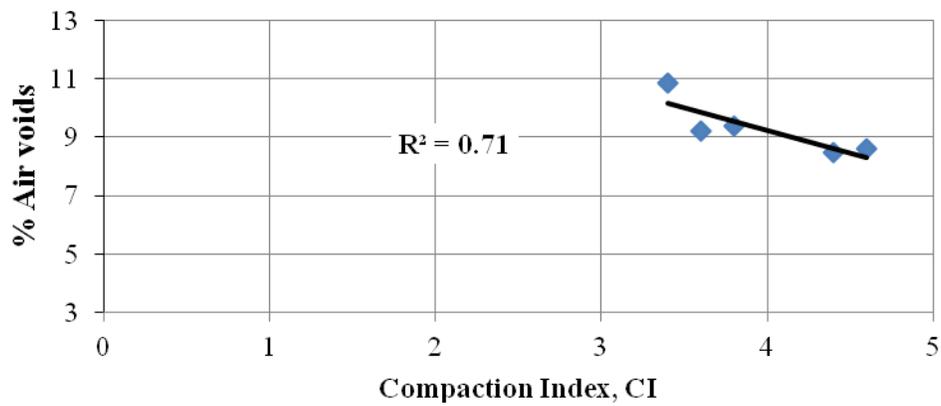
(c) Compaction Index versus the Percent of Air Voids

Figure A-24. Test Section SL 340.
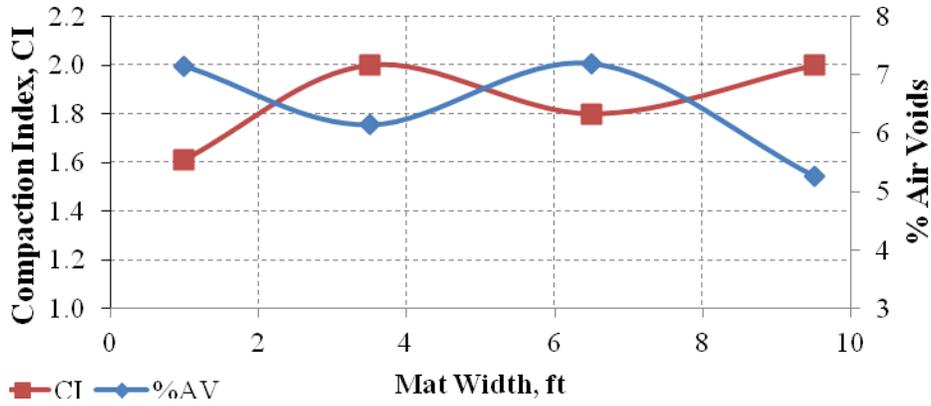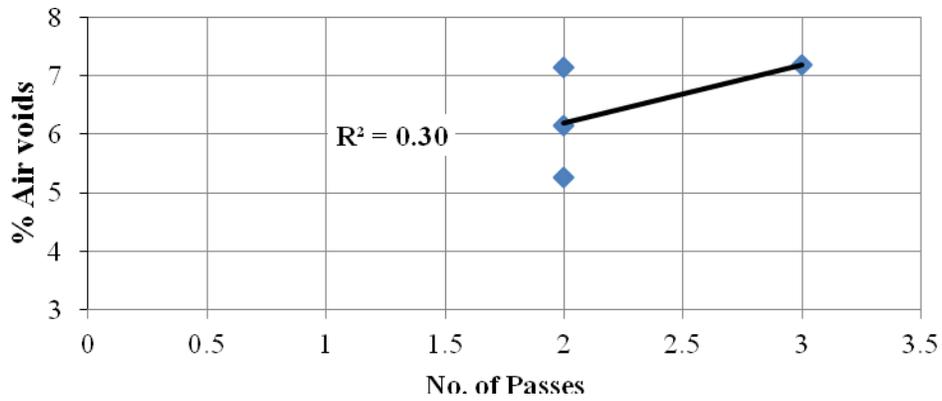
147

(a) CI and Percent of Air Voids Distributions across the Mat

(b) Number of Passes versus the Percent of Air Voids
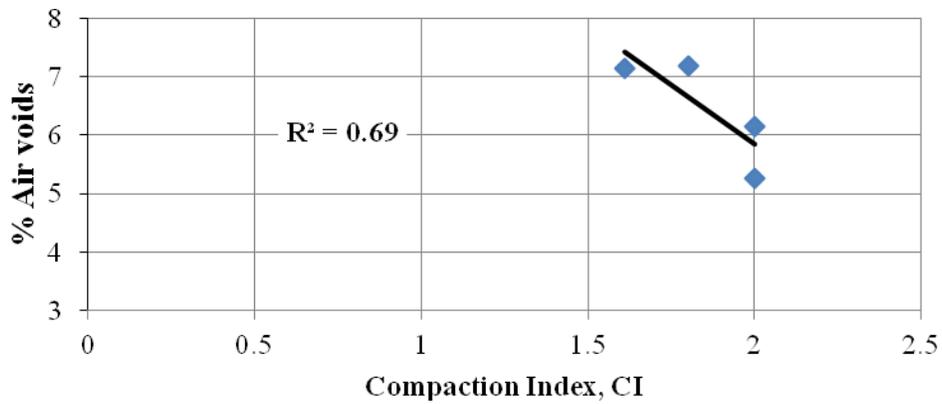
(c) Compaction Index versus the Percent of Air Voids

Figure A-25. Test Section SH 159.